Supporting Information:

Structure-Activity Relationships in Tripodal Transmembrane Anion Transporters: The Effect of Fluorination

Nathalie Busschaert,[1] Marco Wenzel,[1] Mark E. Light,[1] Paulina Iglesias-Hernández,[2] Ricardo Pérez-Tomás[2] and Philip A. Gale,[1]*

Chemistry, University of Southampton, Southampton, SO17 1BJ, UK, and Department of Pathology and Experimental Therapeutics, Cancer Cell Biology Research Group, Universidad de Barcelona, Barcelona, Spain. Corresponding author: philip.gale@soton.ac.uk

[1] University of Southampton

[2] Universidad de Barcelona

S1. OVERVIEW OF COMPOUNDS

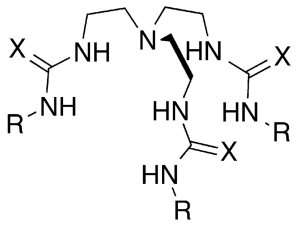

1 X=O, R=Ph
2 X=O, R=*p*-C_6H_4F
3 X=O, R=C_6F_5
4 X=O, R=*p*-$C_6H_4(CF_3)$
5 X=O, R=

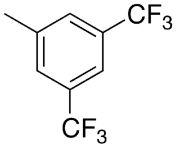

6 X=S, R=Ph
7 X=S, R=*p*-C_6H_4F
8 X=S, R=C_6F_5
9 X=S, R=*p*-$C_6H_4(CF_3)$
10 X=S, R=

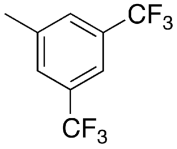

S2. SYNTHESIS

General. ^{1}H NMR (300 MHz) and ^{13}C{^{1}H} NMR (75 MHz) spectra were determined on a Bruker AV300 spectrometer. Chemical shifts (δ) are reported in parts per million (ppm) and calibrated to the residual protio solvent peak in DMSO-d_6 (δ = 2.50 (^{1}H) and 74.2 ppm (^{13}C)). The following abbreviations are used for spin multiplicity: s = singlet, d = doublet, dd = doublet of doublets, t = triplet, q = quartet, m = multiplet, br = broad. Infrared (IR) spectra were recorded on a Matterson Satellite (ATR) and are reported in wavenumbers (cm^{-1}). High resolution electron spray (ES) mass spectra were recorded on a Bruker Apex III. All mass spectra are reported as *m*/*z* (relative intensity). Melting points were determined by a Barnstead Electrothermal 9100 melting point apparatus and were not corrected. All reactions were performed using oven-dried glassware. DCM was distilled over calcium hydride under nitrogen prior to use. All other solvents and reagents were used as provided by the supplier. The syntheses and characterizations of compounds **1**[1], **3**[2] and **6**[1] were performed as previously reported. All other compounds are novel.

1,1',1''-(nitrilotris(ethane-2,1-diyl))tris(3-(4-fluorophenyl)urea) (2). 0.30 mL (2.00 mmol) of tris(2-aminoethyl)amine was dissolved in 20 mL dichloromethane and 0.60 mL (6.63 mmol) 4-fluorophenyl isocyanate was added. The mixture was stirred overnight at room temperature

under nitrogen atmosphere. A precipitate was formed and subsequently filtered off and washed with dichloromethane. The white solid was then dried overnight in vacuo (1.04 g, 1.86 mmol). Yield: 93%; Mp: decomposition; ^{1}H NMR (300 MHz, DMSO-d_6) δ ppm 2.58 (t, *J*=6.40 Hz, 6 H), 3.17 (q, *J*=6.03 Hz, 6 H), 6.18 (t, *J*=5.27 Hz, 3 H), 7.02 (t, *J*=9.04 Hz, 6 H), 7.37 (dd, *J*=9.23, 5.09 Hz, 6 H), 8.59 (s, 3 H); ^{13}C{^{1}H} NMR (75 MHz, DMSO-d_6) δ ppm 37.48, 53.85, 114.99 (d, *J*=22.12 Hz), 119.26 (d, *J*=7.74 Hz), 136.79, 155.32, 156.80 (d, *J*=236.63 Hz); IR (neat): ν= 3300 (br, NH stretch), 1640 (CO stretch) cm^{-1}; LRMS (ESI+): *m/z*= 596.3 [M+K]$^{+}$; HRMS (ES) for $C_{27}H_{31}F_3N_7O_3$ [M+H]$^{+}$: *m/z*= 558.2435 (calcd), 558.2433 (found).

1,1',1''-(nitrilotris(ethane-2,1-diyl))tris(3-(4-(trifluoromethyl)phenyl)urea) (4). 0.30 mL (2.00 mmol) of tris(2-aminoethyl)amine was dissolved in 20 mL dichloromethane and 0.86 mL (6.75 mmol) 4-trifluoromethylphenyl isocyanate was added. The mixture was stirred overnight at room temperature under nitrogen atmosphere. A white precipitate was formed and subsequently filtered off and washed with dichloromethane. The white solid was then dried overnight in vacuo (1.41 g, 2.00 mmol). Yield: 100%; Mp: 239.9-242.3 °C; ^{1}H NMR (300 MHz, DMSO-d_6) δ ppm 2.62 (t, *J*=6.40 Hz, 6 H), 3.21 (q, *J*=6.03 Hz, 6 H), 6.30 (t, *J*=5.27 Hz, 3 H), 7.54 (m, 12 H), 8.95 (s, 3 H); ^{13}C{^{1}H} NMR (75 MHz, DMSO-d_6) δ ppm 37.50, 53.61, 117.18, 120.85 (q, *J*=32.07 Hz), 124.59 (q, *J*=270.91 Hz), 125.84 (q, *J*=3.32 Hz), 144.14, 154.85; IR (neat): ν= 3290 (br, NH stretch), 1650 (CO stretch) cm^{-1}; LRMS (ESI+): *m/z*= 708.3 [M+H]$^{+}$, 730.3 [M+Na]$^{+}$; HRMS (ES) for $C_{30}H_{31}F_9N_7O_3$ [M+H]$^{+}$: m/z= 708.2339 (calcd), 708.2345 (found).

1,1',1''-(nitrilotris(ethane-2,1-diyl))tris(3-(3,5-bis(trifluoromethyl)phenyl)urea) (5). 0.25 mL (1.67 mmol) of tris(2-aminoethyl)amine was dissolved in 20 mL dichloromethane and 0.87 mL (5.01 mmol) 3,5-bis(trifluoromethyl)phenyl isocyanate was added. The mixture was stirred overnight at room temperature under nitrogen atmosphere. A precipitate was formed and subsequently filtered off and washed with dichloromethane. The white solid was then dried overnight in vacuo (1.48 g, 1.62 mmol). Yield: 97%; Mp: 224.0-224.9 °C; ^{1}H NMR (300 MHz, DMSO-d_6) δ ppm 2.63 (t, *J*=6.04 Hz, 6 H), 3.22 (q, *J*=5.49 Hz, 6 H), 6.40 (t, *J*=5.31 Hz, 3 H), 7.44 (s, 3 H), 7.98 (s, 6 H), 9.25 (s, 3 H); ^{13}C{^{1}H} NMR (75 MHz, DMSO-d_6) δ ppm 37.67, 53.49, 113.23, 116.95, 123.24 (q, *J*=274.20 Hz), 130.21 (q, *J*=32.07 Hz), 142.41, 154.81; IR (neat): ν= 3290 (br, NH stretch), 1650 (CO stretch) cm^{-1}; LRMS (ESI+): *m/z*= 912.5 [M+H]$^{+}$,

934.3 $[M+Na]^+$; HRMS (ES) for $C_{33}H_{28}F_{18}N_7O_3$ $[M+H]^+$: *m/z*= 912.1961 (calcd), 912.1960 (found).

1,1',1''-(nitrilotris(ethane-2,1-diyl))tris(3-(4-fluorophenyl)thiourea) (7). A solution of 4-fluorophenyl isothiocyanate (0.62g, 4.05 mmol) and triethylamine (0.20 mL) in 10 mL chloroform was heated to reflux under nitrogen. A solution of 0.20 mL (1.33 mmol) tris(2-aminoethyl)amine in 40 mL chloroform was added dropwise to this mixture over a period of 2 hours. The resulting mixture was then left to reflux overnight under nitrogen. Chloroform was removed under reduced pressure and the resulting residue was purified by column chromatography (5% methanol in dichloromethane) to give a white foam (0.63 g, 1.04 mmol). Yield: 78%; Mp: decomposition; ^{1}H NMR (300 MHz, DMSO-d_6) δ ppm 2.71 (t, *J*=6.22 Hz, 6 H), 3.55 (br. s., 6 H), 7.15 (t, *J*=8.78 Hz, 6 H), 7.37 (dd, J=8.97, 4.94 Hz, 6 H), 7.59 (br. s., 3 H), 9.57 (s, 3 H); ^{13}C{^{1}H} NMR (75 MHz, DMSO-d_6) δ ppm 41.88, 52.09, 115.22 (d, *J*=22.64 Hz), 125.79, 135.32, 158.98 (d, *J*=240.75 Hz), 180.55; IR (neat): ν= 3190 (br, NH stretch), 1500 (CS stretch) cm^{-1}; LRMS (ESI+): *m/z*= 628.3 $[M+Na]^+$; HRMS (ES) for $C_{27}H_{31}F_3N_7S_3$ $[M+H]^+$: *m/z*= 606.1750 (calcd), 606.1753 (found).

1,1',1''-(nitrilotris(ethane-2,1-diyl))tris(3-(perfluorophenyl)thiourea) (8). 1.50 mL (10.62 mmol) pentafluorophenyl isothiocyanate was dissolved in 10 mL dry dichloromethane at roomtemperature under nitrogen. A solution of 0.50 mL tris(2-aminoethyl)amine (3.34 mmol) in 15 mL dry dichloromethane was added dropwise to this solution. The resulting mixture was left to stir overnight at room temperature under nitrogen. A precipitate was formed and subsequently filtered off and washed with dichloromethane. The white solid was then dried on air overnight (2.64 g, 3.21 mmol). Yield: 96%; Mp: 189.1-190.9 °C; ^{1}H NMR (300 MHz, DMSO-d_6) δ ppm 2.73 (br. s, 6 H), 3.58 (br. s., 6 H), 8.10 (br. s., 3 H), 9.31 (br. s., 3 H); ^{13}C{^{1}H} NMR (75 MHz, DMSO-d_6) δ ppm 42.79, 51.93, 114.99 (t, *J*=14.37 Hz), 137.19 (d of m, *J*=250.44 Hz), 139.46 (d of m, *J*=250.44 Hz), 143.97 (d of m, *J*=247.68 Hz), 182.39; LRMS (ESI+): *m/z*= 822.4 $[M+H]^+$, 844.4 $[M+Na]^+$; HRMS (ES) for $C_{27}H_{19}F_{15}N_7S_3$ $[M+H]^+$: *m/z*= 822.0644 (calcd), 822.0638 (found).

1,1',1''-(nitrilotris(ethane-2,1-diyl))tris(3-(4-(trifluoromethyl)phenyl)thiourea) (9). 0.30 mL (2.00 mmol) of tris(2-aminoethyl)amine was dissolved in 20 mL dichloromethane and 1.28 g (6.30 mmol) 4-trifluoromethylphenyl isothiocyanate was added. The mixture was stirred overnight at room temperature under nitrogen atmosphere. A precipitate was formed and subsequently filtered off and washed with dichloromethane. The white solid was then recrystalized from ethanol and dried overnight in vacuo at 100 °C to remove all solvents (1.09 g, 1.44 mmol). Yield: 72%; Mp: 192.3-193.6 °C; ^{1}H NMR (300 MHz, DMSO-d_6) δ ppm 2.79 (t, *J*=6.97 Hz, 6 H), 3.63 (br. s., 6 H), 7.66 (m, 12 H), 7.97 (br. s., 3 H), 9.95 (br. s., 3 H); ^{13}C{^{1}H} NMR (75 MHz, DMSO-d_6) δ ppm 41.85, 51.86, 121.81, 123.39 (q, *J*=33.18 Hz), 124.37 (q, *J*=272.02 Hz), 125.66, 143.26, 180.19; LRMS (ESI+): *m*/*z*= 756.3 $[M+H]^+$, 778.6 $[M+Na]^+$; HRMS (ES) for $C_{30}H_{31}F_9N_7S_3$ $[M+H]^+$: *m*/*z*= 756.1654 (calcd), 756.1668 (found).

1,1',1''-(nitrilotris(ethane-2,1-diyl))tris(3-(3,5-bis(trifluoromethyl)phenyl)thiourea) (10). 0.25 mL (1.67 mmol) of tris(2-aminoethyl)amine was dissolved in 20 mL dichloromethane and 0.91 mL (5.03 mmol) 3,5-bis(trifluoromethyl)phenyl isothiocyanate was added. The mixture was stirred overnight at room temperature under nitrogen atmosphere. A precipitate was formed and subsequently filtered off and washed with dichloromethane. The white solid was then dried overnight in vacuo (1.40 g, 1.46 mmol). Yield: 87%; Mp: 174.5-183.2 °C; ^{1}H NMR (300 MHz, DMSO-d_6) δ ppm 2.83 (t, *J*=6.04 Hz, 6 H), 3.65 (br. s., 6 H), 7.65 (s, 3 H), 8.05 (br. s., 3 H), 8.20 (s, 6 H), 10.09 (br. s., 3 H); ^{13}C{^{1}H} NMR (75 MHz, DMSO-d_6) δ ppm 41.74, 51.47, 115.89, 121.61, 123.14 (q, *J*=272.00 Hz), 129.95 (q, *J*=32.07 Hz), 141.74, 180.30; IR (neat): ν= 3230 (br, NH stretch), 3060 (br, NH stretch), 1560 (CS stretch) cm^{-1}; LRMS (ESI+): *m*/*z*= 960.2 $[M+H]^+$, 981.9 $[M+Na]^+$; HRMS (ES) for $C_{33}H_{28}F_{18}N_7S_3$ $[M+H]^+$: *m*/*z*= 960.1275 (calcd), 960.1293 (found).

S3. NMR SPECTRA

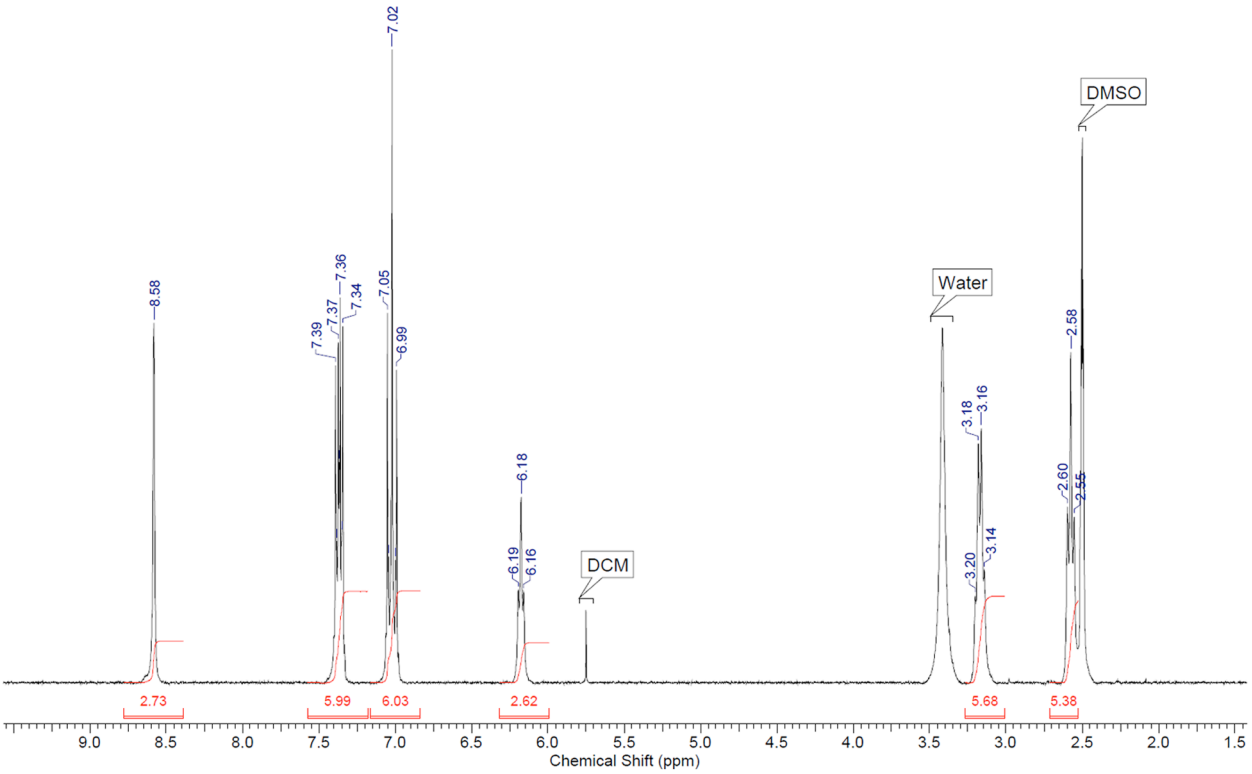

Figure S1. [1]H NMR spectrum of compound **2** in DMSO-d_6 at 298K.

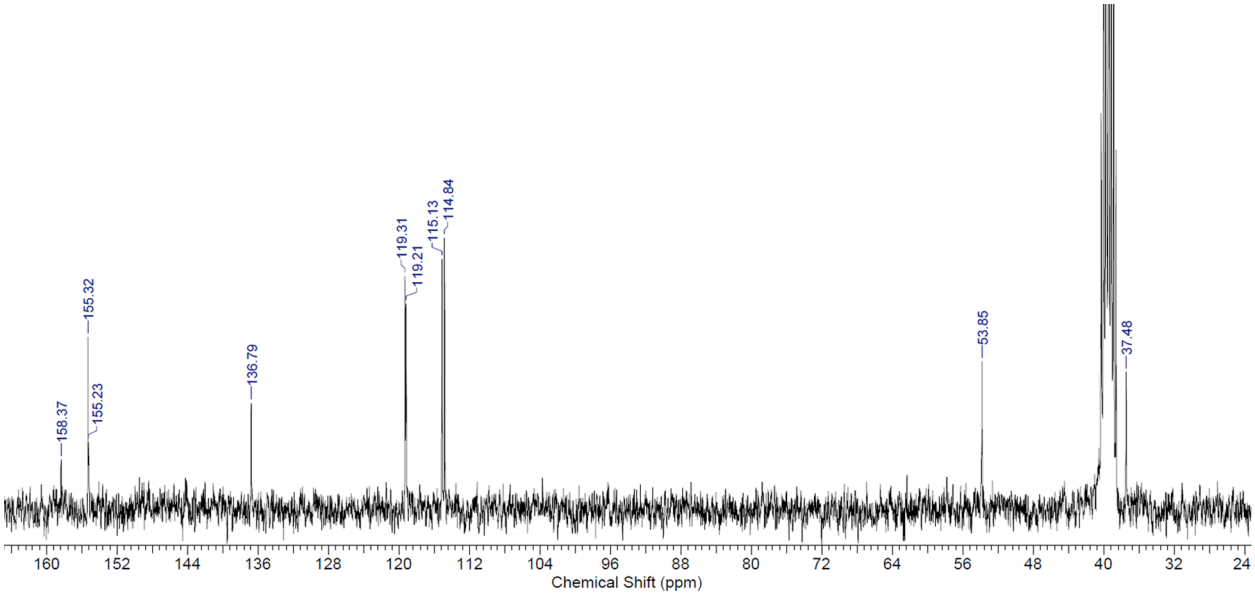

Figure S2. [13]C NMR spectrum of compound **2** in DMSO-d_6 at 298K.

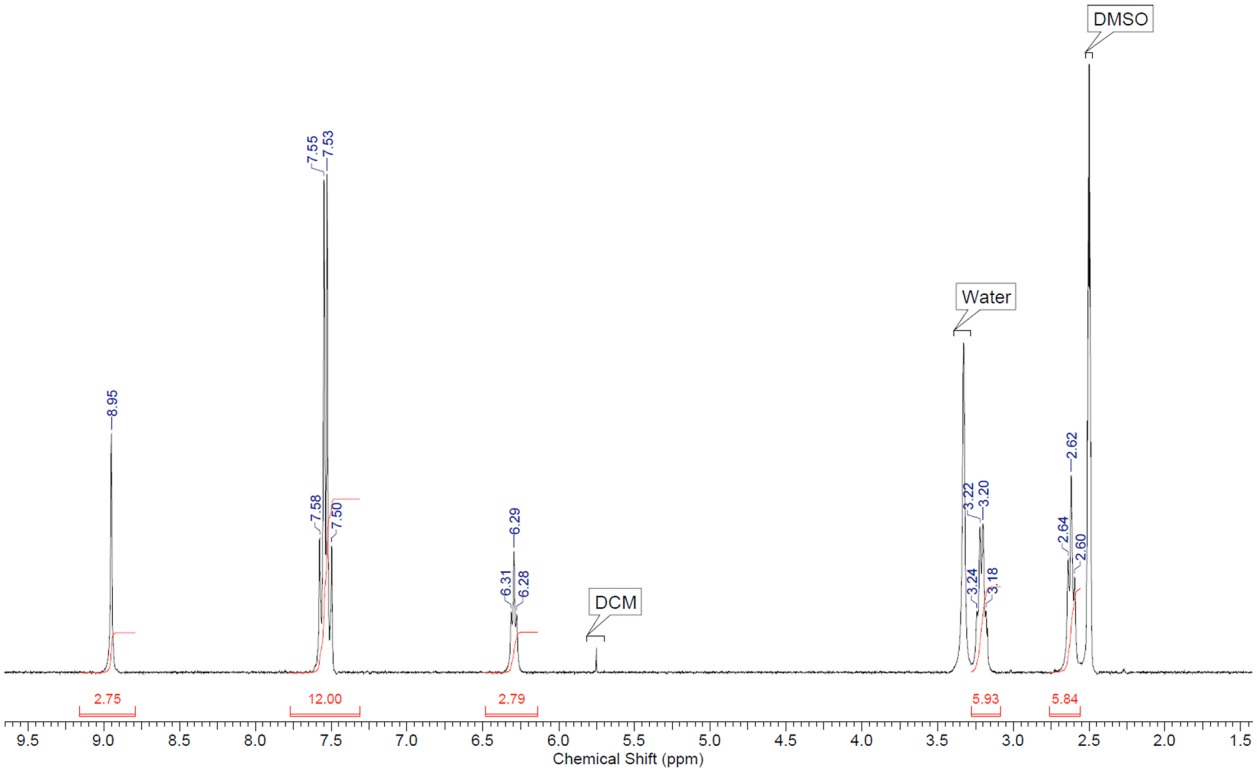

Figure S3. [1]H NMR spectrum of compound **4** in DMSO-d_6 at 298K.

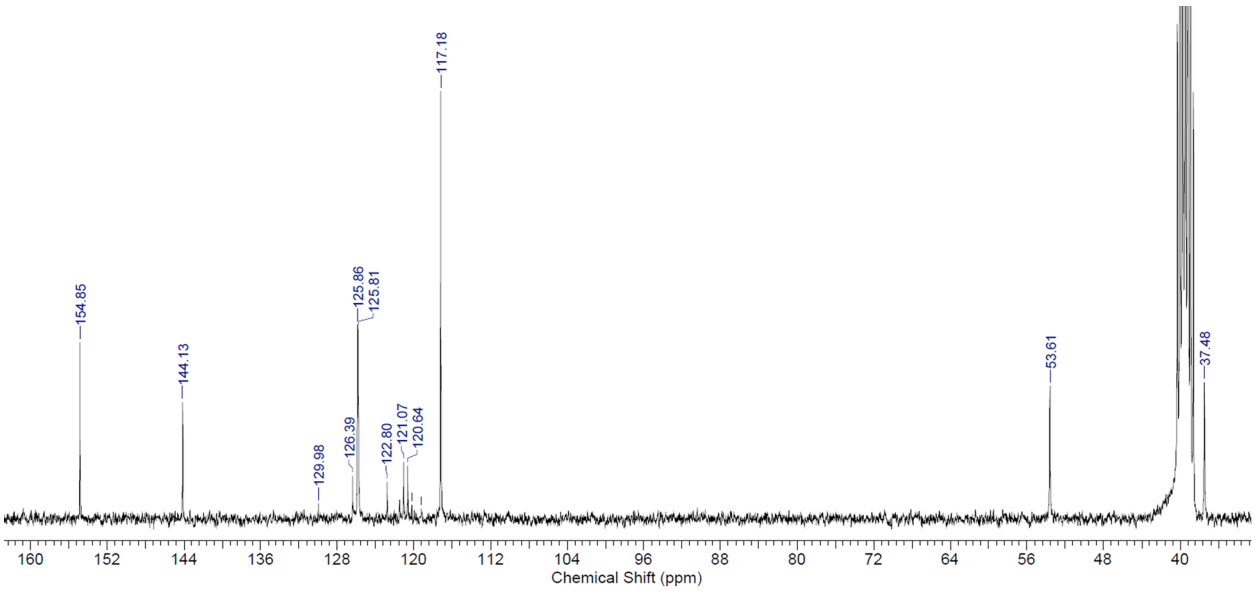

Figure S4. [13]C NMR spectrum of compound **4** in DMSO-d_6 at 298K.

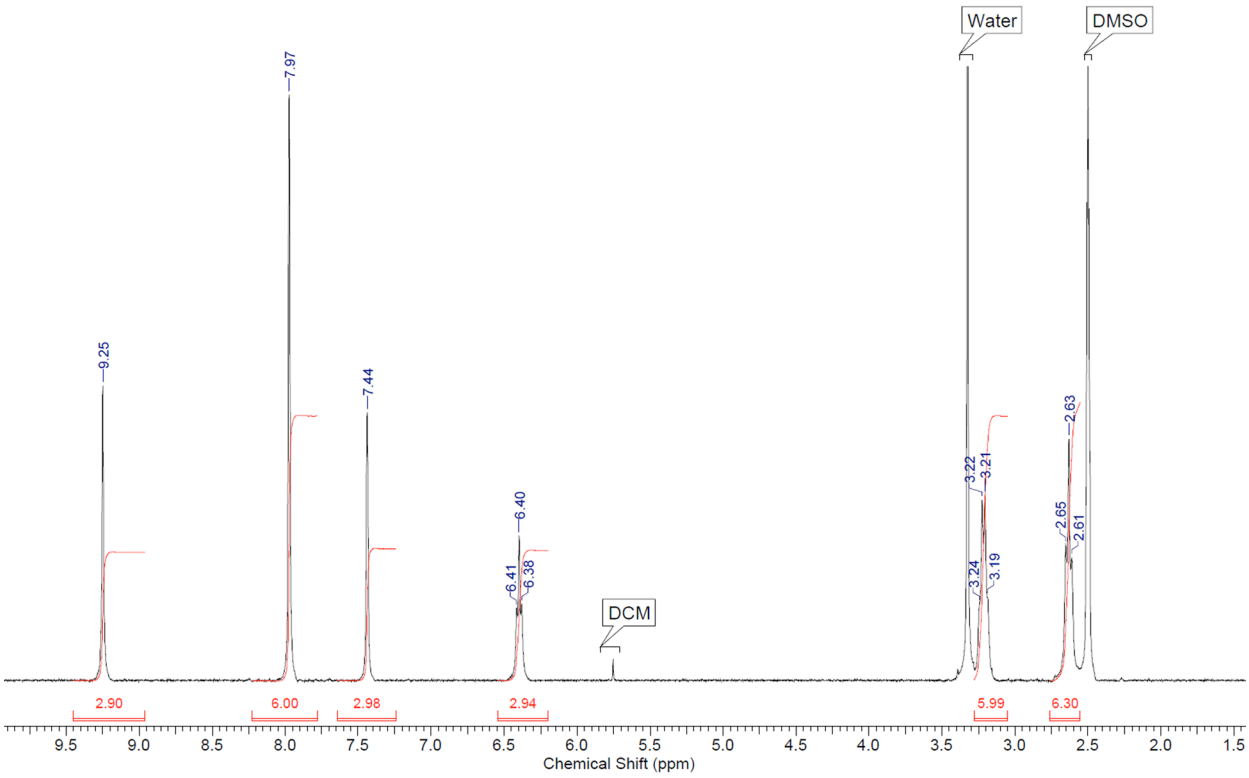

Figure S5. [1]H NMR spectrum of compound **5** in DMSO-d_6 at 298K.

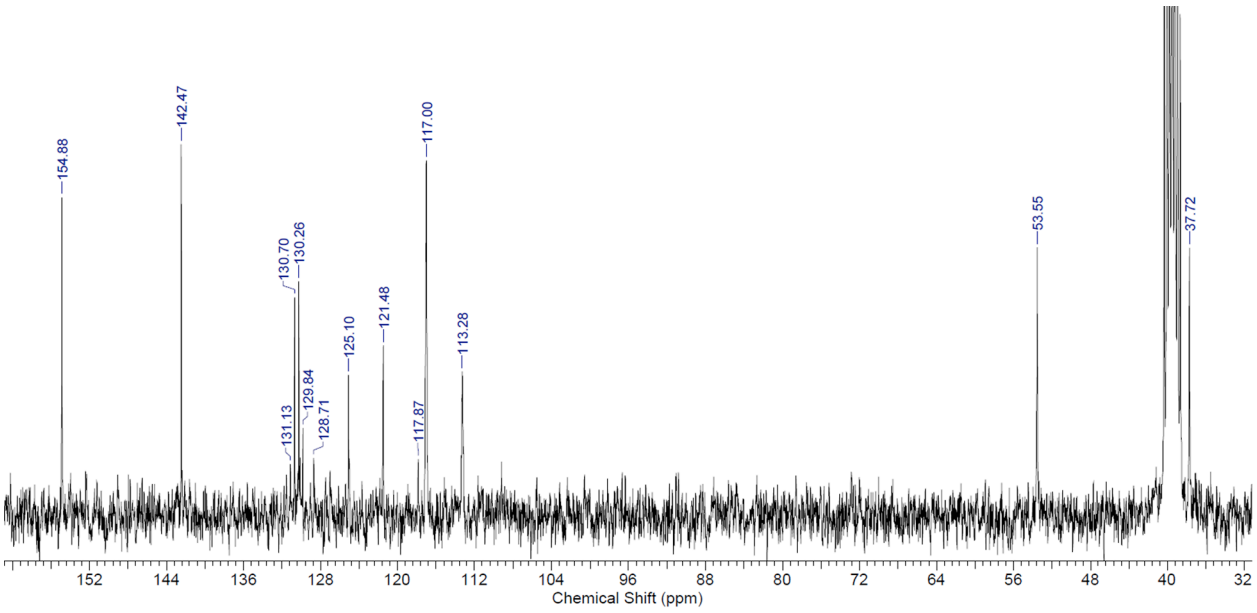

Figure S6. [13]C NMR spectrum of compound **5** in DMSO-d_6 at 298K.

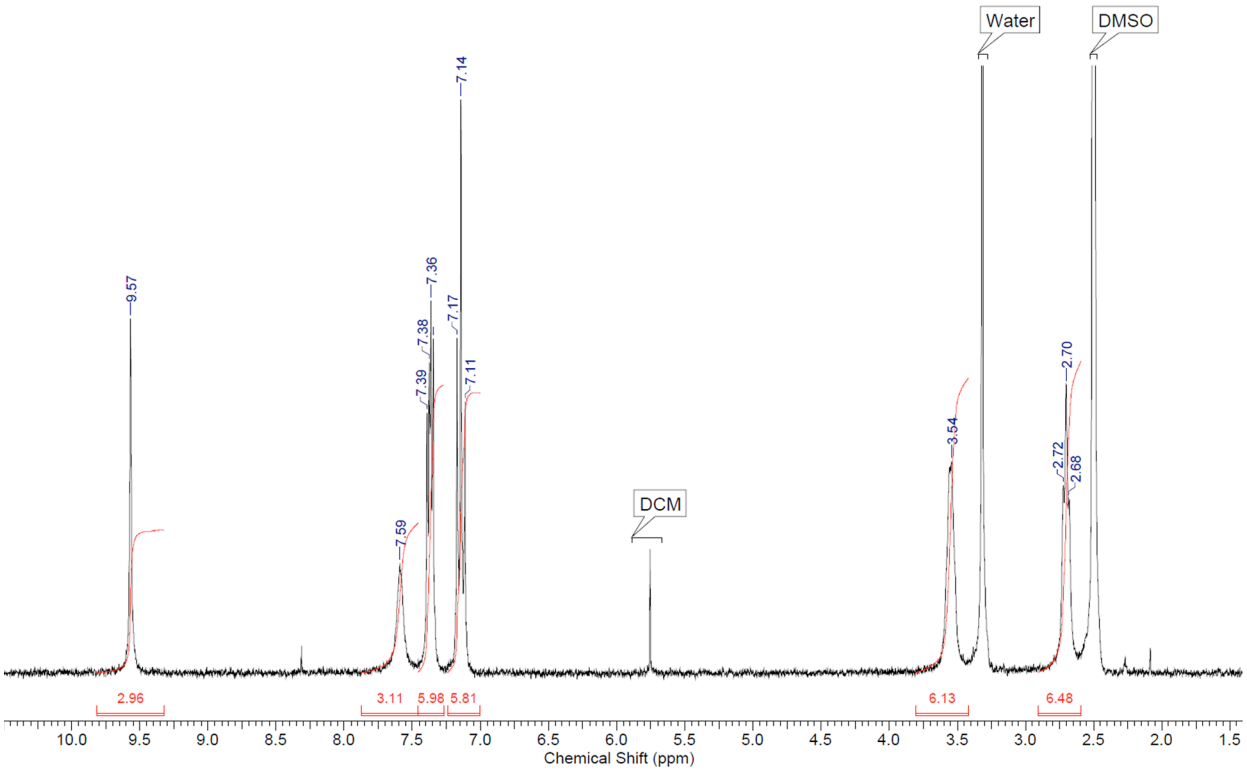

Figure S7. [1]H NMR spectrum of compound **7** in DMSO-d_6 at 298K.

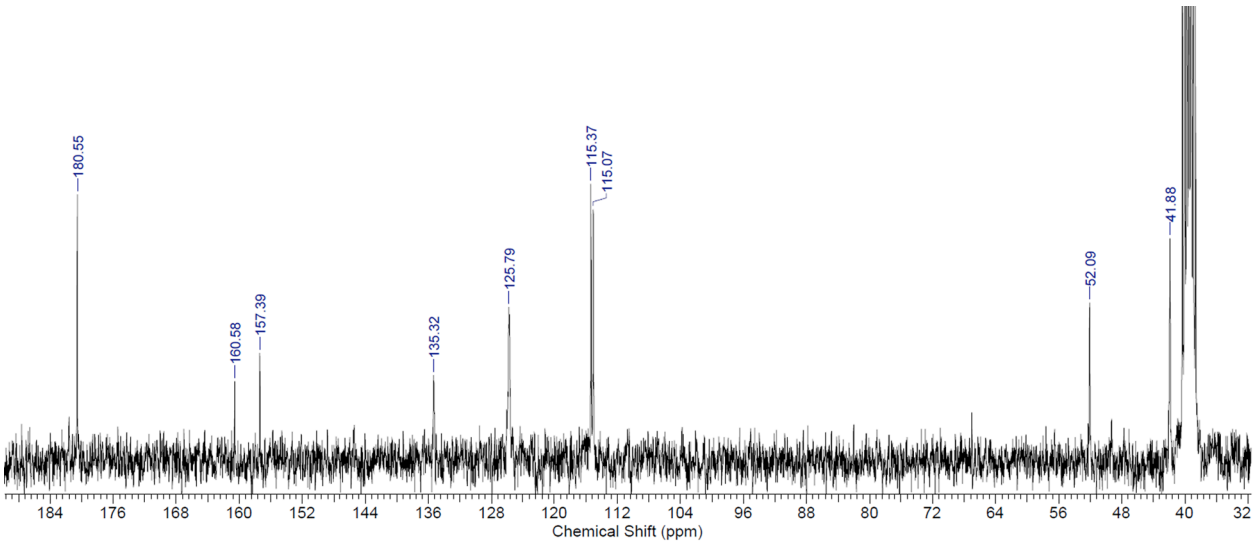

Figure S8. [13]C NMR spectrum of compound **7** in DMSO-d_6 at 298K.

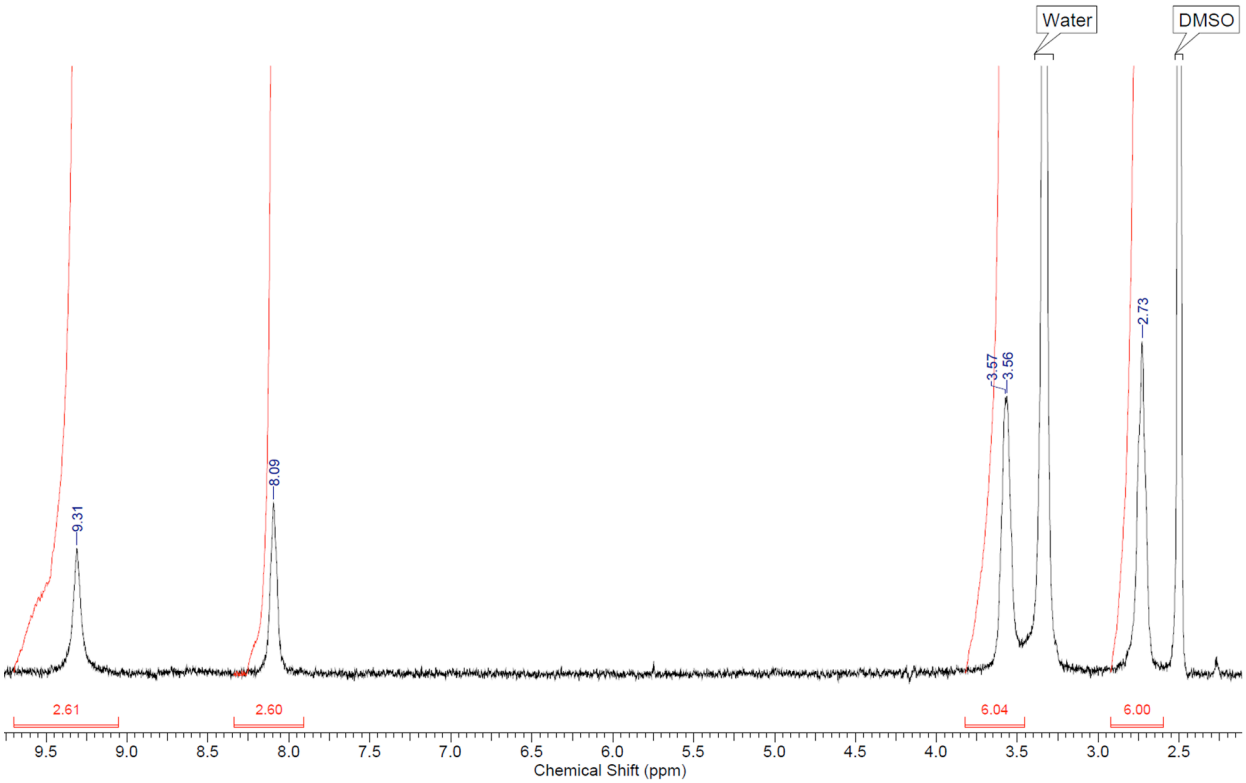

Figure S9. [1]H NMR spectrum of compound **8** in DMSO-d_6 at 298K.

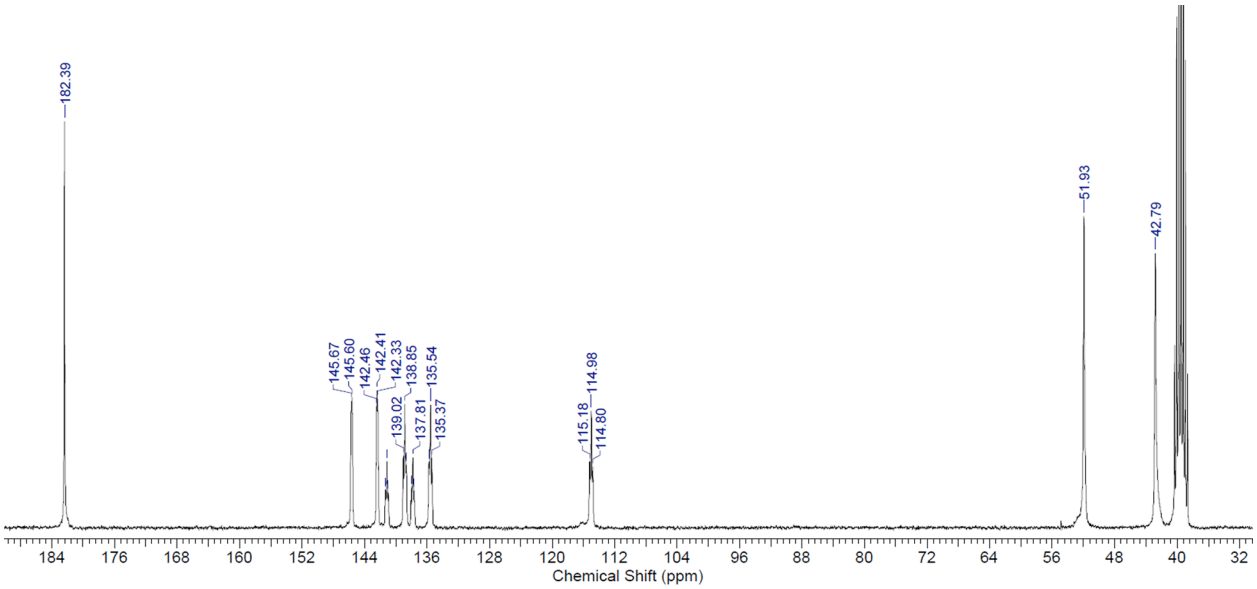

Figure S10. [13]C NMR spectrum of compound **8** in DMSO-d_6 at 298K.

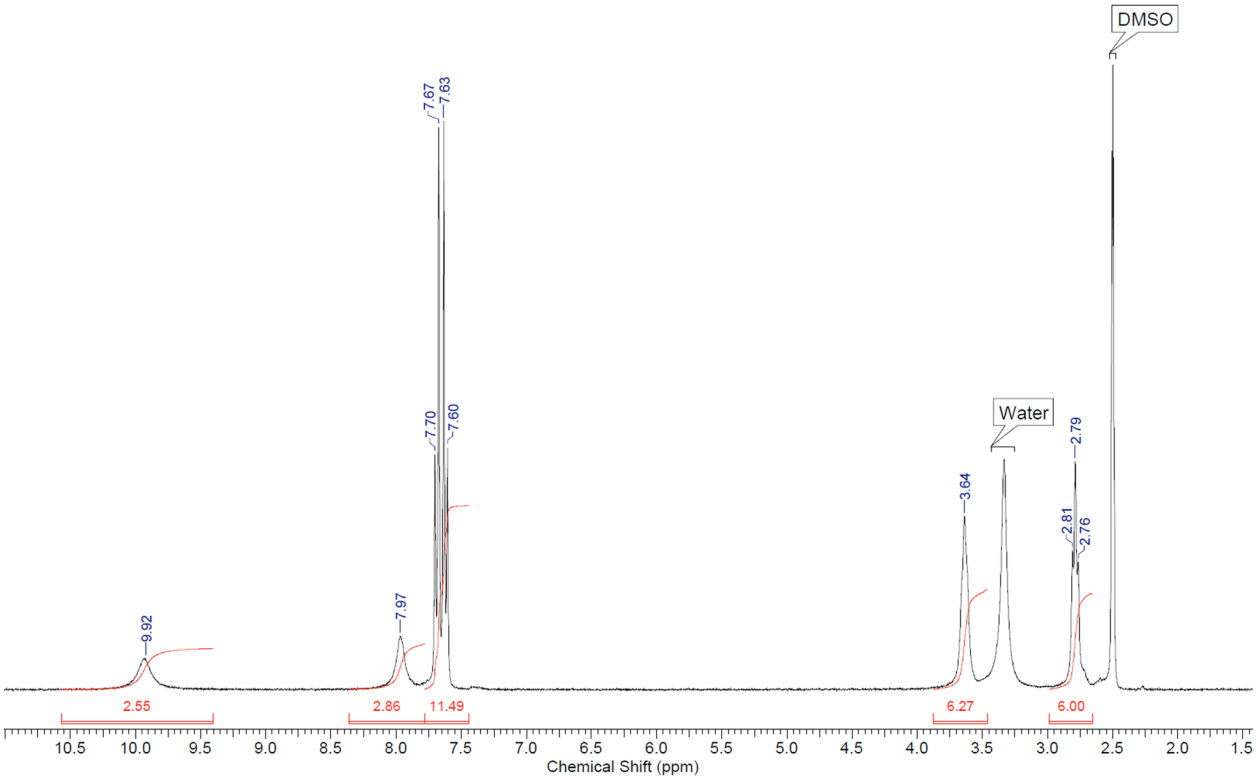

Figure S11. [1]H NMR spectrum of compound **9** in DMSO-d_6 at 298K.

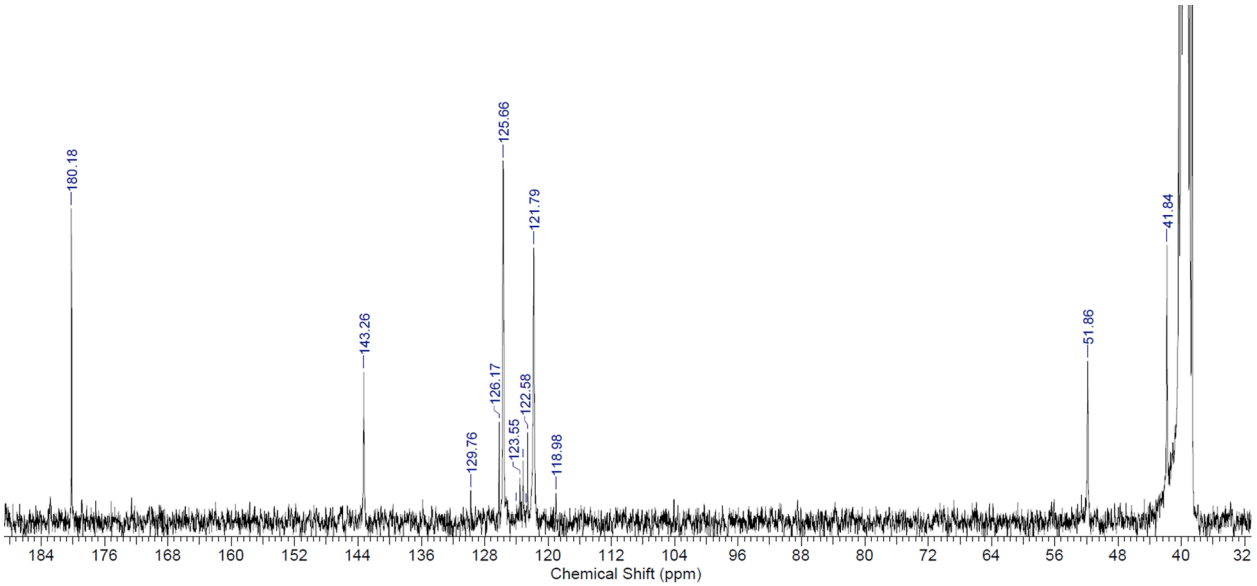

Figure S12. [13]C NMR spectrum of compound **9** in DMSO-d_6 at 298K.

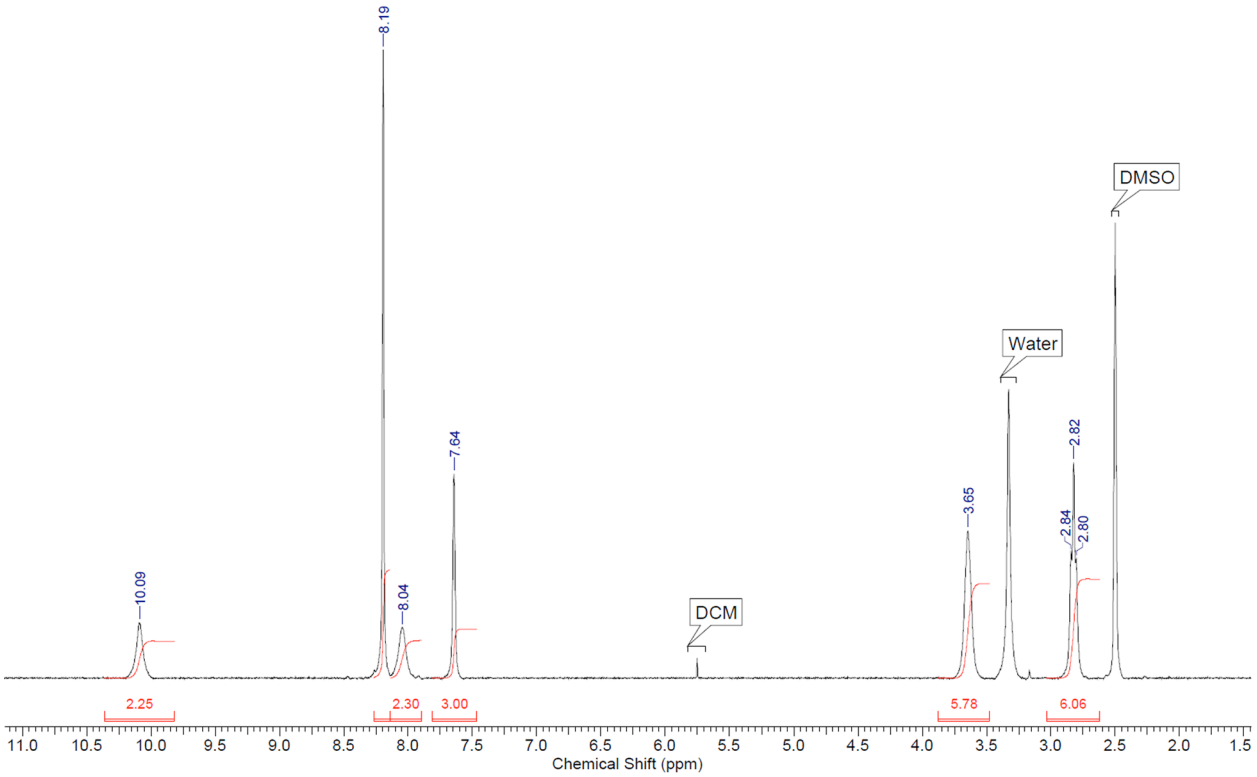

Figure S13. ^{1}H NMR spectrum of compound **10** in DMSO-d_6 at 298K.

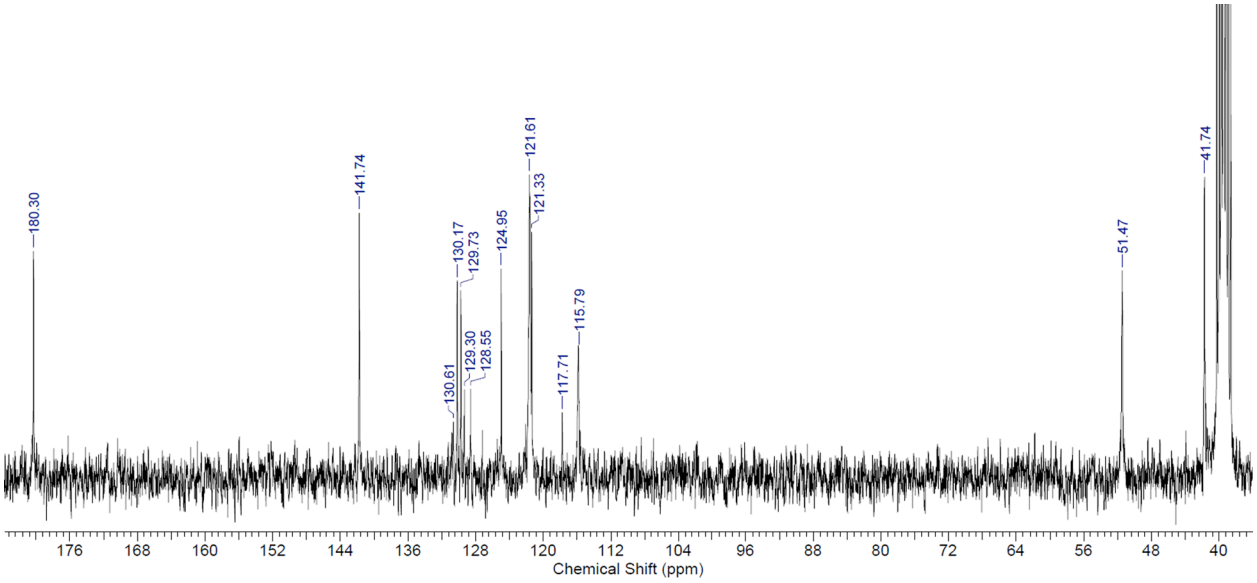

Figure S14. ^{13}C NMR spectrum of compound **10** in DMSO-d_6 at 298K.

S4. NMR BINDING STUDIES

S4.1 Overview and experimental procedure

NMR titrations were performed by addition of aliquots of the putative anionic guest as the tetrabutylammonium (TBA) or tetraethylammonium (TEA) salt (0.15 M), in a solution of the receptor (0.01 M) in DMSO-d_6/0.5% H_2O, to a 0.01 M solution of the receptor in DMSO-d_6/0.5% H_2O. Both salt and receptor were dried under high vacuum prior to use. ^{1}H NMR spectra were recorded on a Bruker AV300 spectrometer and calibrated to the residual protio solvent peak in DMSO-d_6 (δ = 2.50 ppm). In most cases a change in the chemical shift of both (thio)urea NH protons was observed. Where possible, the WinEQNMR2 computer program[3] was used to curve-fit the data and to obtain binding constants (using a 1:1 model unless otherwise stated). The results are summarized in Table S1. Data for compound **1**, **3** and **6** have been reported before and are given for comparison.[1,2,4,5] Stack plots and fitplots can be found in figures S15-S63.

Job plot analyses were performed in a separate experiment. 10 NMR tubes were filled with 0.5 mL of a DMSO-d_6/water solution containing 0.01 M of an anion-receptor mixture in different ratios (0.1, 0.2, 0.3, 0.4, 0.5, 0.6, 0.7, 0.8, 0.9 and 1 molar fraction of the receptor). Both salt (TBA or TEA salts of various anions) and receptor were dried under high vacuum prior to use. ^{1}H NMR spectra were recorded on a Bruker AV300 spectrometer and calibrated to the residual protio solvent peak in DMSO-d_6 (δ = 2.50 ppm). Job plots were obtained by plotting the molar fraction of the receptor as a function of the relative change in chemical shift.

Table S1. Binding constants (M^{-1}) of TBA salts to compounds **1**-**10** in DMSO-d_6 containing 0.5 % water at 298K. Data obtained for both NH peaks are given. (n.b. = no binding detected)

	Cl^-	SO_4^{2-}	$H_2PO_4^-$	HCO_3^- [a]	NO_3^-
	Urea based compounds				
1	882 [b]	$>10^4$ [b]	443 [c]	- [b]	n.b. [b]
	777 [b]	$>10^4$ [b]	6363 [c]	- [b]	n.b. [b]
2	575	$>10^4$	452 [c]	365	n.b.
	490	$>10^4$	8099 [c]	200	n.b.
3	166	$>10^4$ [d]	$>10^4$ [e]	$>10^4$ [f]	n.b. [d]
	105				
4	405	$>10^4$	243 [c]	156	n.b.
	271	$>10^4$	4818 [c]	123	n.b.
5	517	$>10^4$	- [g]	- [h]	n.b.
	228	$>10^4$	- [g]	- [h]	n.b.
	Thiourea based compounds				
6	191 [b]	$>10^4$ [b]	256 [c]	- [b]	n.b. [b]
	191 [b]	$>10^4$ [b]	546 [c]	- [b]	n.b. [b]
7	179	$>10^4$	227 [c]	- [h]	n.b.
	165	$>10^4$	947 [c]	- [h]	n.b.
8	128	$>10^4$	130	- [h]	n.b.
	111	$>10^4$	- [h]	- [h]	n.b.
9	156	- [i]	- [g]	- [h]	n.b.
	171	- [i]	- [g]	- [h]	n.b.
10	- [j]	- [i]	- [g]	- [h]	n.b.
	- [j]	- [i]	- [g]	- [h]	n.b.

[a] Anion added as TEA salt. [b] Previously reported data by Busschaert *et al.*[1] [c] Data for DMSO-d_6 with 10% water, data for DMSO-d_6 with 0.5% water could not be fitted (mixed stoichiometries). [d] Data for neat DMSO-d_6 by Gosh *et al.*[2], data for DMSO-d_6 with 0.5% water was obtained for TBACl and showed a significant decrease in binding constants, similar results are expected for the other anions. [e] Data in neat DMSO-d_6 by Ghosh *et al.*[4] [f] Data in neat DMSO-d_6 by Ghosh *et al.*[5], 2:1 model. [g] New peaks due to deprotonation of bound $H_2PO_4^-$ and subsequent binding of HPO_4^{2-}. [h] Peak broadening. [i] Data could not be fitted, but suggest strong 1:1 binding ($K_a > 10^4$ M^{-1}). [j] Data could not be fitted to any model, probably mixture of stoichiometries.

S4.2 Interaction with TBACl

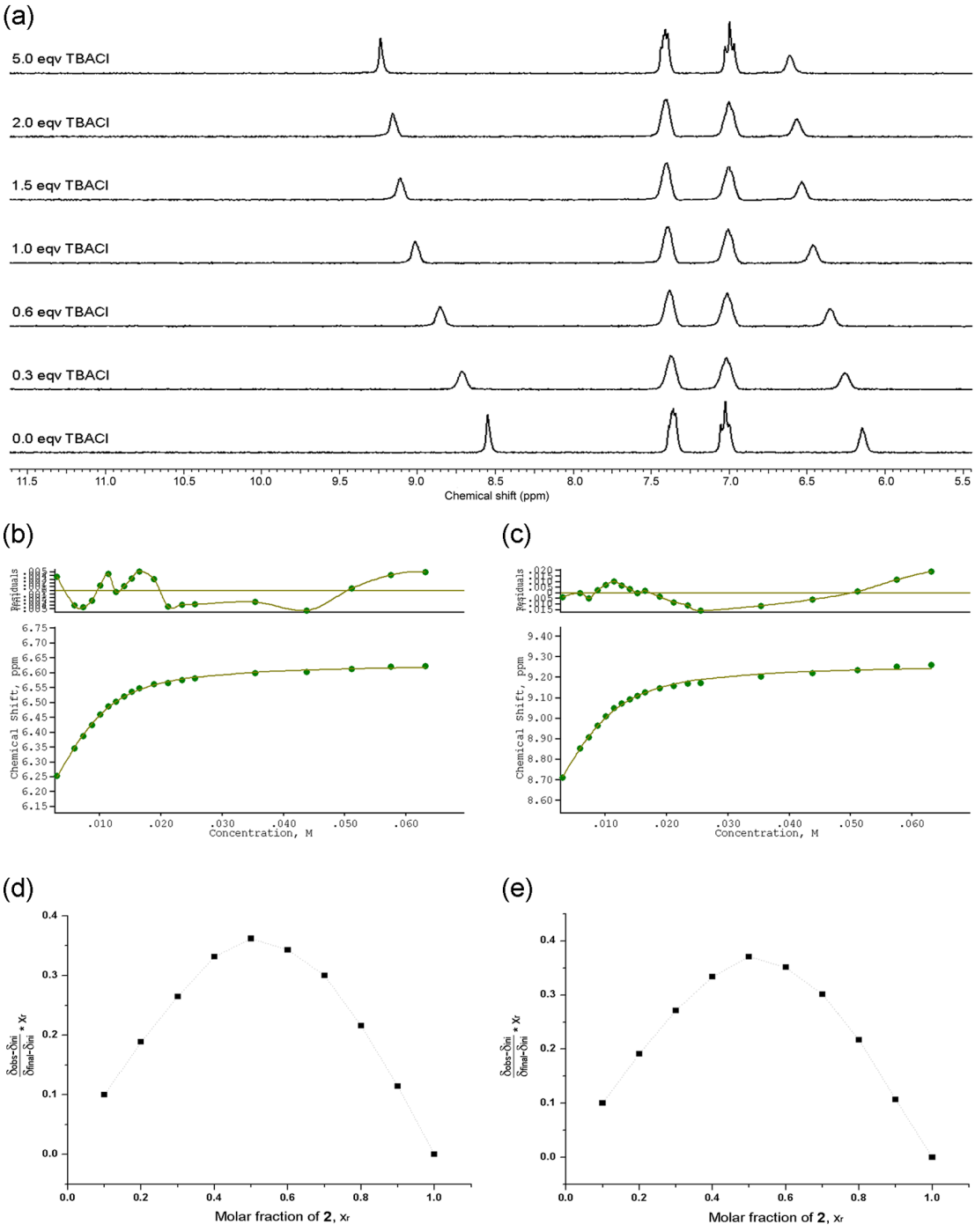

Figure S15. ^{1}H NMR titration of compound **2** with TBACl in DMSO-d_6 with 0.5 % water at 298K. (a) Stack plot. (b) Fitplot for NH proton at δ = 6.18 ppm. K_a = 575 M^{-1} (error 4 %). (c) Fitplot for NH proton at δ = 8.59 ppm. K_a = 490 M^{-1} (error 8 %). (d) Job plot analysis for NH proton at δ = 6.18 ppm. (e) Job plot analysis for NH proton at δ = 8.59 ppm.

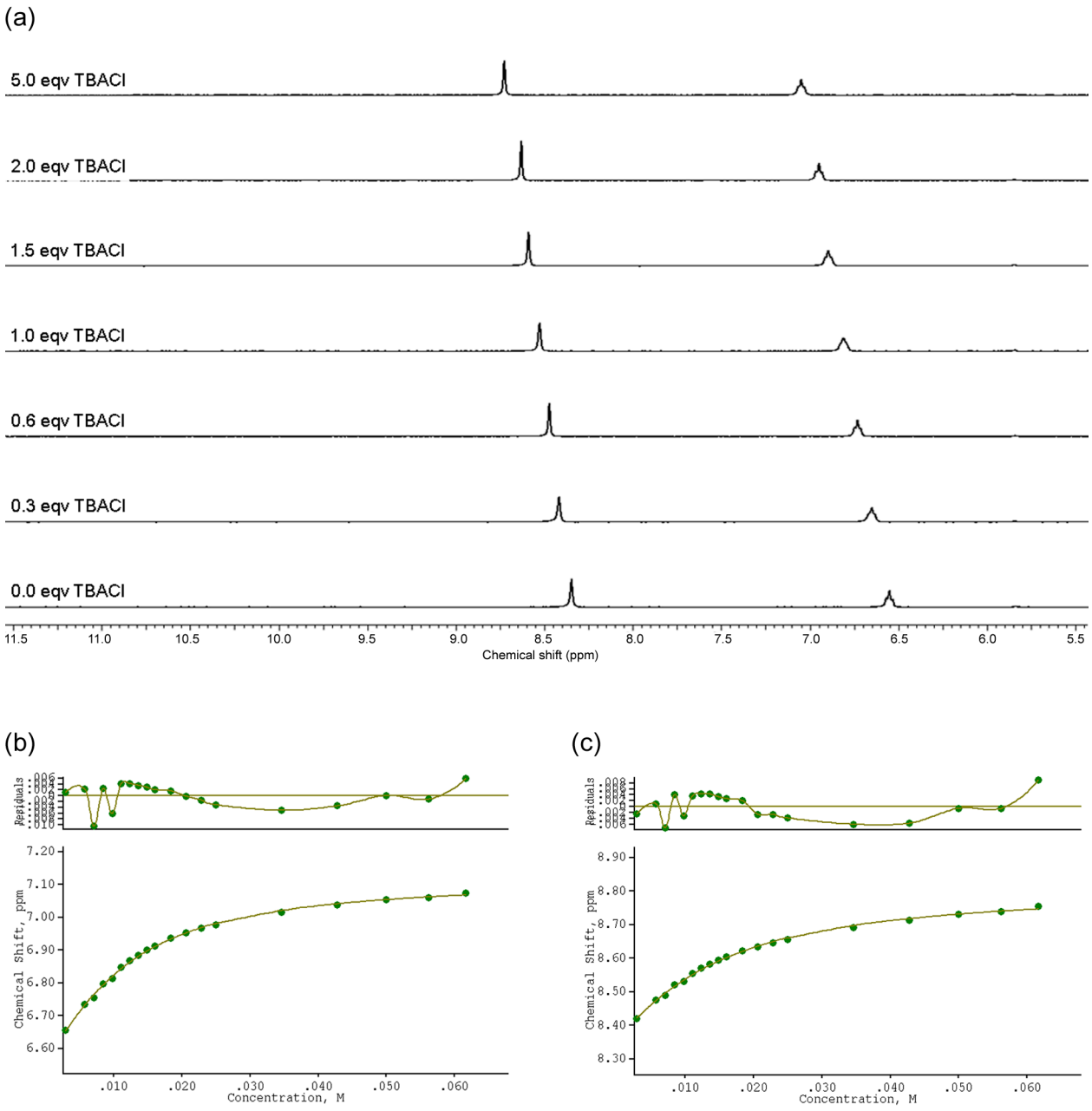

Figure S16. ^{1}H NMR titration of compound **3** with TBACl in DMSO-d_6 with 0.5 % water at 298K. (a) Stack plot. (b) Fitplot for NH proton at δ = 6.56 ppm. K_a = 166 M^{-1} (error 4 %). (c) Fitplot for NH proton at δ = 8.36 ppm. K_a = 105 M^{-1} (error 6 %).

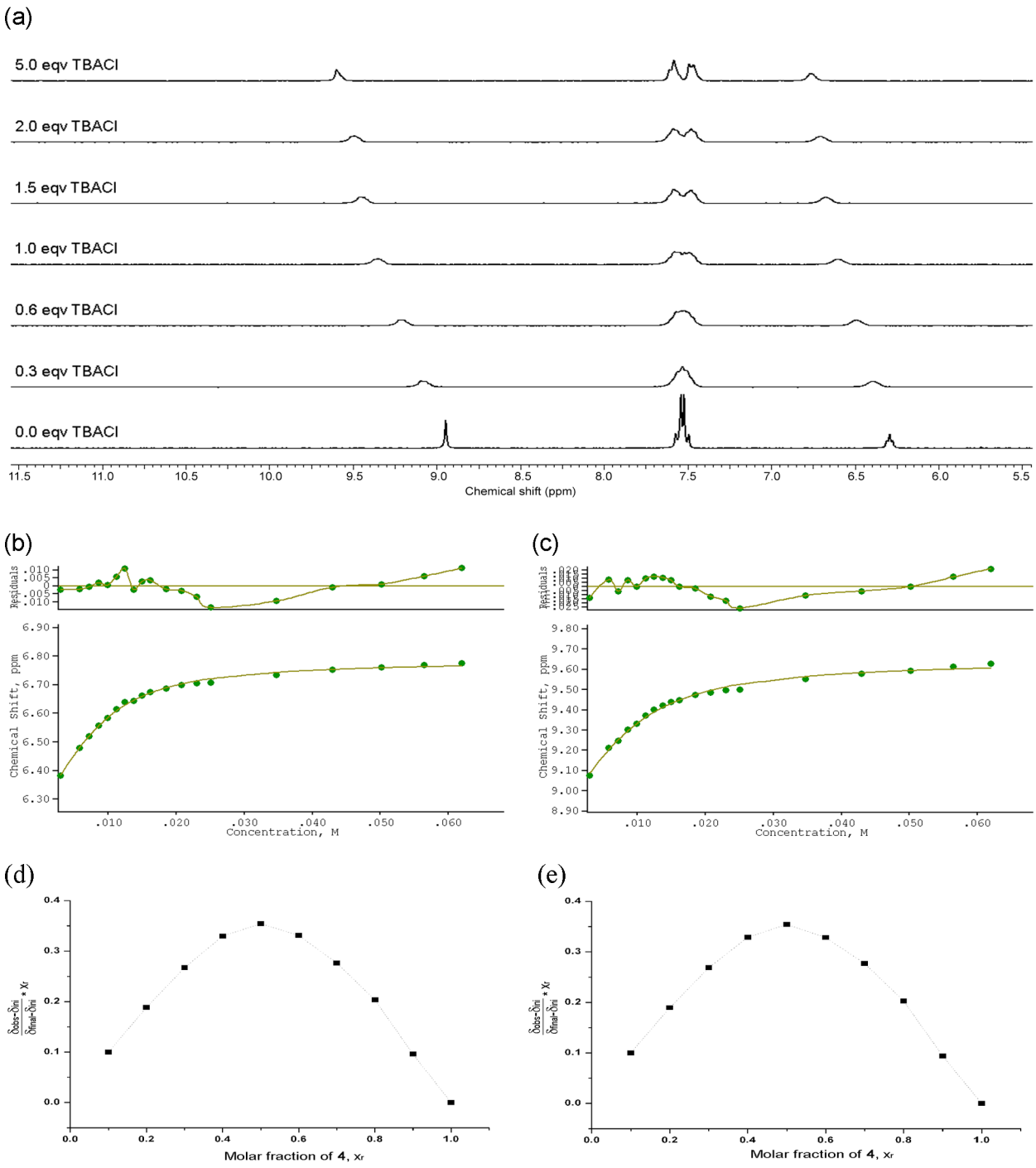

Figure S17. ^{1}H NMR titration of compound **4** with TBACl in DMSO-d_6 with 0.5 % water at 298K. (a) Stack plot. (b) Fitplot for NH proton at δ = 6.30 ppm. K_a = 405 M^{-1} (error 7 %). (c) Fitplot for NH proton at δ = 8.95 ppm. K_a = 271 M^{-1} (error 10 %). (d) Job plot analysis for NH proton at δ = 6.30 ppm. (e) Job plot analysis for NH proton at δ = 8.95 ppm.

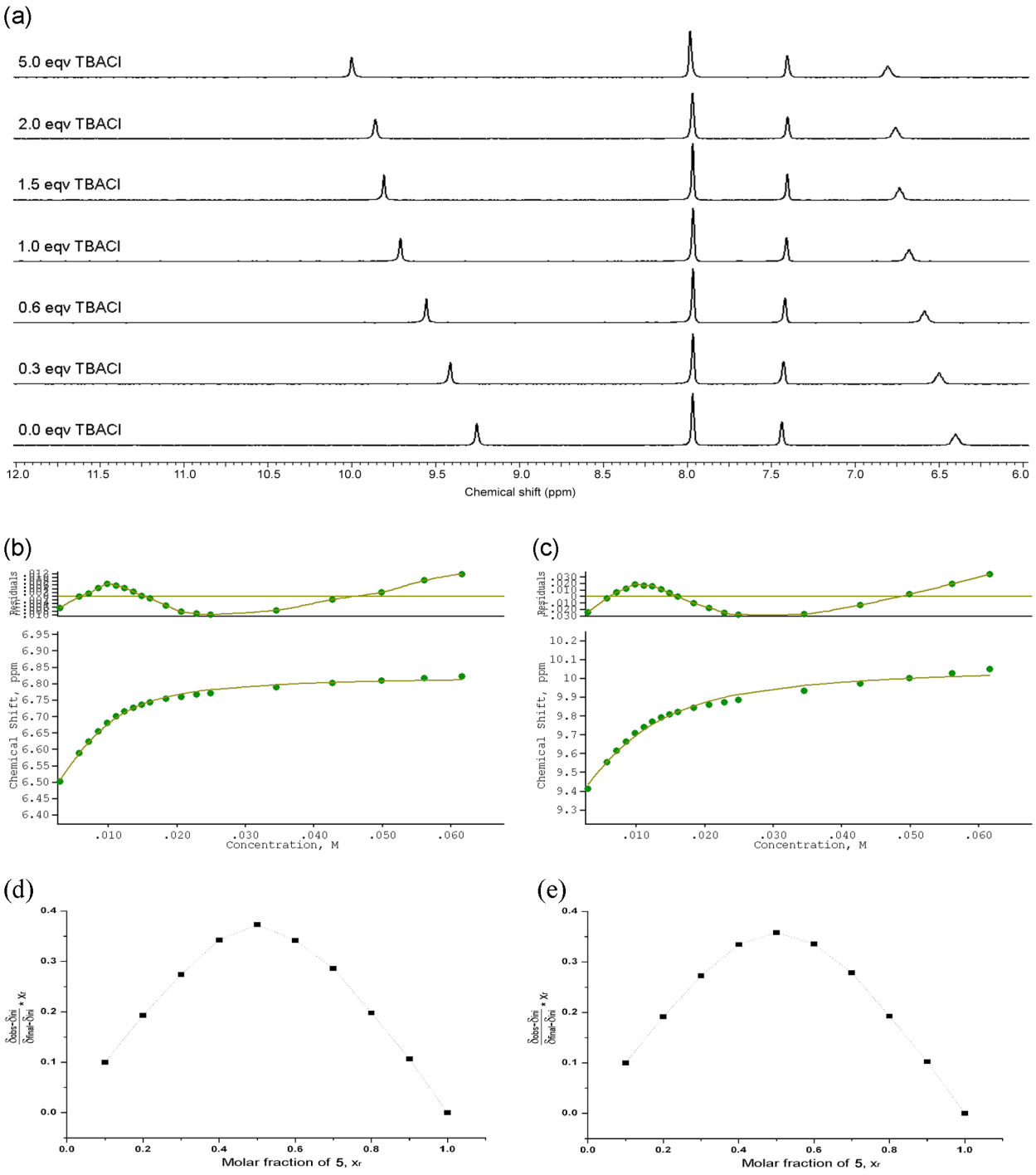

Figure S18. ^{1}H NMR titration of compound **5** with TBACl in DMSO-d_6 with 0.5 % water at 298K. (a) Stack plot. (b) Fitplot for NH proton at δ = 6.40 ppm. K_a = 517 M^{-1} (error 9 %). (c) Fitplot for NH proton at δ = 9.25 ppm. K_a = 228 M^{-1} (error 14 %). (d) Job plot analysis for NH proton at δ = 6.40 ppm. (e) Job plot analysis for NH proton at δ = 9.25 ppm.

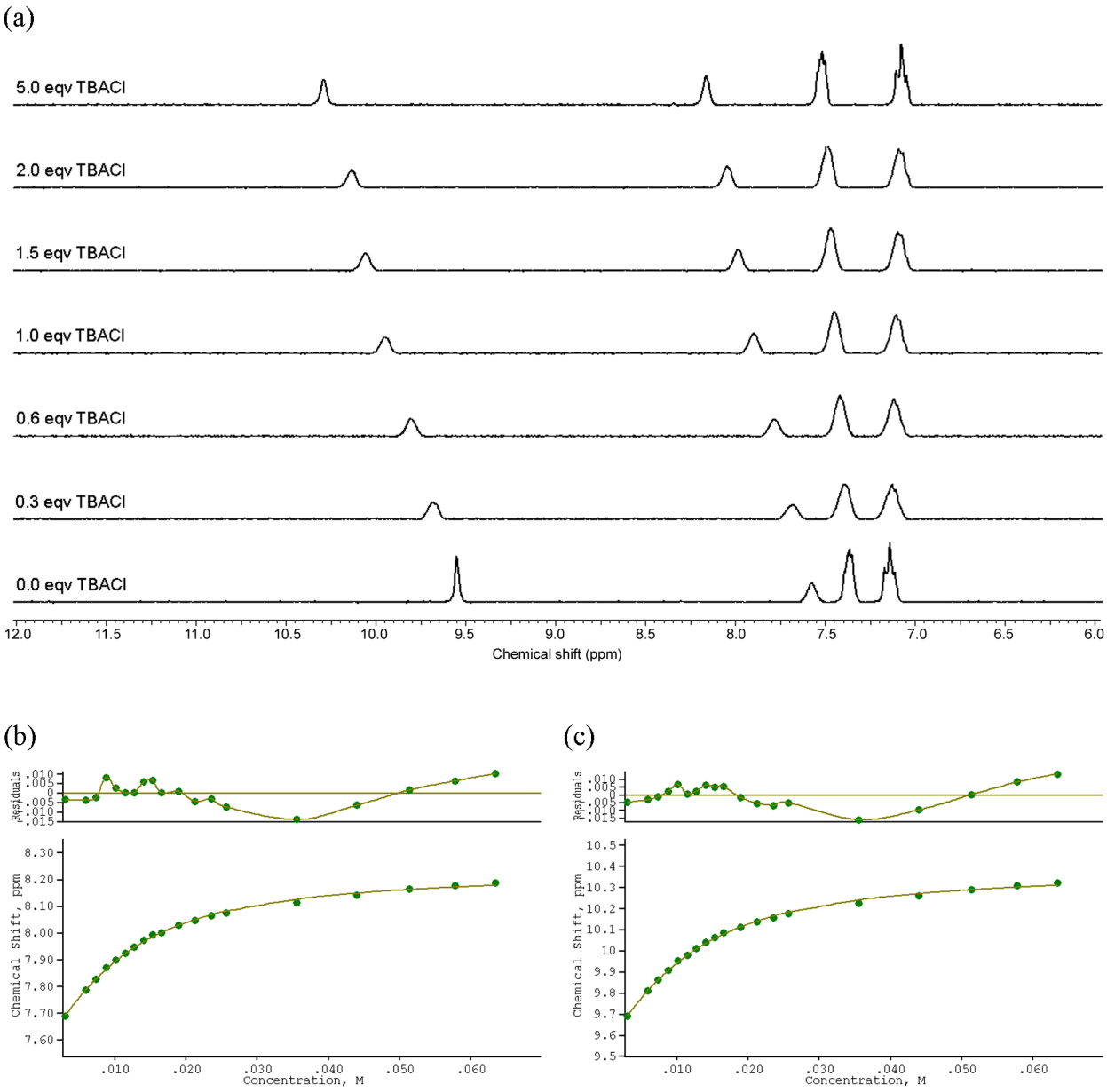

Figure S19. ^{1}H NMR titration of compound **7** with TBACl in DMSO-d_6 with 0.5 % water at 298K. (a) Stack plot. (b) Fitplot for NH proton at δ = 7.59 ppm. K_a = 179 M^{-1} (error 6 %). (c) Fitplot for NH proton at δ = 9.57 ppm. K_a = 165 M^{-1} (error 5 %).

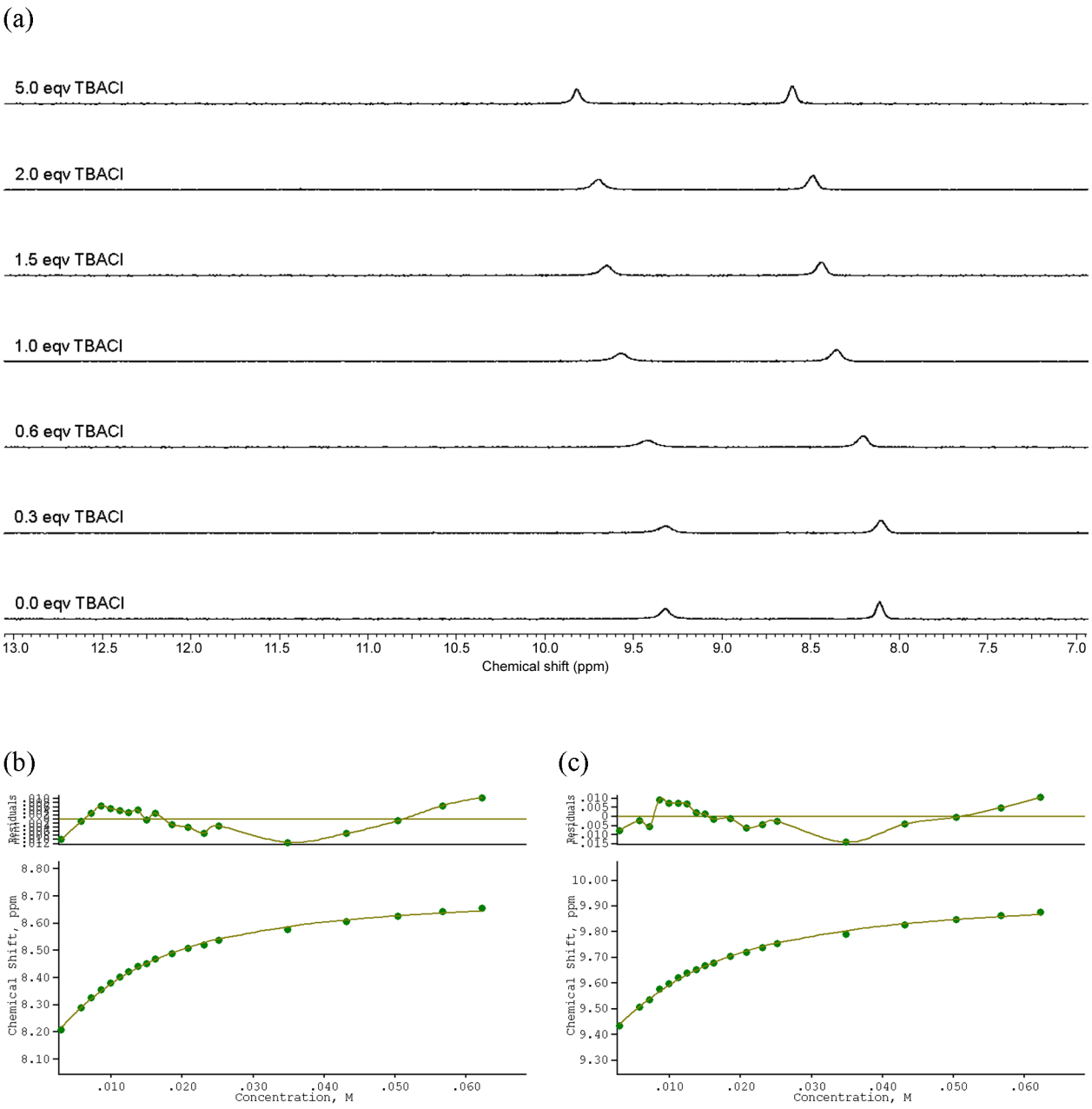

Figure S20. ^{1}H NMR titration of compound **8** with TBACl in DMSO-d_6 with 0.5 % water at 298K. (a) Stack plot. (b) Fitplot for NH proton at δ = 8.10 ppm. K_a = 128 M^{-1} (error 6 %). (c) Fitplot for NH proton at δ = 9.31 ppm. K_a = 111 M^{-1} (error 7 %).

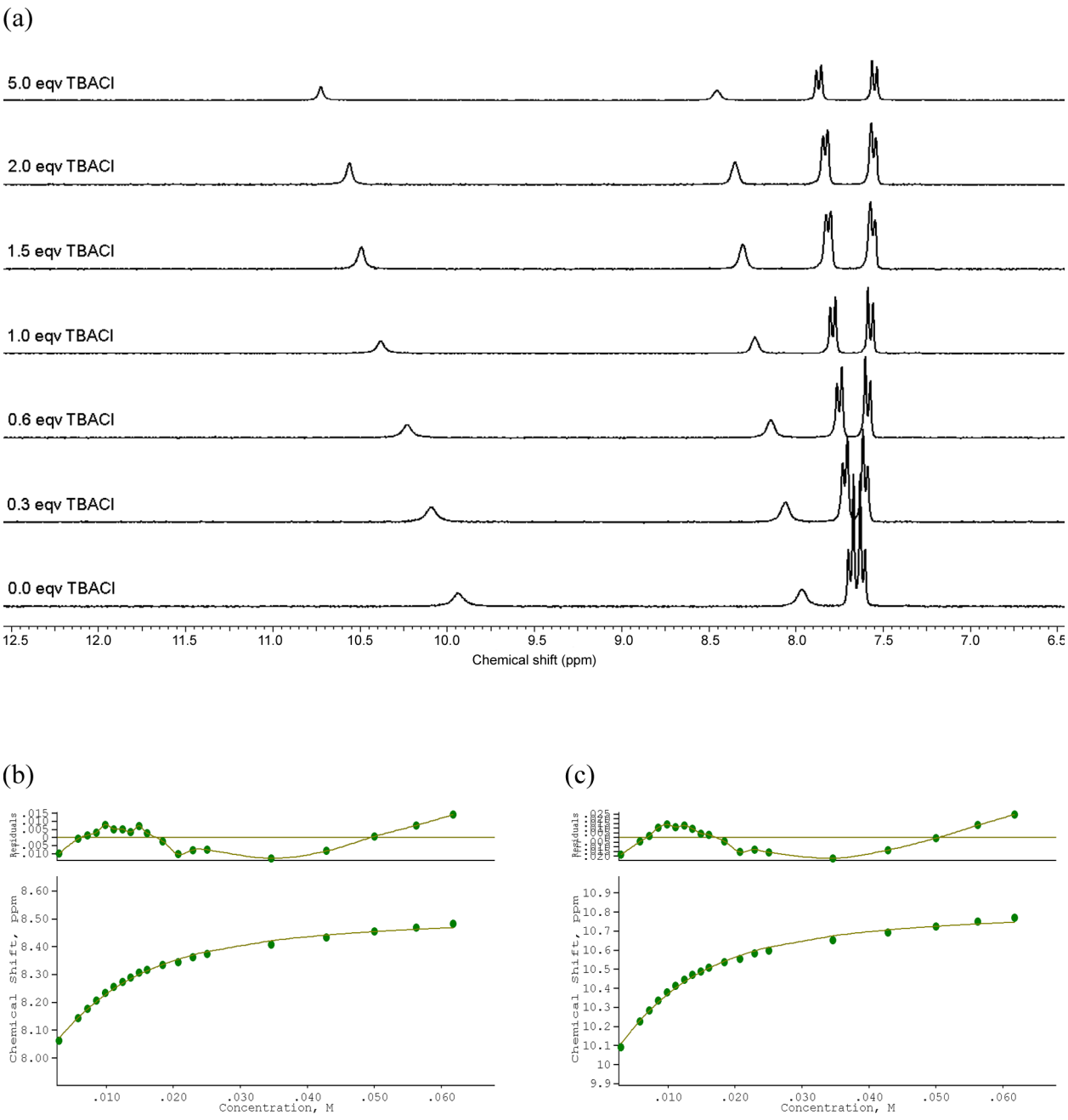

Figure S21. ^{1}H NMR titration of compound **9** with TBACl in DMSO-d_6 with 0.5 % water at 298K. (a) Stack plot. (b) Fitplot for NH proton at δ = 7.97 ppm. K_a = 157 M^{-1} (error 7 %). (c) Fitplot for NH proton at δ = 9.95 ppm. K_a = 172 M^{-1} (error 10 %).

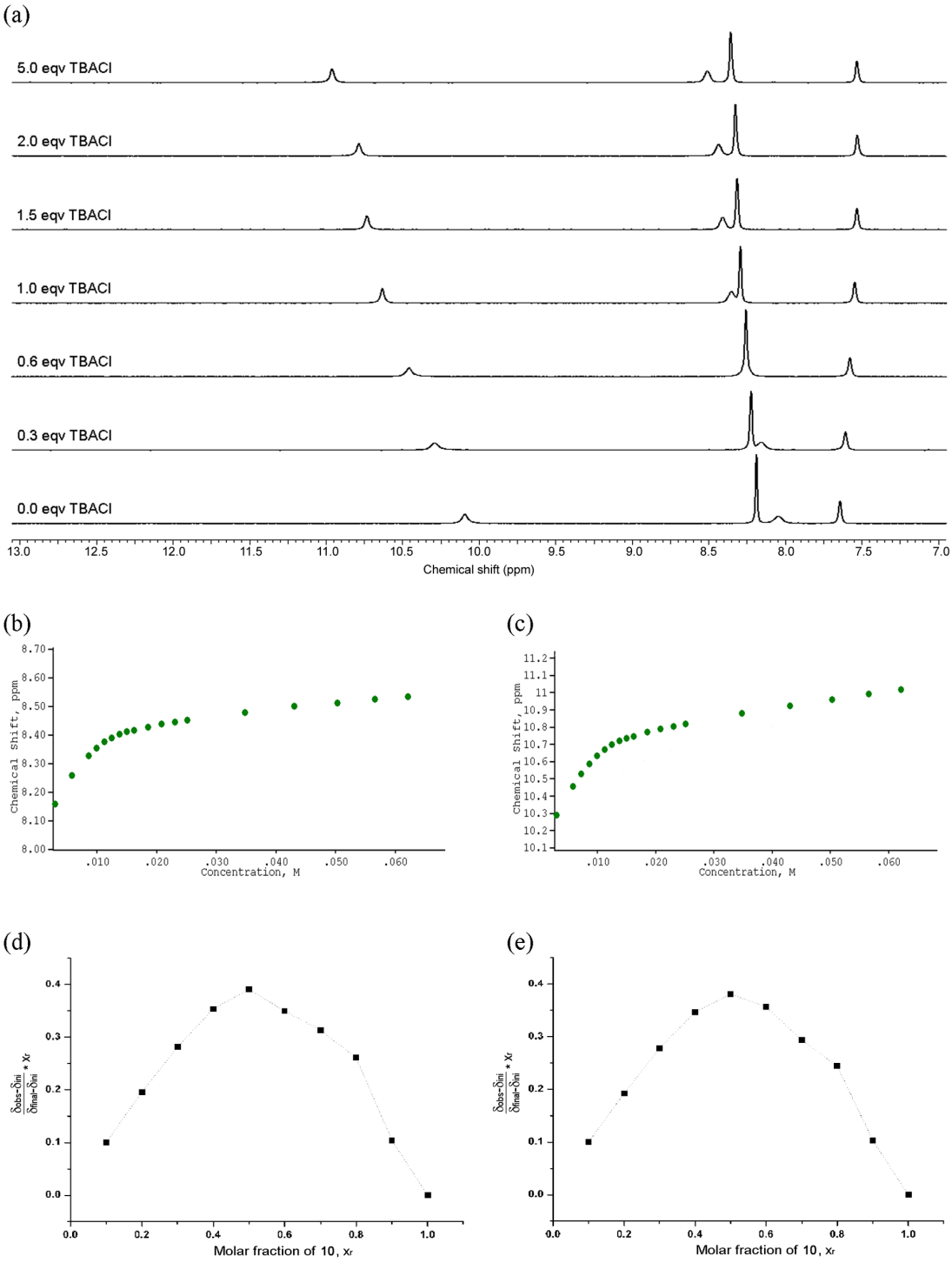

Figure S22. ^{1}H NMR titration of compound **10** with TBACl in DMSO-d_6 with 0.5 % water at 298K. (a) Stack plot. (b) Change in chemical shift for NH proton at δ = 8.05 ppm. Data could not be fitted. (c) Change in chemical shift for NH proton at δ = 10.09 ppm. Data could not be fitted. (d) Job plot analysis for NH proton at δ = 8.05 ppm. (e) Job plot analysis for NH proton at δ = 10.09 ppm.

S4.3 Interaction with TBA_2SO_4

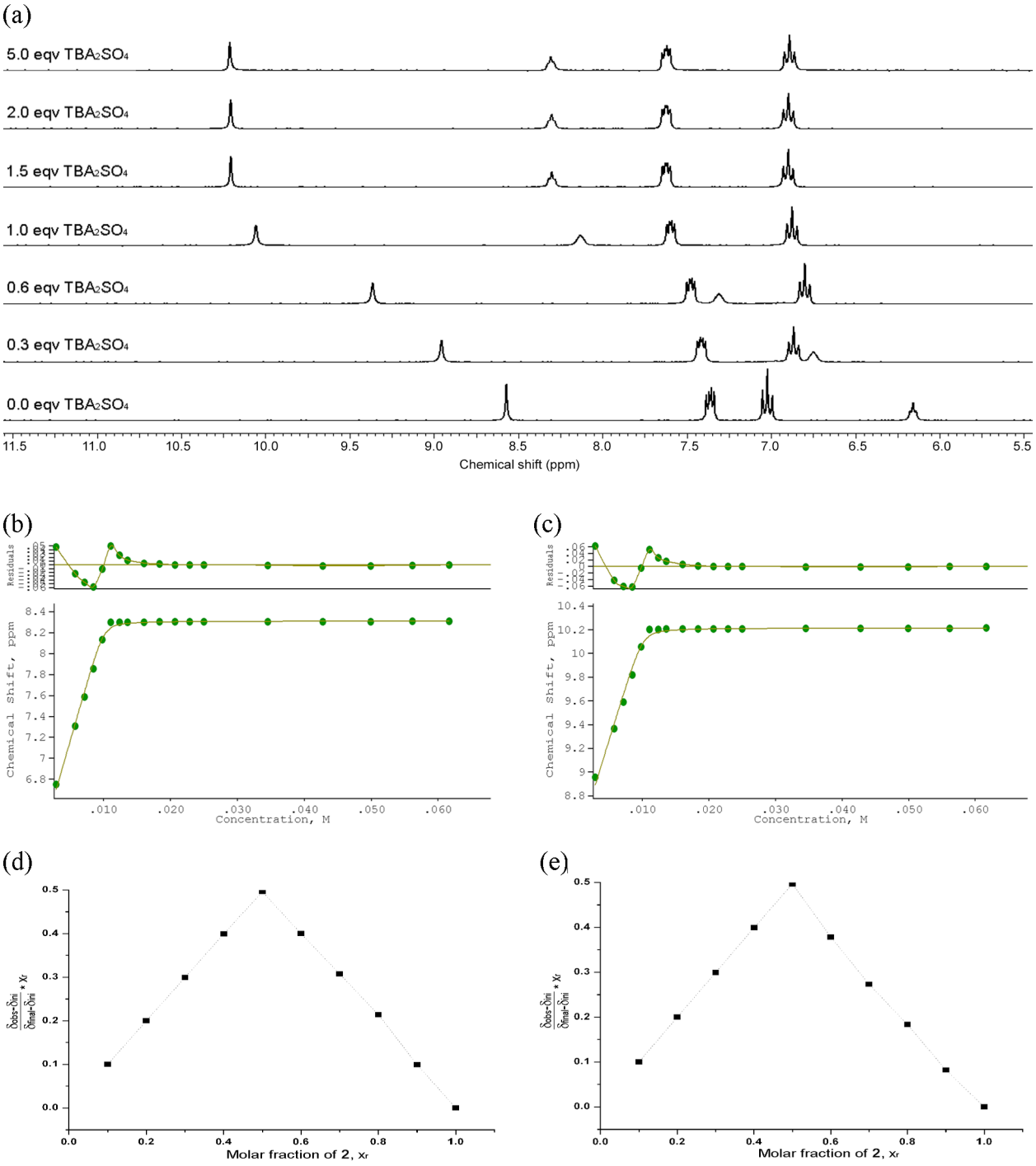

Figure S23. ^{1}H NMR titration of compound **2** with TBA_2SO_4 in DMSO-d_6 with 0.5 % water at 298K. (a) Stack plot. (b) Fitplot for NH proton at δ = 6.18 ppm. $K_a > 10^4$ M^{-1}. (c) Fitplot for NH proton at δ = 8.59 ppm. $K_a > 10^4$ M^{-1}. (d) Job plot analysis for NH proton at δ = 6.18 ppm. (e) Job plot analysis for NH proton at δ = 8.59 ppm.

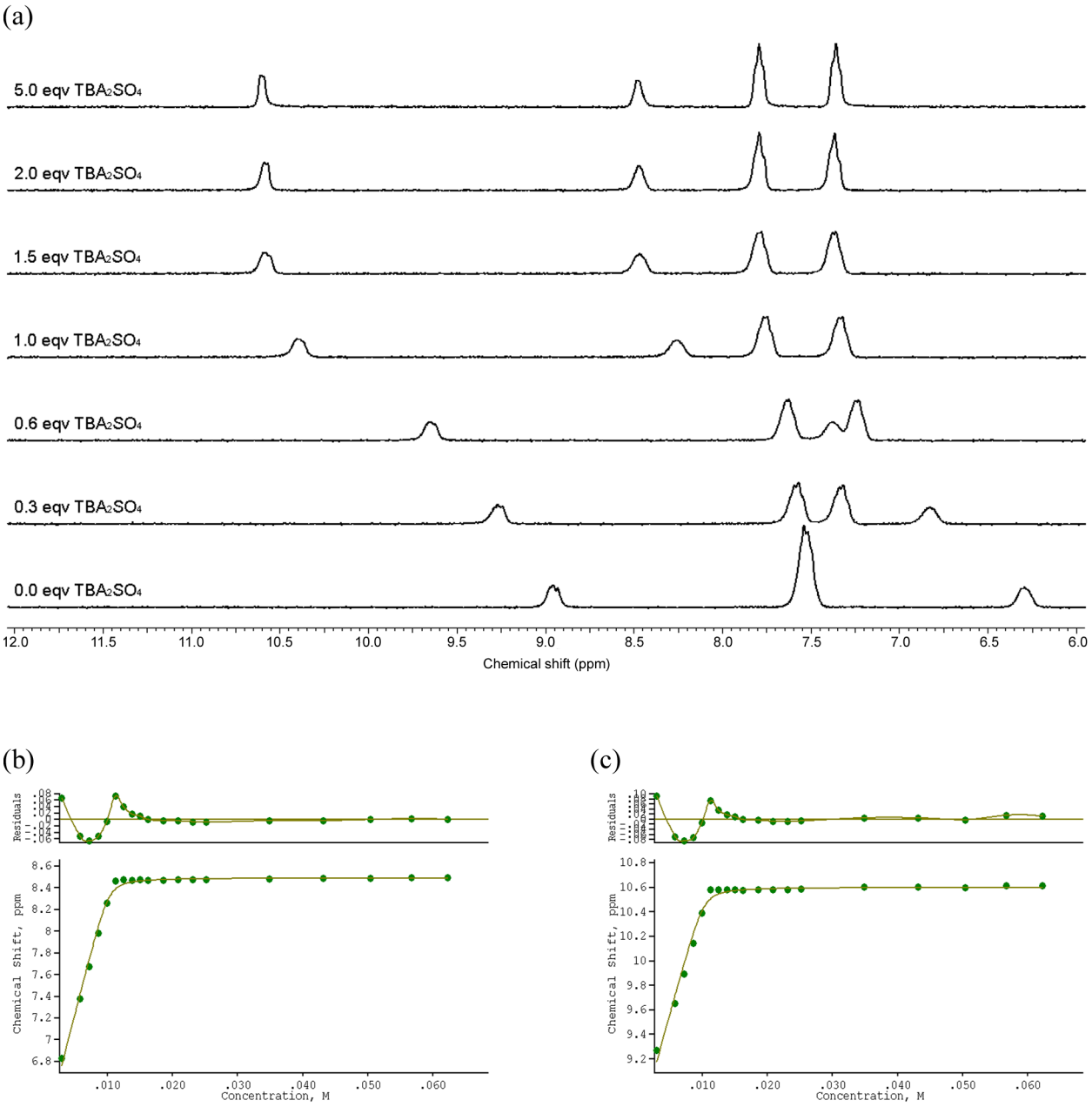

Figure S24. ^{1}H NMR titration of compound **4** with TBA_2SO_4 in DMSO-d_6 with 0.5 % water at 298K. (a) Stack plot. (b) Fitplot for NH proton at δ = 6.30 ppm. $K_a > 10^4$ M^{-1}. (c) Fitplot for NH proton at δ = 8.95 ppm. $K_a > 10^4$ M^{-1}.

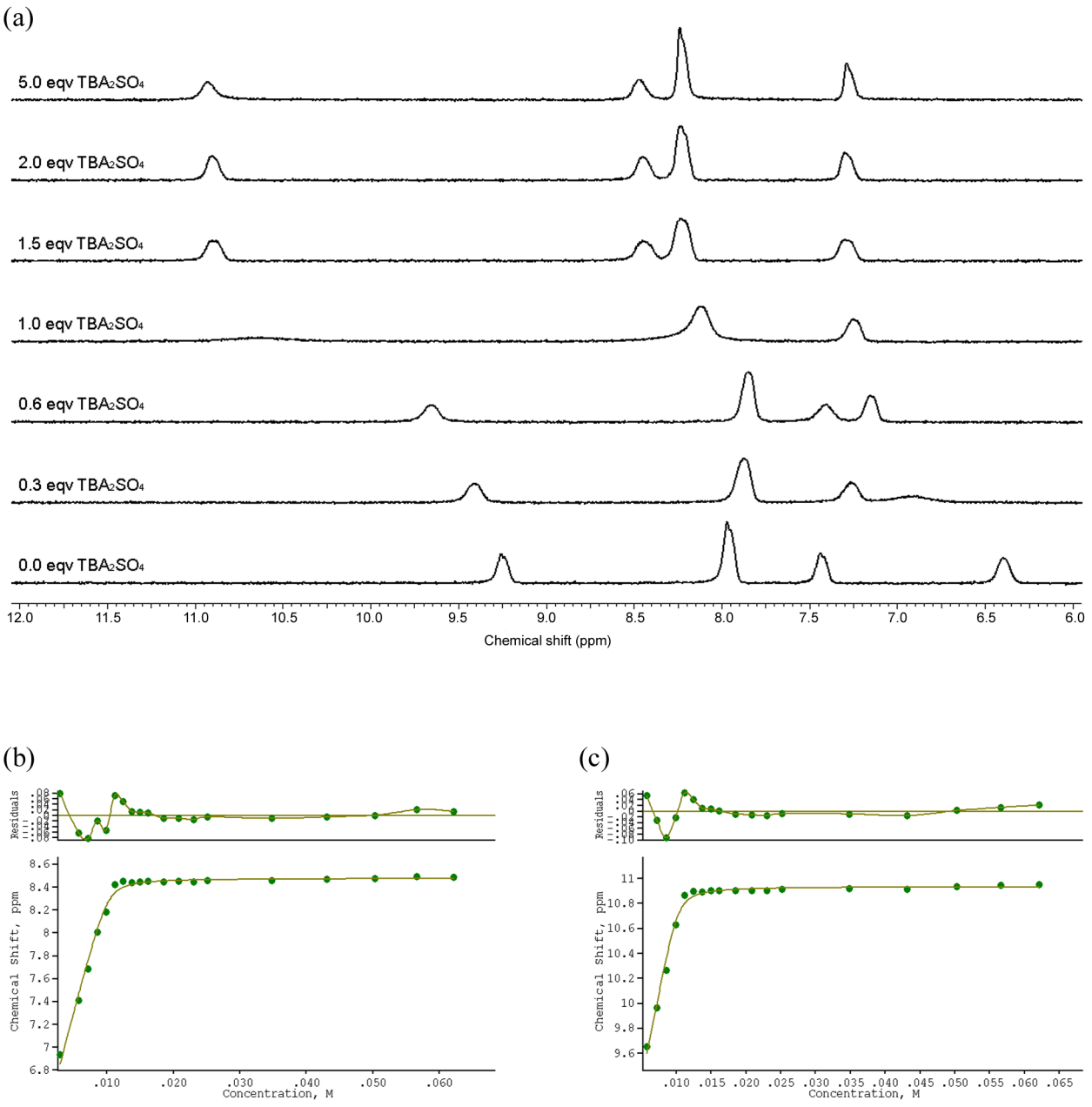

Figure S25. ^{1}H NMR titration of compound **5** with TBA_2SO_4 in DMSO-d_6 with 0.5 % water at 298K. (a) Stack plot. (b) Fitplot for NH proton at δ = 6.40 ppm. $K_a > 10^4$ M^{-1}. (c) Fitplot for NH proton at δ = 9.25 ppm. $K_a > 10^4$ M^{-1}.

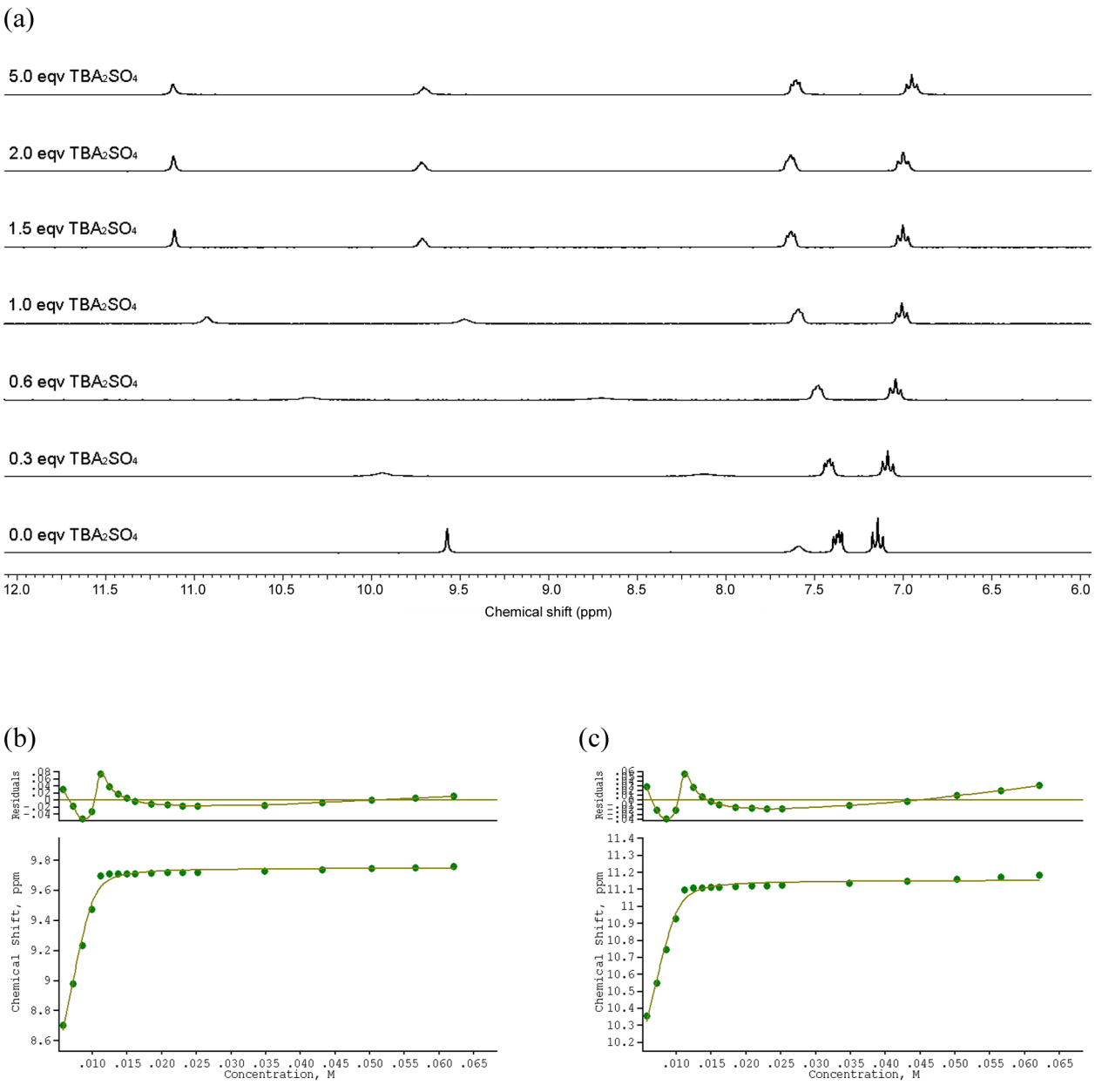

Figure S26. ^{1}H NMR titration of compound **7** with TBA_2SO_4 in DMSO-d_6 with 0.5 % water at 298K. (a) Stack plot. (b) Fitplot for NH proton at δ = 7.59 ppm. $K_a > 10^4$ M^{-1}. (c) Fitplot for NH proton at δ = 9.57 ppm. $K_a > 10^4$ M^{-1}.

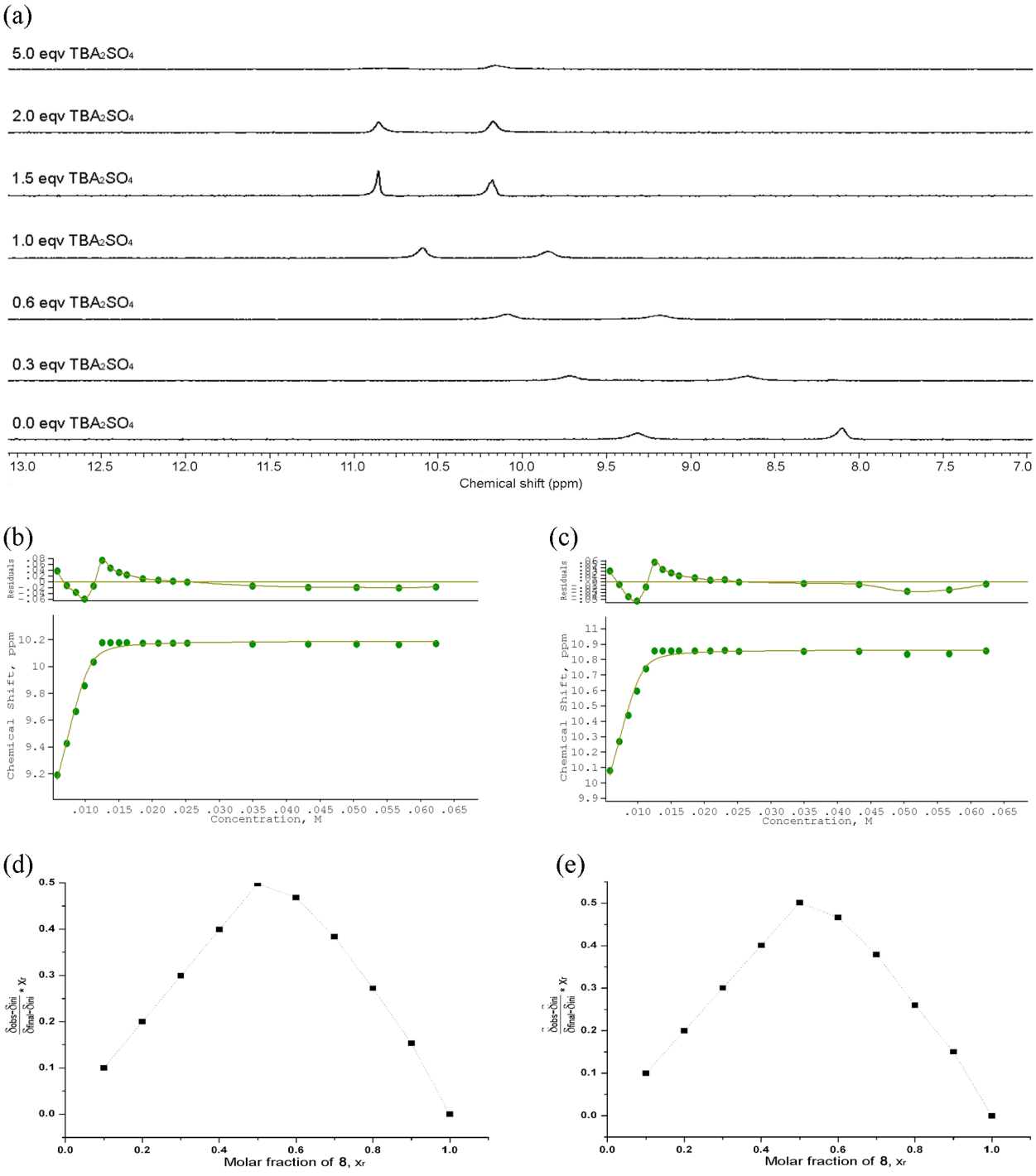

Figure S27. ^{1}H NMR titration of compound **8** with TBA_2SO_4 in DMSO-d_6 with 0.5 % water at 298K. (a) Stack plot. (b) Fitplot for NH proton at δ = 8.10 ppm. $K_a > 10^4$ M^{-1}. (c) Fitplot for NH proton at δ = 9.31 ppm. $K_a > 10^4$ M^{-1}. (d) Job plot analysis for NH proton at δ = 8.10 ppm. (e) Job plot analysis for NH proton at δ = 9.31 ppm.

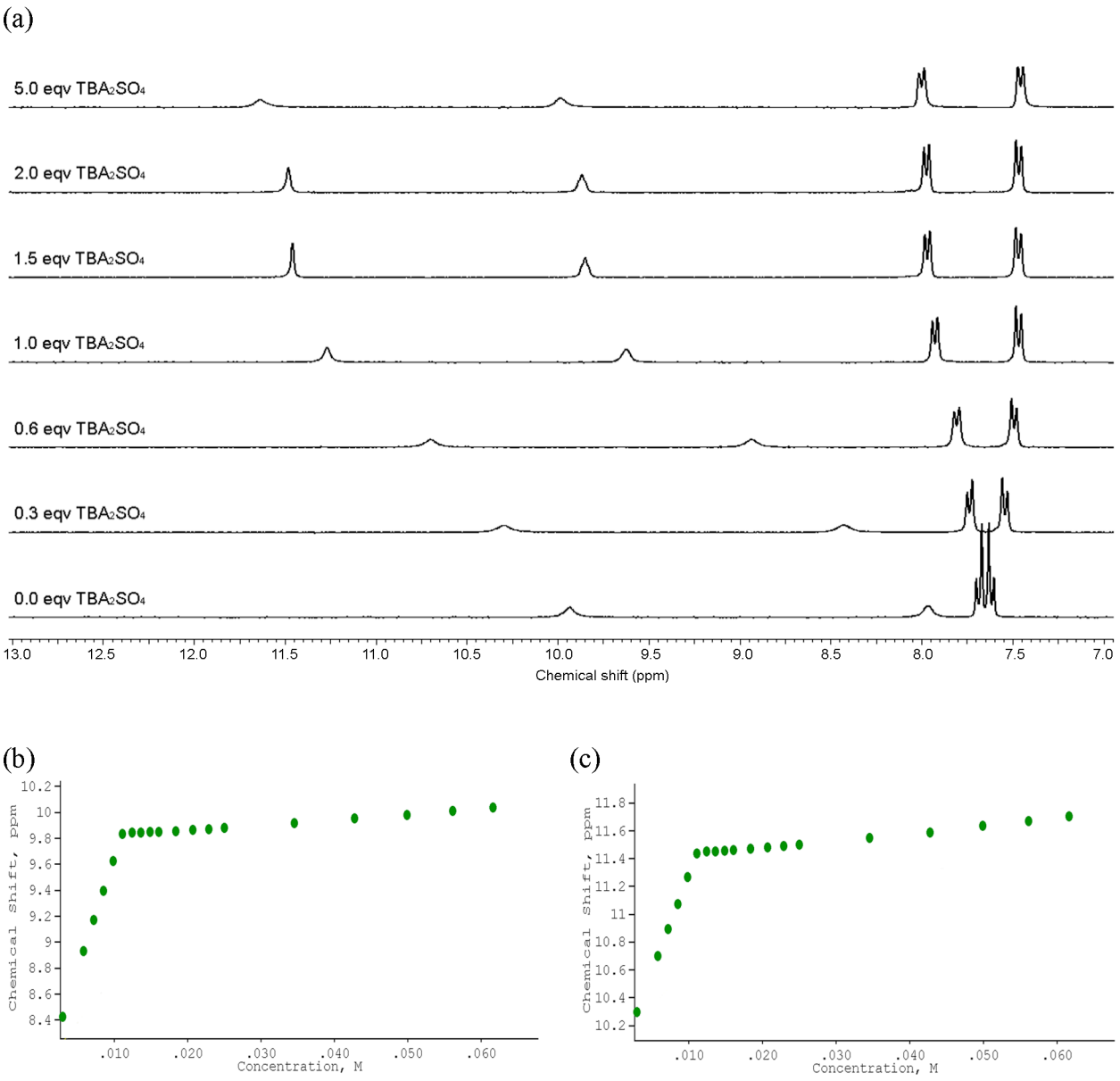

Figure S28. ^{1}H NMR titration of compound **9** with TBA_2SO_4 in DMSO-d_6 with 0.5 % water at 298K. (a) Stack plot. (b) Change in chemical shift for NH proton at δ = 7.97 ppm. Data could not be fitted (but estimated $K_a > 10^4$ M^{-1}). (c) Change in chemical shift for NH proton at δ = 9.95 ppm. Data could not be fitted (but estimated $K_a > 10^4$ M^{-1}).

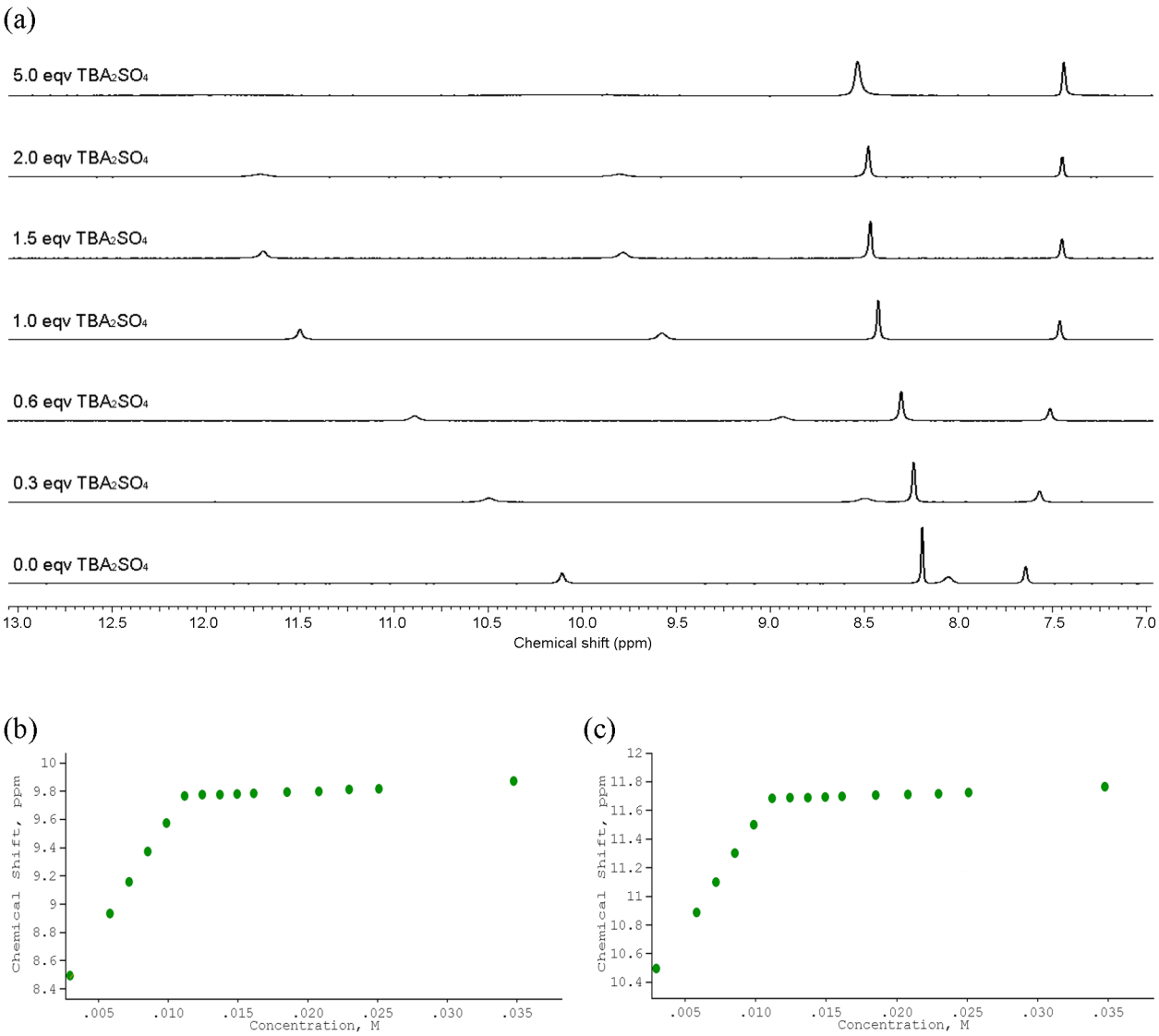

Figure S29. ^{1}H NMR titration of compound **10** with TBA_2SO_4 in DMSO-d_6 with 0.5 % water at 298K. (a) Stack plot. (b) Change in chemical shift for NH proton at δ = 8.05 ppm. Data could not be fitted (but estimated $K_a > 10^4$ M^{-1}). (c) Change in chemical shift for NH proton at δ = 10.09 ppm. Data could not be fitted (but estimated $K_a > 10^4$ M^{-1}).

S4.4 Interaction with $TBAH_2PO_4$ (in DMSO-d_6 with 0.5% water)

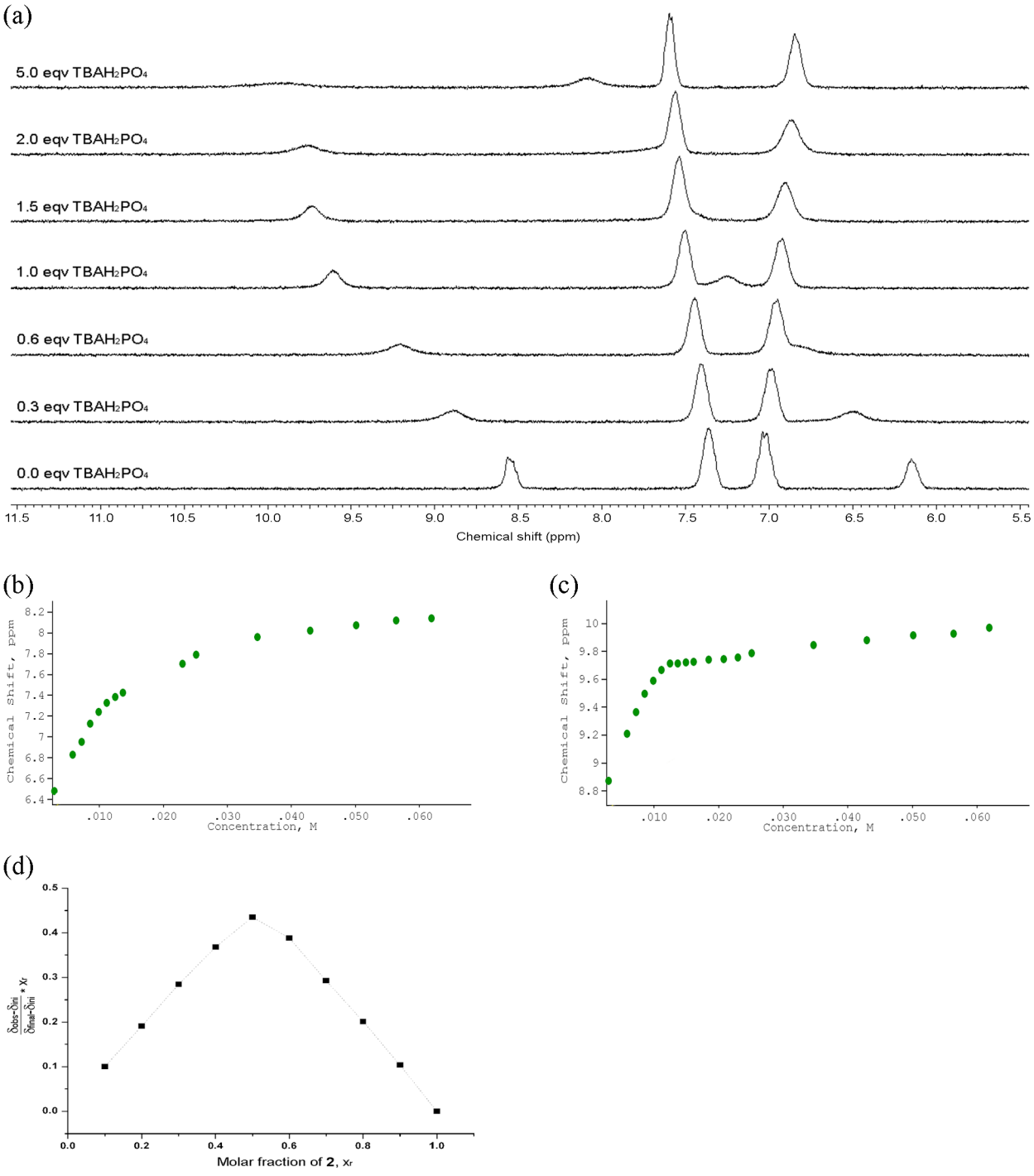

Figure S30. ^{1}H NMR titration of compound **2** with $TBAH_2PO_4$ in DMSO-d_6 with 0.5 % water at 298K. (a) Stack plot. (b) Change in chemical shift for NH proton at δ = 6.18 ppm. $K_a > 10^4$ M^{-1}. (c) Change in Chemical shift for NH proton at δ = 8.59 ppm. $K_a > 10^4$ M^{-1}. (d) Job plot analysis for NH proton at δ = 8.59 ppm.

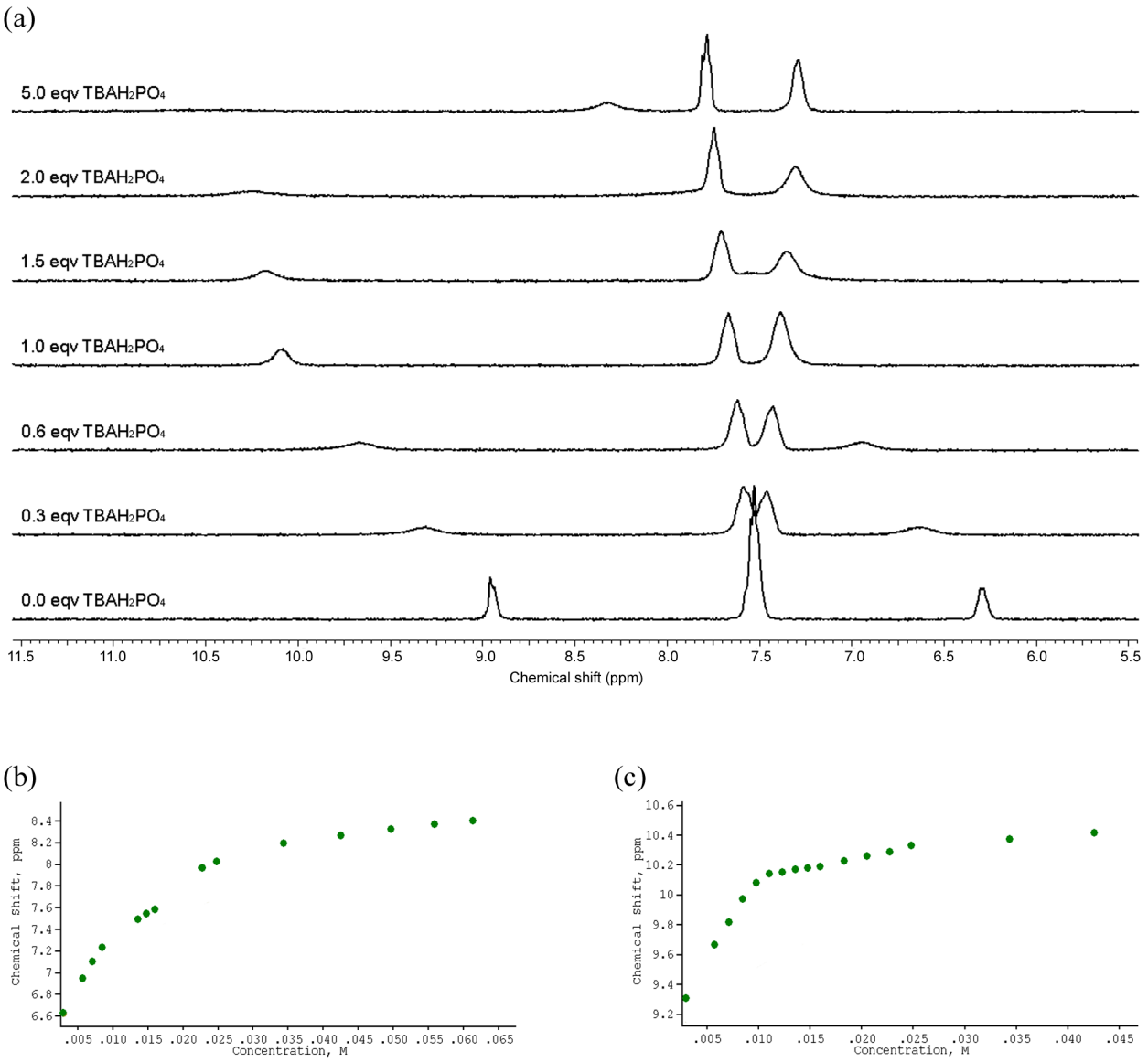

Figure S31. ^{1}H NMR titration of compound **4** with $TBAH_2PO_4$ in DMSO-d_6 with 0.5 % water at 298K. (a) Stack plot. (b) Change in chemical shift for NH proton at δ = 6.30 ppm. Data could not be fitted. (c) Change in chemical shift for NH proton at δ = 8.95 ppm. Data could not be fitted.

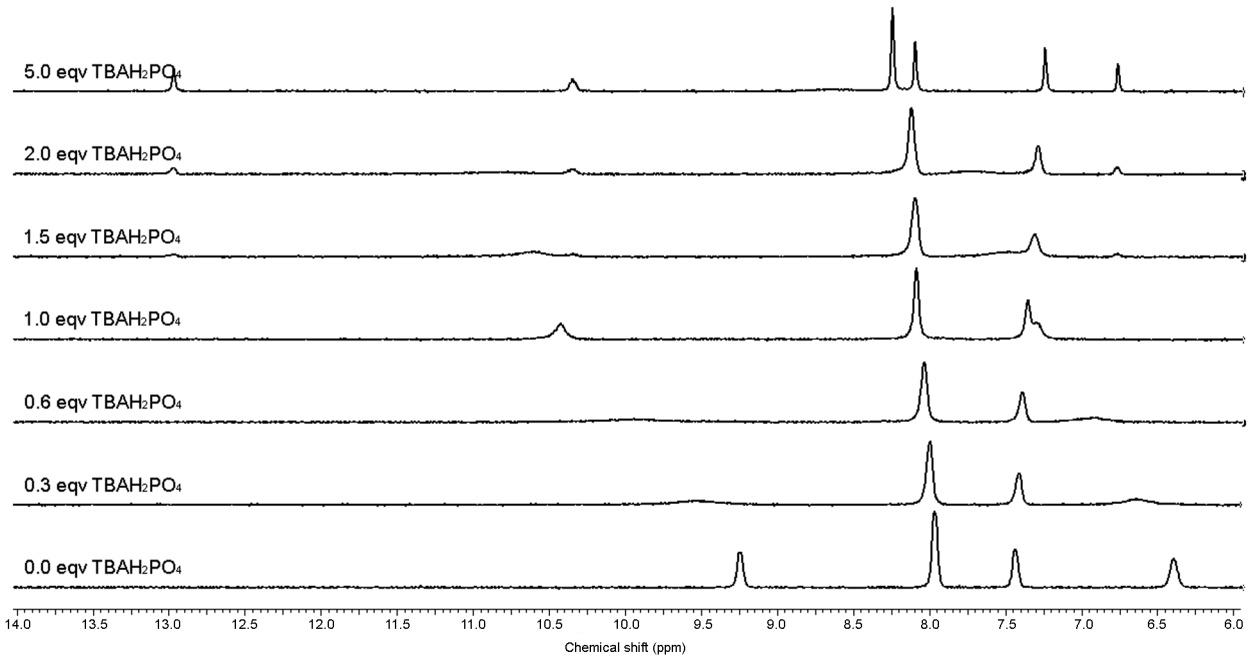

Figure S32. ^{1}H NMR titration of compound **5** with $TBAH_2PO_4$ in DMSO-d_6 with 0.5 % water at 298K. Stack plot. New peaks emerge due to deprotonation of bound $H_2PO_4^-$.

(a)

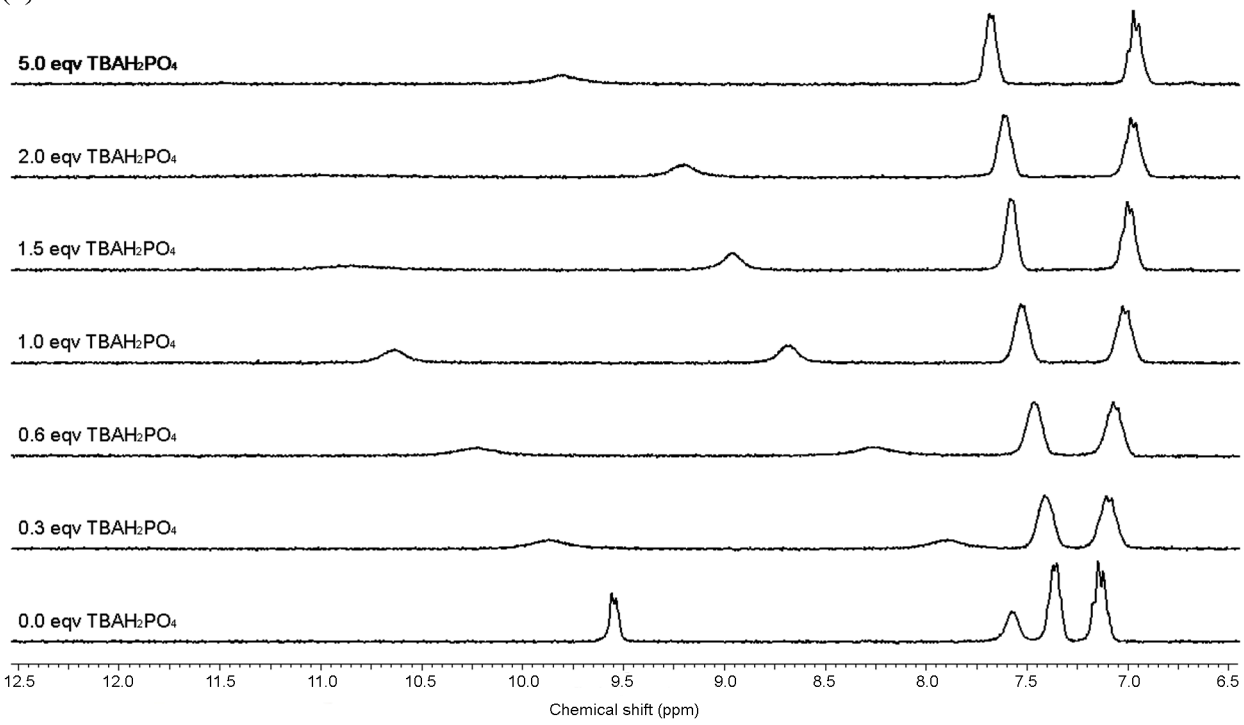

(b)

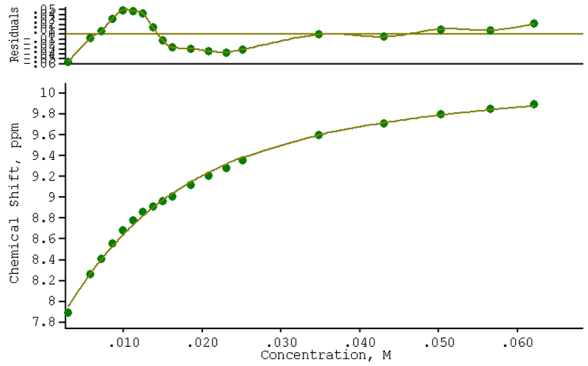

Figure S33. ^{1}H NMR titration of compound **7** with $TBAH_2PO_4$ in DMSO-d_6 with 0.5 % water at 298K. (a) Stack plot. (b) Fitplot for NH proton at δ = 7.59 ppm. K_a = 115 M^{-1} (error 8 %). Data for NH proton at δ = 9.57 ppm could not be fitted due to peak broadening.

(a)

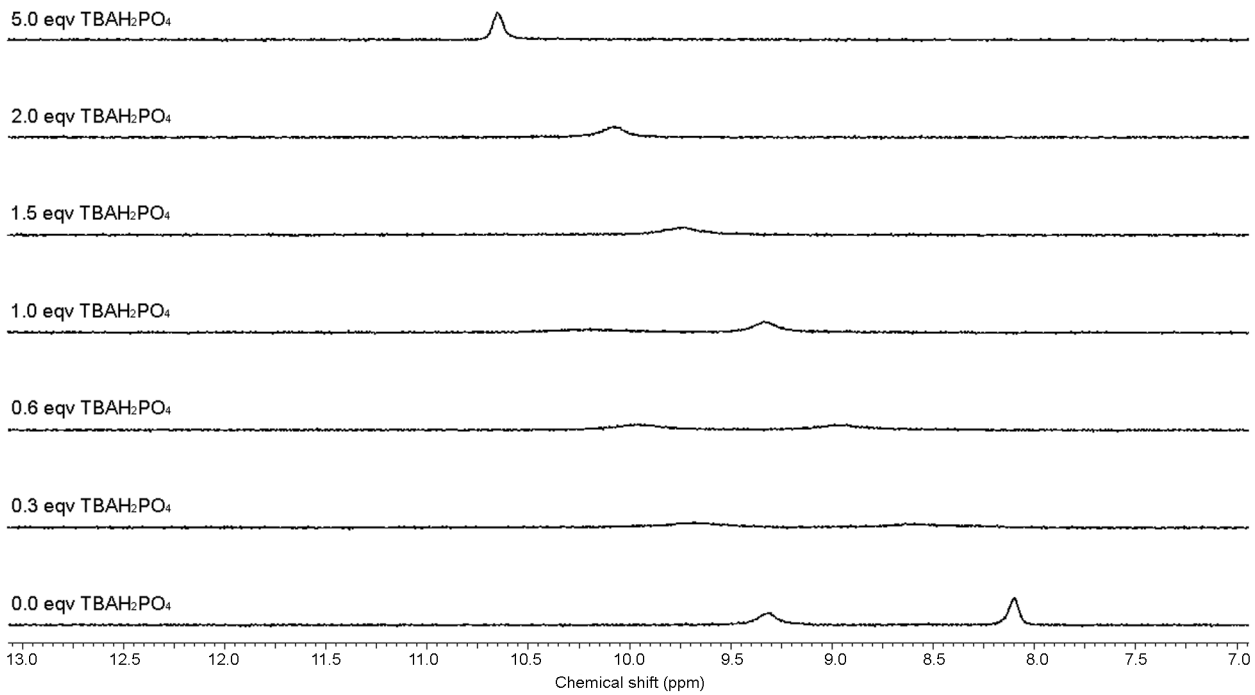

(b)

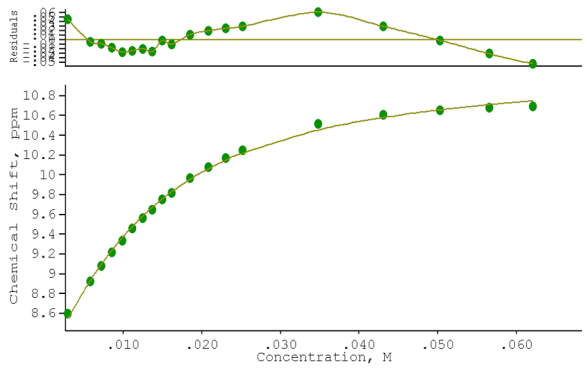

Figure S34. ^{1}H NMR titration of compound **8** with $TBAH_2PO_4$ in DMSO-d_6 with 0.5 % water at 298K. (a) Stack plot. (b) Fitplot for NH proton at δ = 8.10 ppm. K_a = 130 M^{-1} (error 6 %). Data for NH proton at δ = 9.31 ppm could not be fitted due to peak broadening.

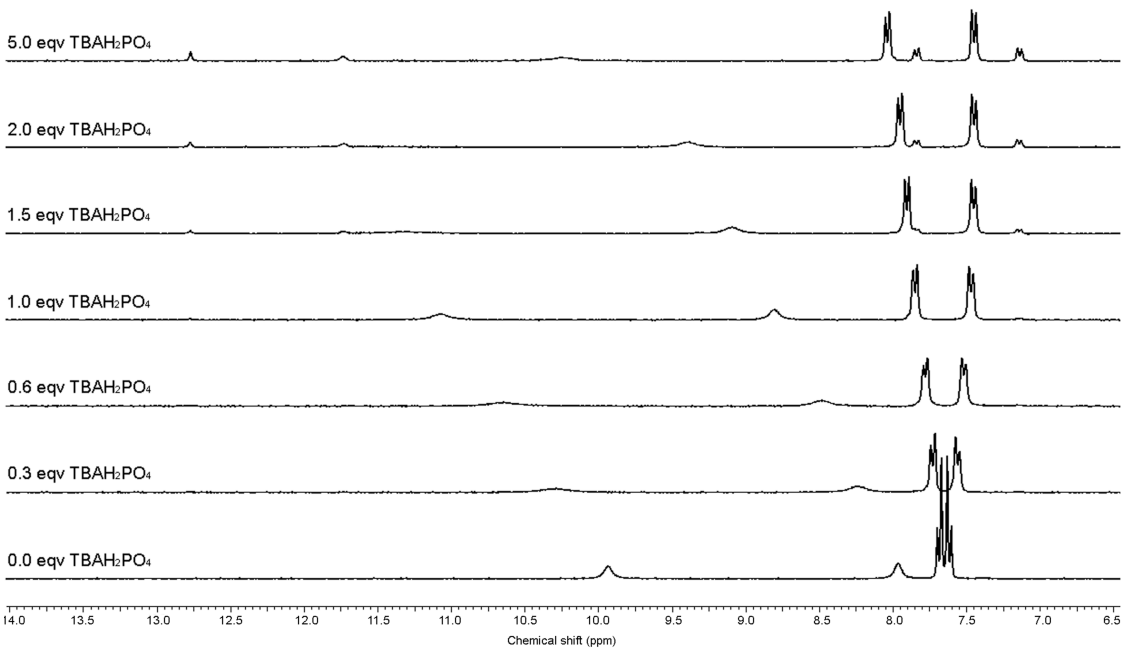

Figure S35. ^{1}H NMR titration of compound **9** with $TBAH_2PO_4$ in DMSO-d_6 with 0.5 % water at 298K. Stack plot. New peaks due to deprotonation of bound $H_2PO_4^-$.

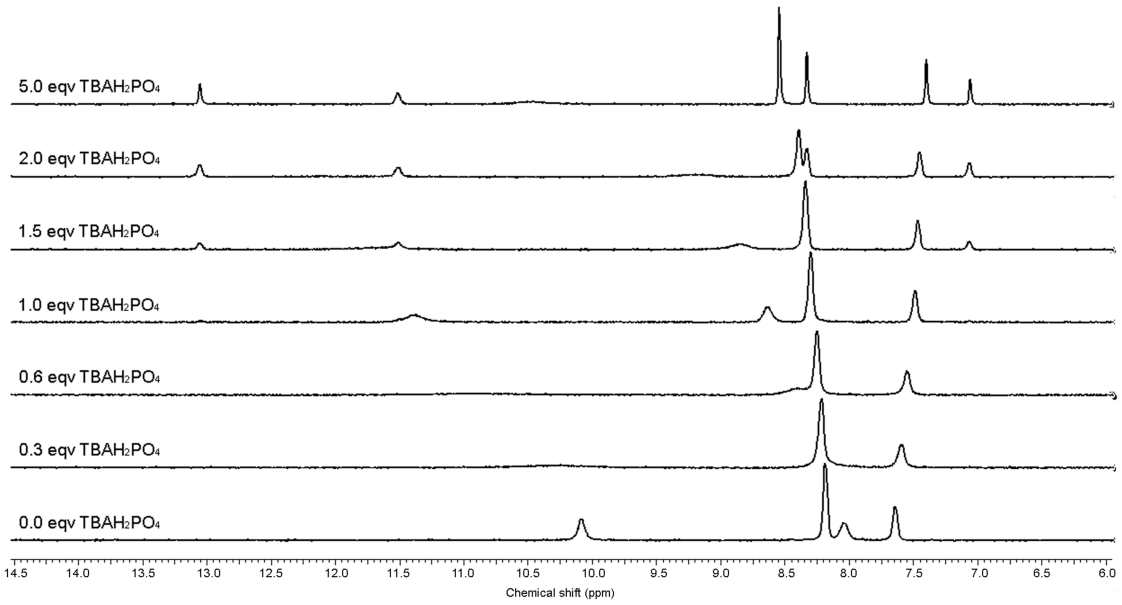

Figure S36. ^{1}H NMR titration of compound **10** with $TBAH_2PO_4$ in DMSO-d_6 with 0.5 % water at 298K. Stack plot. New peaks due to deprotonation of bound $H_2PO_4^-$.

S4.5 Interaction with $TBAH_2PO_4$ (in DMSO-d_6 with 10 % water)

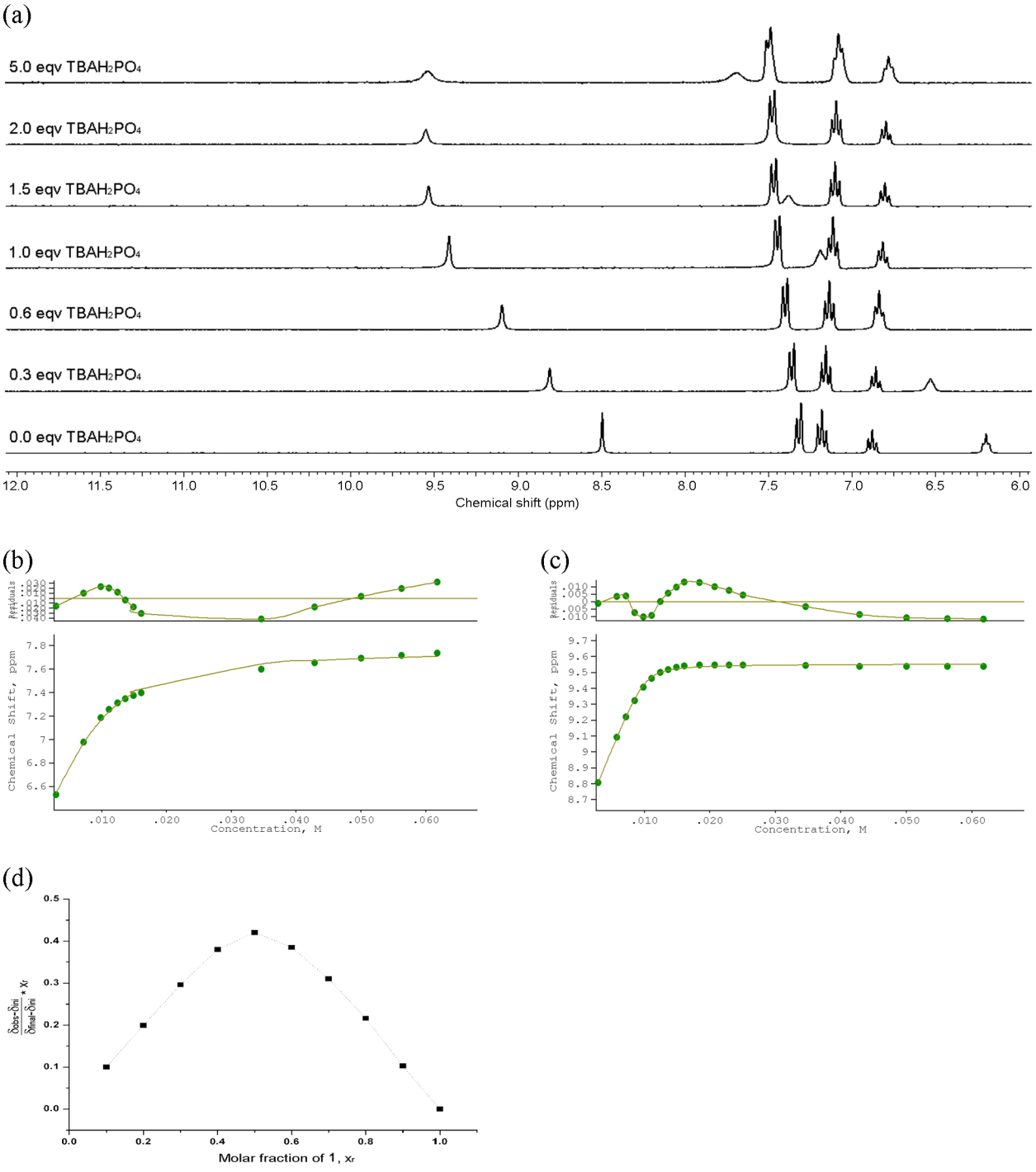

Figure S37. ^{1}H NMR titration of compound **1** with $TBAH_2PO_4$ in DMSO-d_6 with 10 % water at 298K. (a) Stack plot. (b) Fitplot for NH proton at δ = 6.20 ppm. K_a = 443 M^{-1} (error 10 %). (c) Fitplot for NH proton at δ = 8.49 ppm. K_a = 6363 M^{-1} (error 11 %). (d) Job plot analysis for NH proton at δ = 8.49 ppm. (Job plot for NH at δ = 6.20 ppm not possible due to peak overlap).

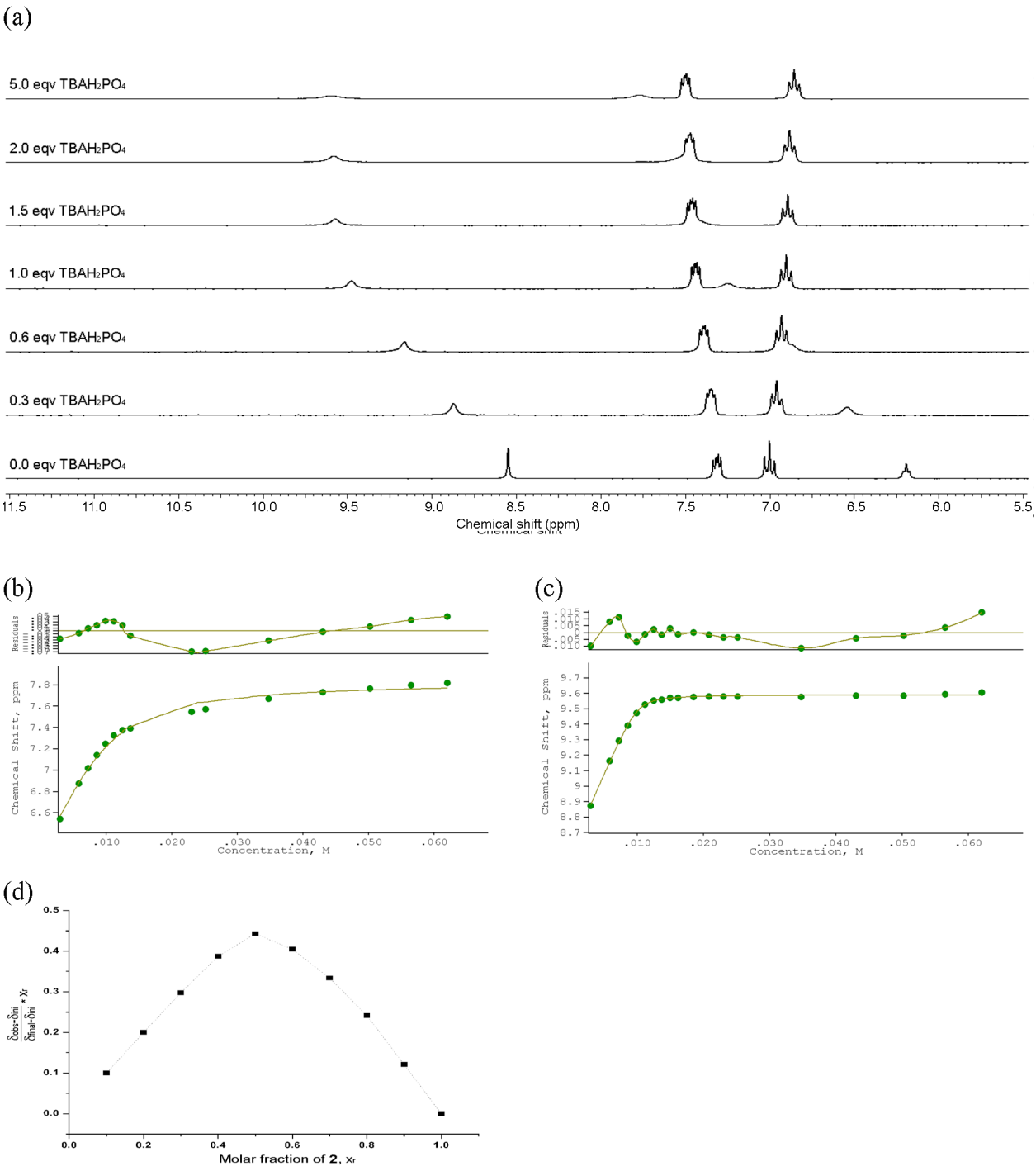

Figure S38. ^{1}H NMR titration of compound **2** with $TBAH_2PO_4$ in DMSO-d_6 with 10 % water at 298K. (a) Stack plot. (b) Fitplot for NH proton at δ = 6.18 ppm. K_a = 452 M^{-1} (error 15 %). (c) Fitplot for NH proton at δ = 8.59 ppm. K_a =8099 M^{-1} (error 8 %). (d) Job plot analysis for NH proton at δ = 8.59 ppm. (Job plot for NH at δ = 6.18 ppm not possible due to peak overlap).

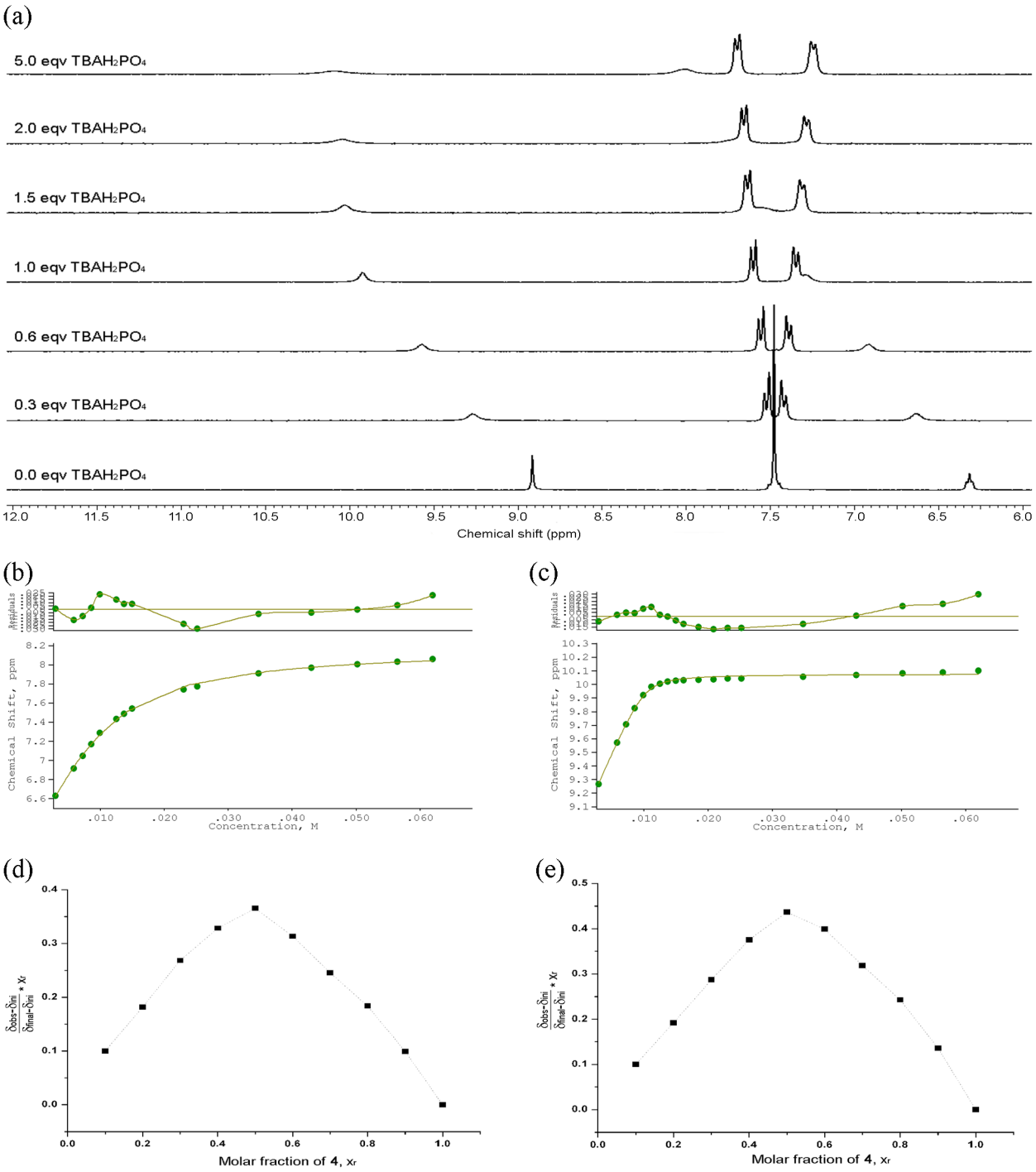

Figure S39. ^{1}H NMR titration of compound **4** with $TBAH_2PO_4$ in DMSO-d_6 with 10 % water at 298K. (a) Stack plot. (b) Fitplot for NH proton at δ = 6.30 ppm. K_a = 243 M^{-1} (error 6 %). (c) Fitplot for NH proton at δ = 8.95 ppm. K_a = 4818 M^{-1} (error 13 %). (d) Job plot analysis for NH proton at δ = 6.30 ppm. (e) Job plot analysis for NH proton at δ = 8.95 ppm.

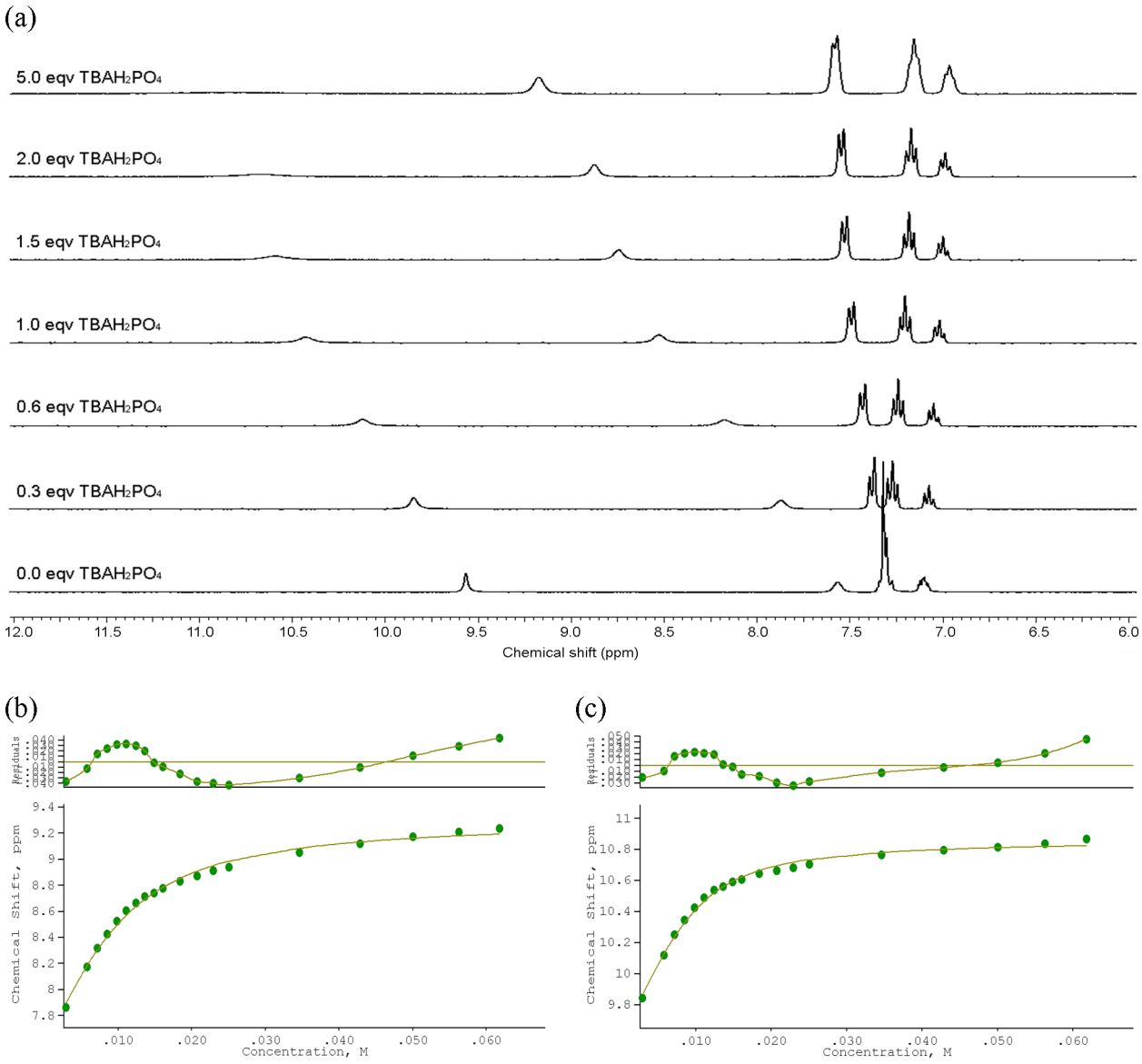

Figure S40. ^{1}H NMR titration of compound **6** with $TBAH_2PO_4$ in DMSO-d_6 with 10 % water at 298K. (a) Stack plot. (b) Fitplot for NH proton at δ = 7.56 ppm. K_a = 256 M^{-1} (error 10 %). (c) Fitplot for NH proton at δ = 9.56 ppm. K_a = 546 M^{-1} (error 11 %).

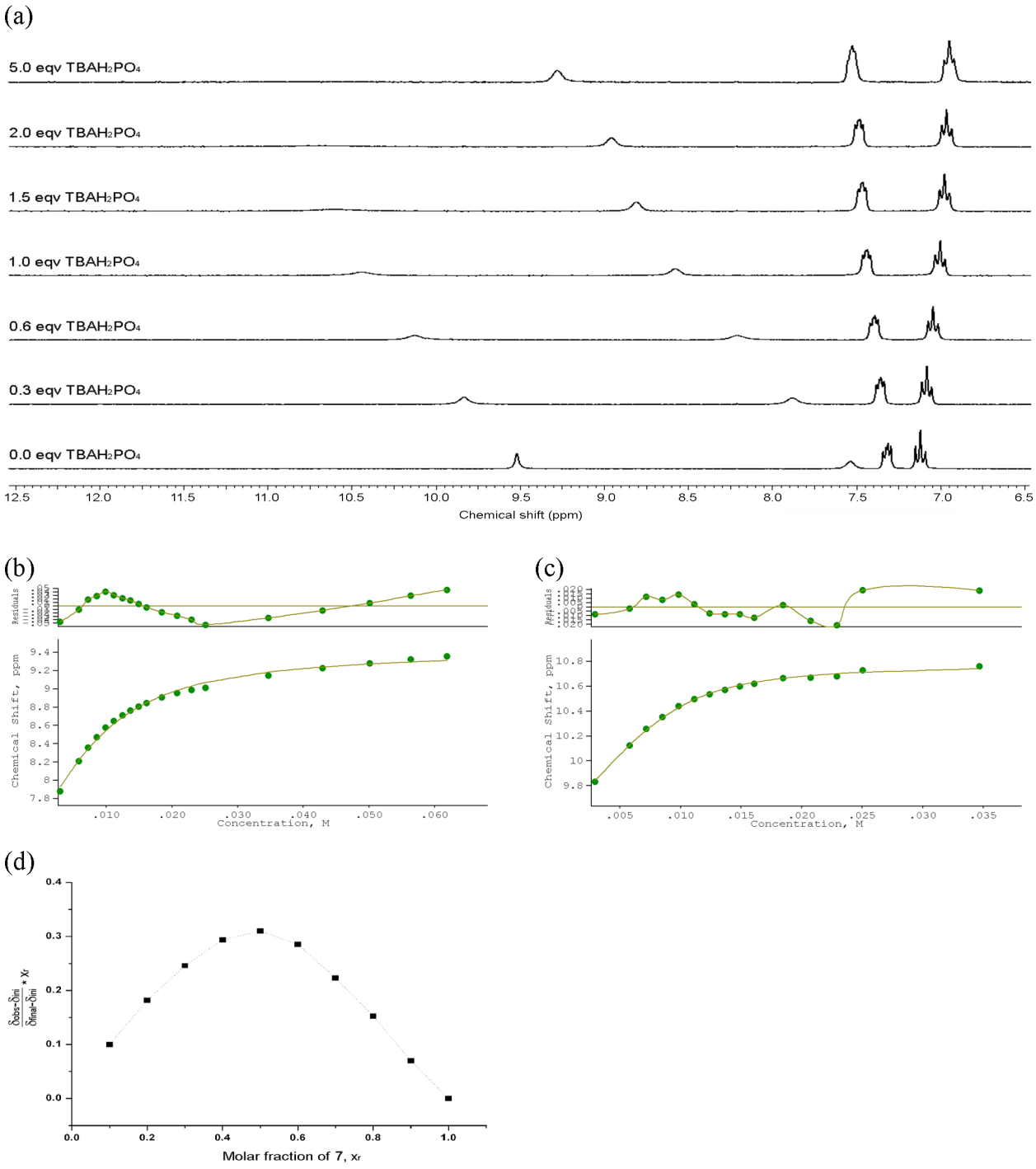

Figure S41. ^{1}H NMR titration of compound **7** with $TBAH_2PO_4$ in DMSO-d_6 with 10 % water at 298K. (a) Stack plot. (b) Fitplot for NH proton at δ = 7.59 ppm. K_a = 227 M^{-1} (error 10 %). (c) Fitplot for NH proton at δ = 9.57 ppm. K_a = 947 M^{-1} (error 7 %). (d) Job plot analysis for NH proton at δ = 7.59 ppm. (Job plot analysis for NH proton at δ = 9.57 ppm not possible due to peak broadening.

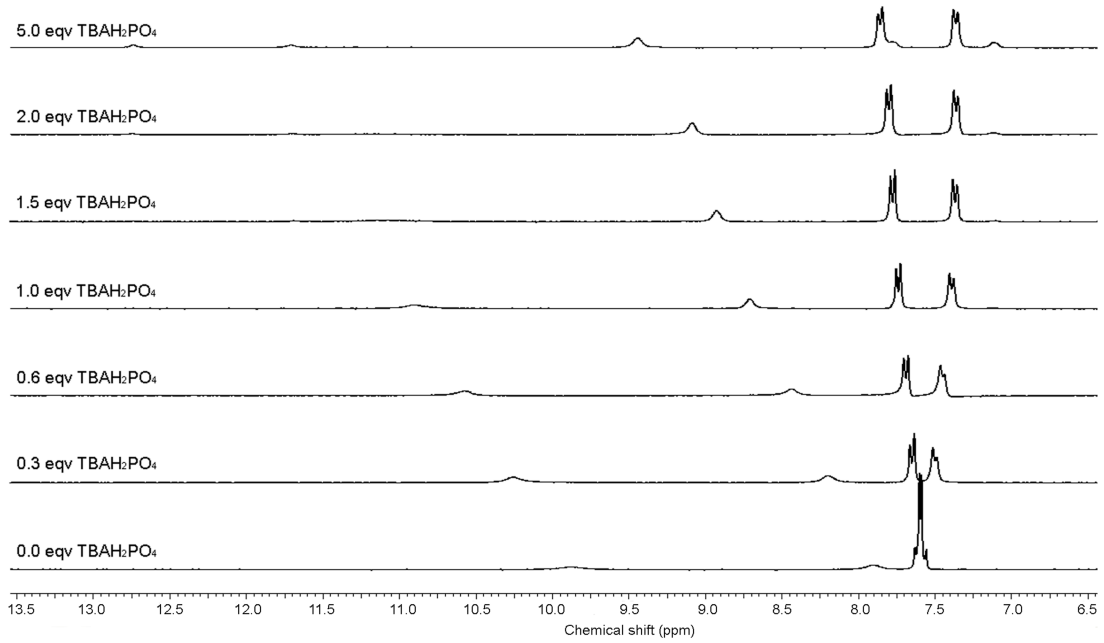

Figure S42. ^{1}H NMR titration of compound **9** with $TBAH_2PO_4$ in DMSO-d_6 with 10 % water at 298K. Stack plot. New peaks due to deprotonation of bound $H_2PO_4^-$.

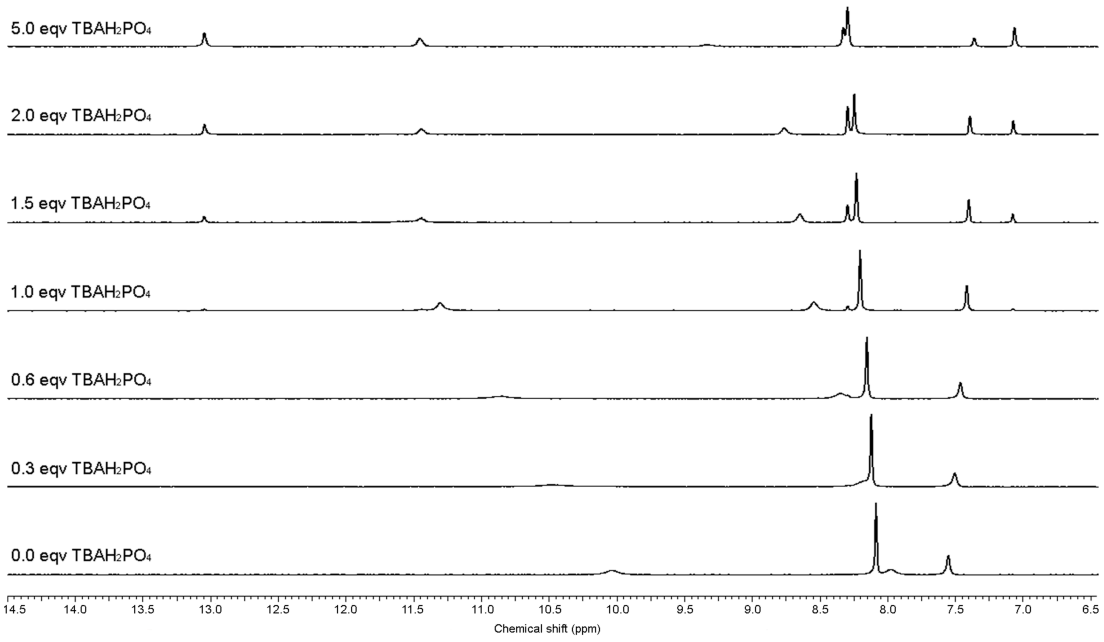

Figure S43. ^{1}H NMR titration of compound **10** with $TBAH_2PO_4$ in DMSO-d_6 with 10 % water at 298K. Stack plot. New peaks due to deprotonation of bound $H_2PO_4^-$.

S4.6 Interaction with TBA OH

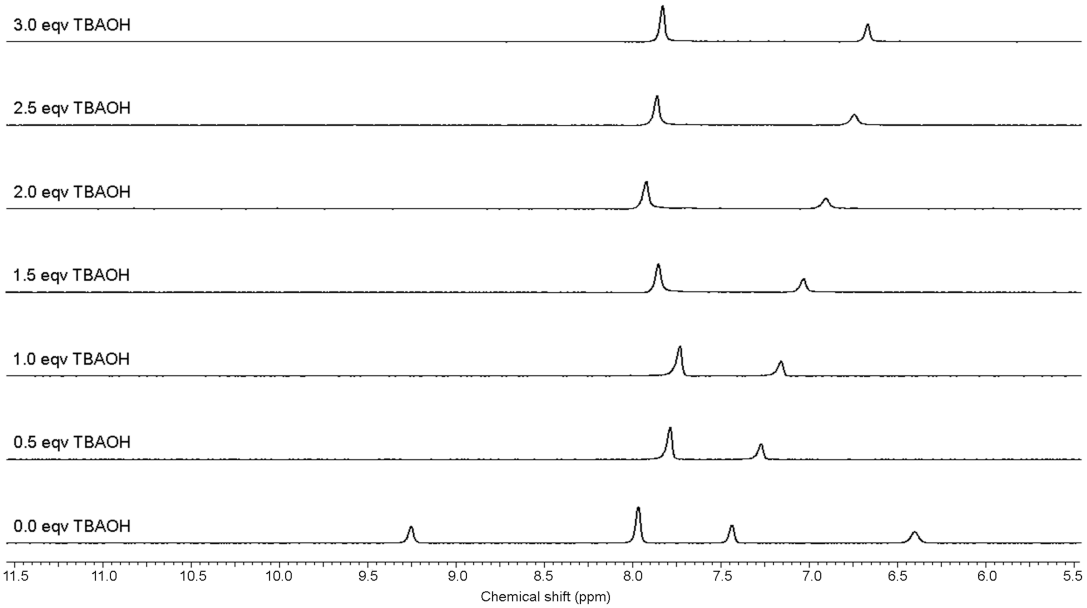

Figure S44. ^{1}H NMR titration of compound **5** with TBA OH in DMSO-d_6 with 0.5 % water at 298K. Stack plot.

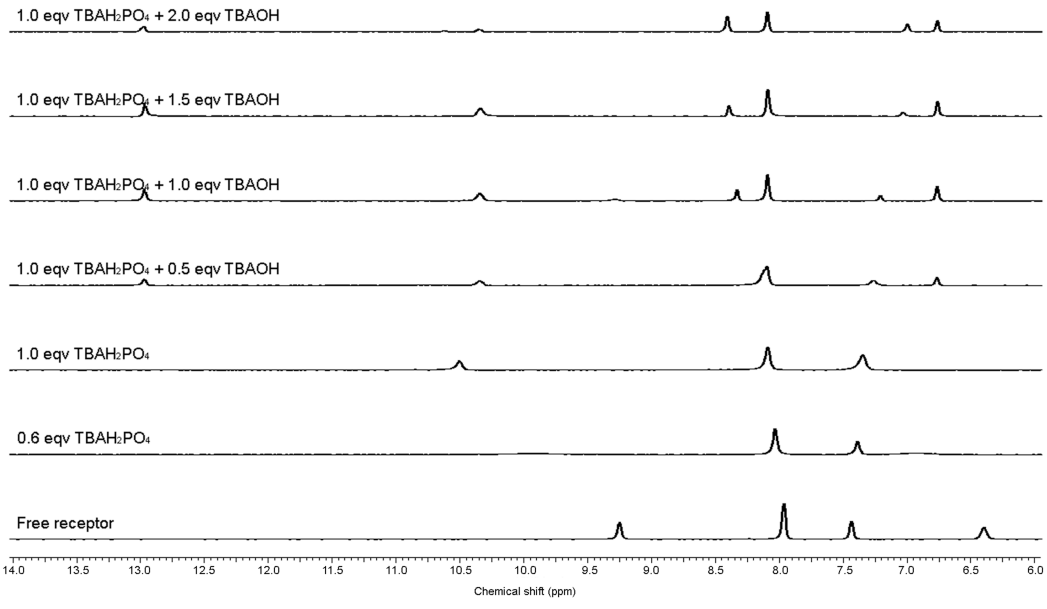

Figure S45. ^{1}H NMR titration of compound **5** with $TBAH_2PO_4$ and TBA OH in DMSO-d_6 with 0.5 % water at 298K. Stack plot.

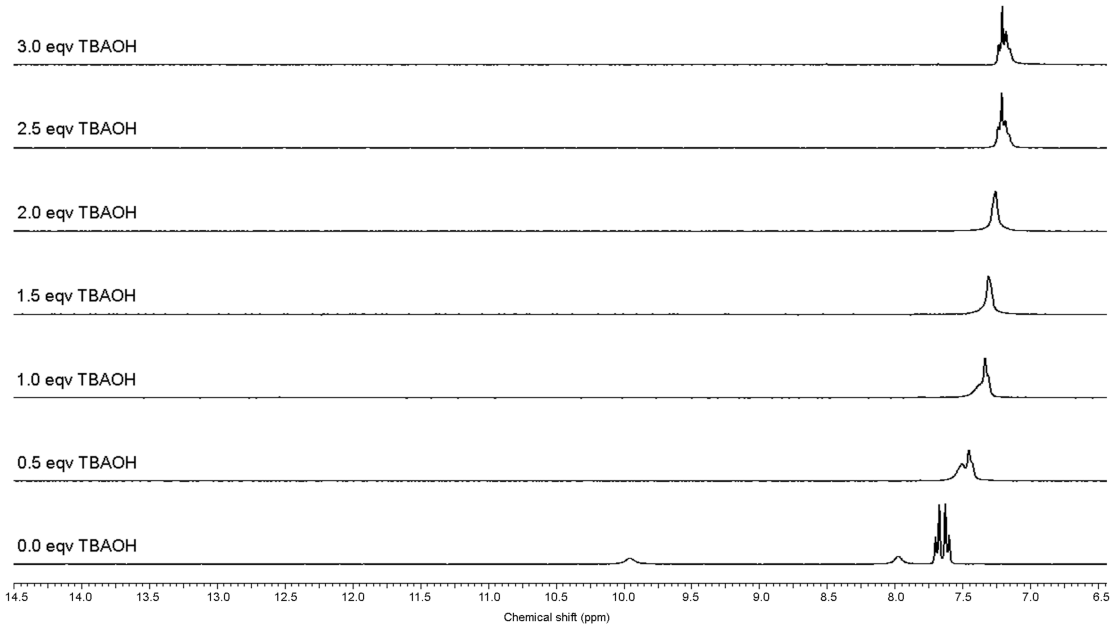

Figure S46. ^{1}H NMR titration of compound **9** with TBA OH in DMSO-d_6 with 0.5 % water at 298K. Stack plot.

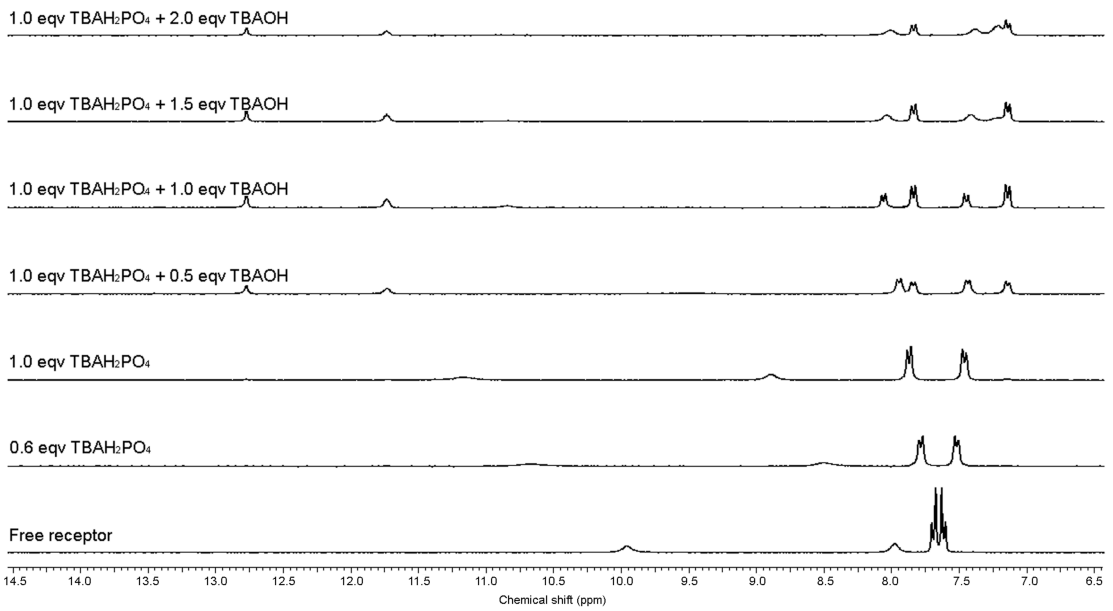

Figure S47. ^{1}H NMR titration of compound **9** with $TBAH_2PO_4$ and TBA OH in DMSO-d_6 with 0.5 % water at 298K. Stack plot.

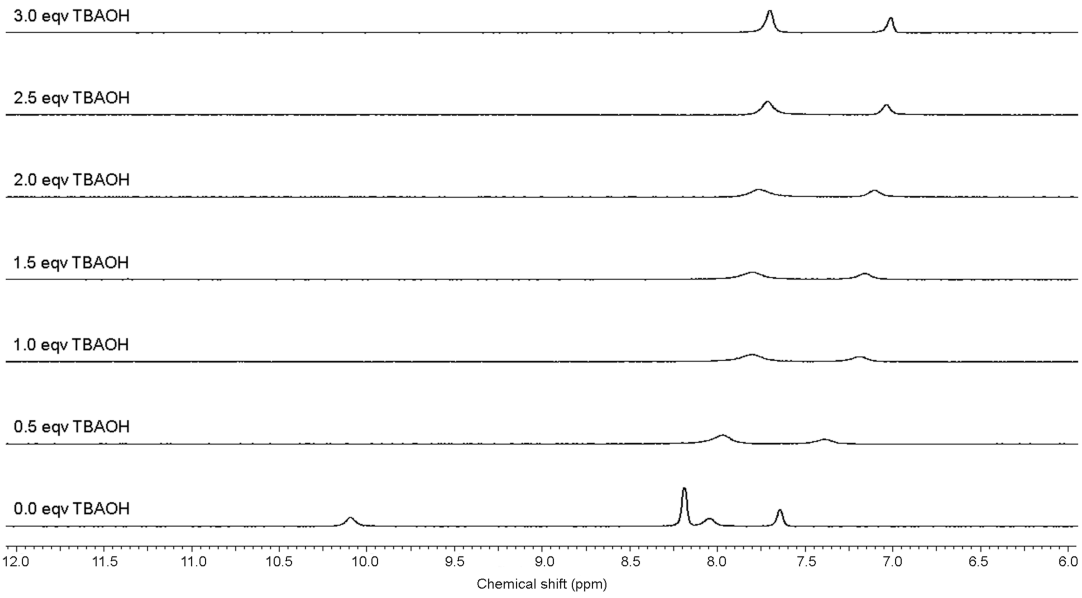

Figure S48. ^{1}H NMR titration of compound **10** with TBA OH in DMSO-d_6 with 0.5 % water at 298K. Stack plot.

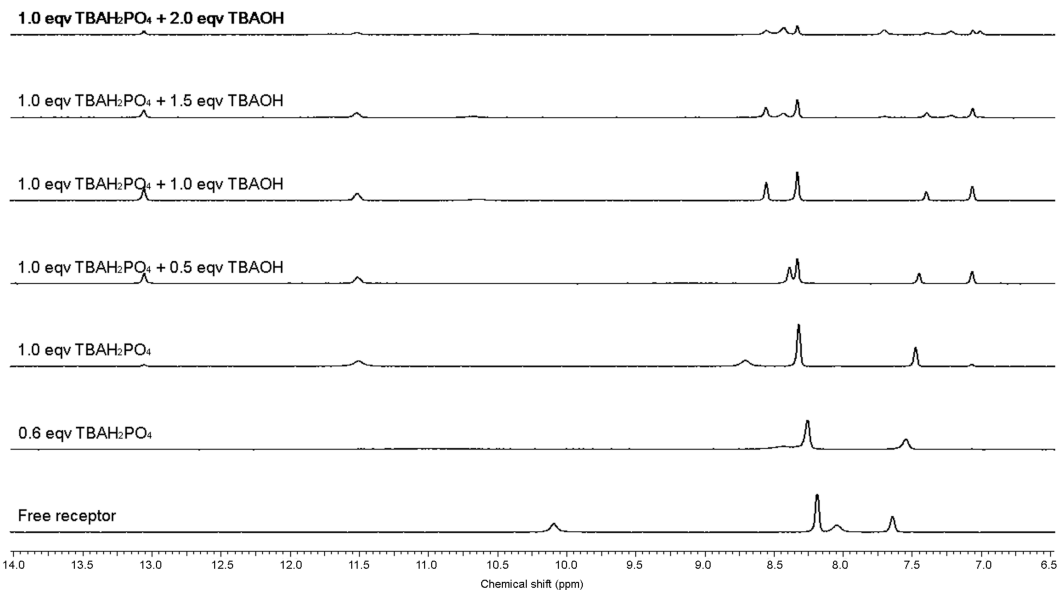

Figure S49. ^{1}H NMR titration of compound **10** with $TBAH_2PO_4$ and TBA OH in DMSO-d_6 with 0.5 % water at 298K. Stack plot.

S4.7 Interaction with $TEAHCO_3$

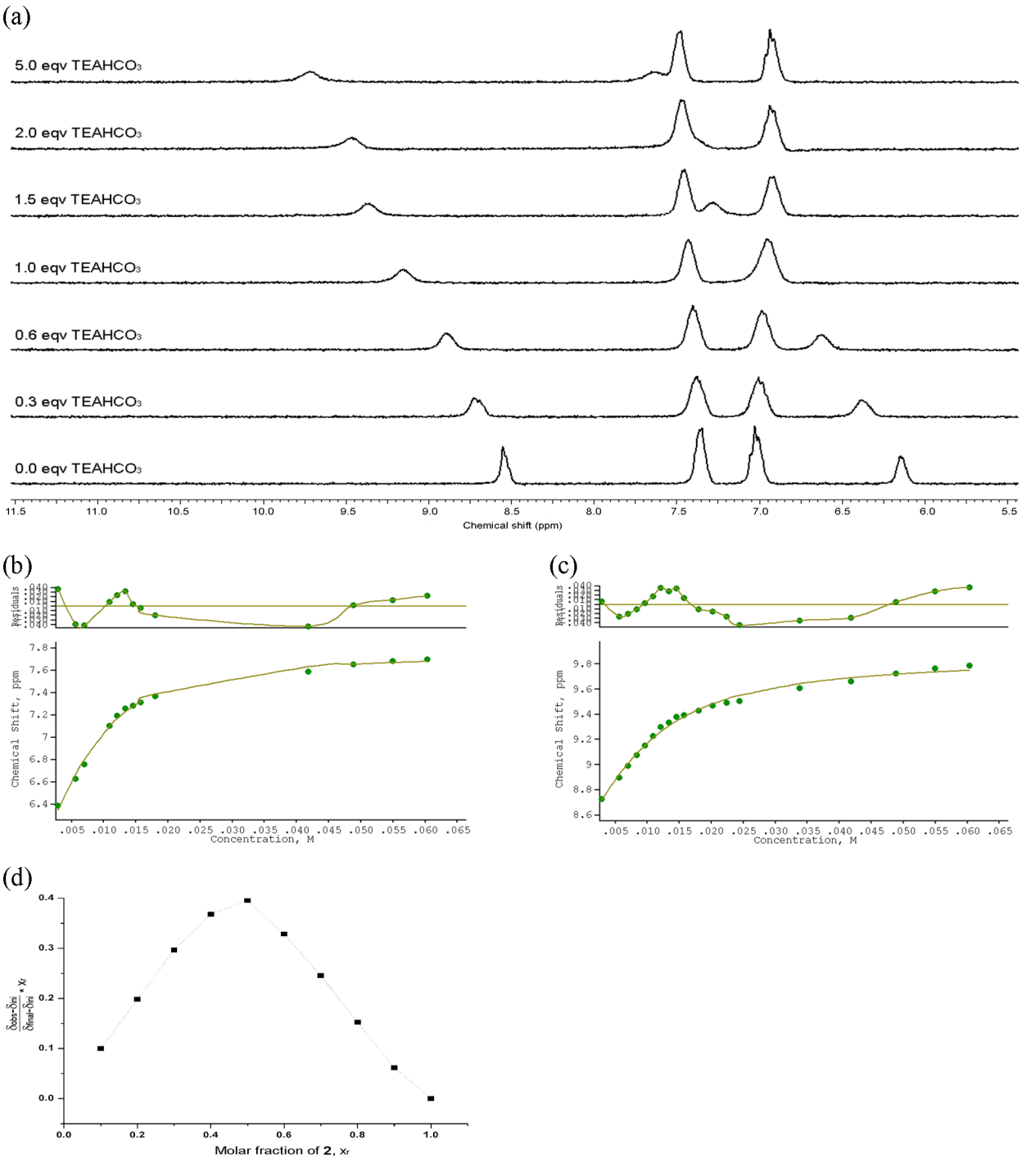

Figure S50. ^{1}H NMR titration of compound **2** with $TEAHCO_3$ in DMSO-d_6 with 0.5 % water at 298K. (a) Stack plot. (b) Fitplot for NH proton at δ = 6.18 ppm. K_a = 365 M^{-1} (error 11 %). (c) Fitplot for NH proton at δ = 8.59 ppm. K_a = 200 M^{-1} (error 12 %). (d) Job plot analysis for NH proton at δ = 8.59 ppm. (Job plot for NH at δ = 6.18 ppm not possible due to peak overlap)

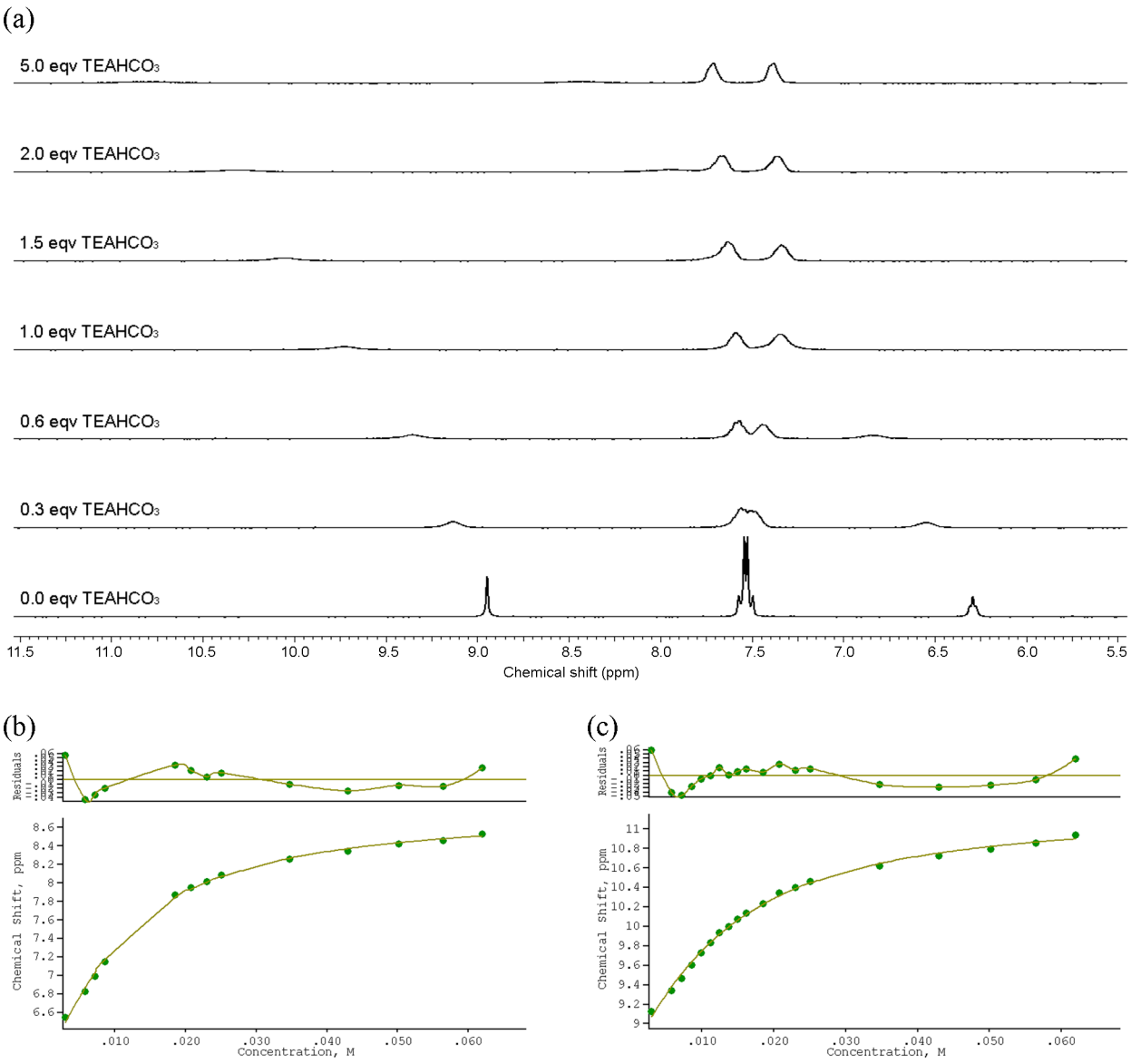

Figure S51. ^{1}H NMR titration of compound **4** with $TEAHCO_3$ in DMSO-d_6 with 0.5 % water at 298K. (a) Stack plot. (b) Fitplot for NH proton at δ = 6.30 ppm. K_a = 156 M^{-1} (error 9 %). (c) Fitplot for NH proton at δ = 8.95 ppm. K_a = 123 M^{-1} (error 7 %).

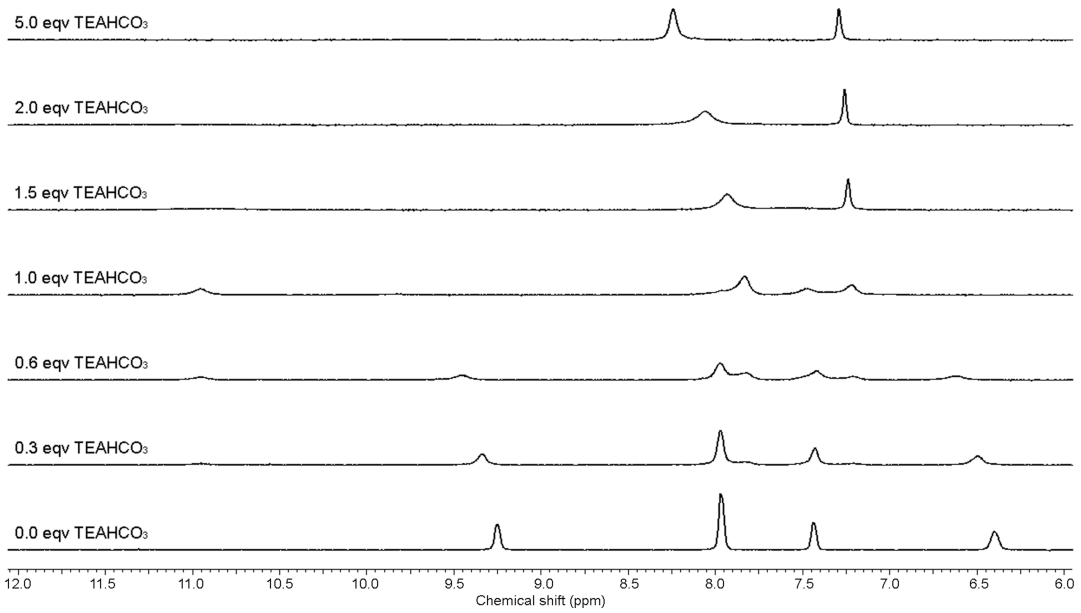

Figure S52. ^{1}H NMR titration of compound **5** with $TEAHCO_3$ in DMSO-d_6 with 0.5 % water at 298K. Stack plot. Peak broadening hindered determination of binding constants.

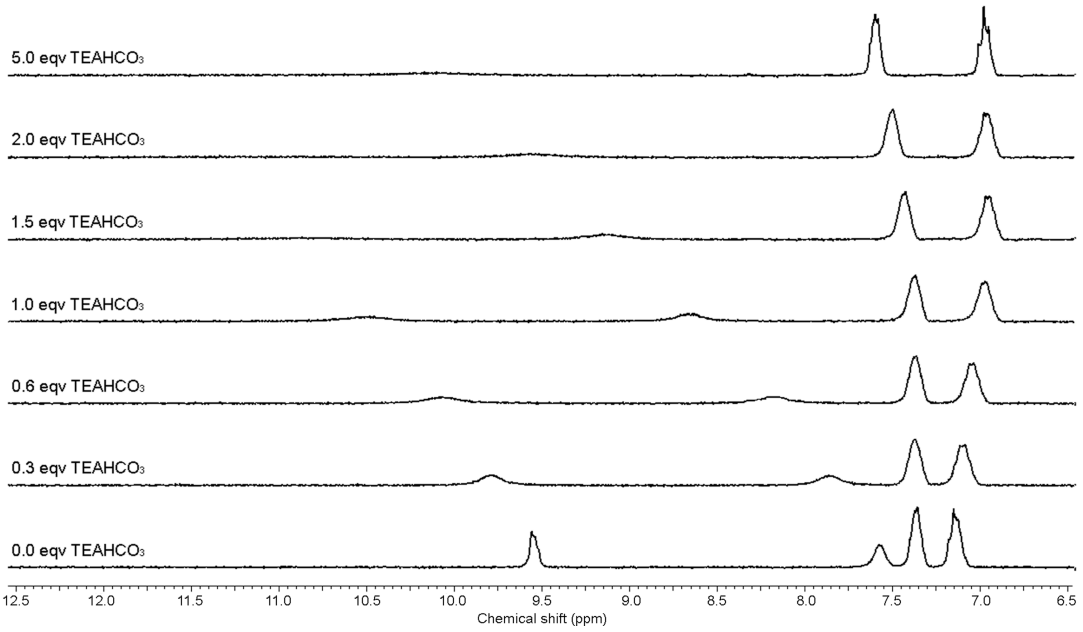

Figure S53. ^{1}H NMR titration of compound **7** with $TEAHCO_3$ in DMSO-d_6 with 0.5 % water at 298K. Stack plot. Peak broadening hindered determination of binding constants.

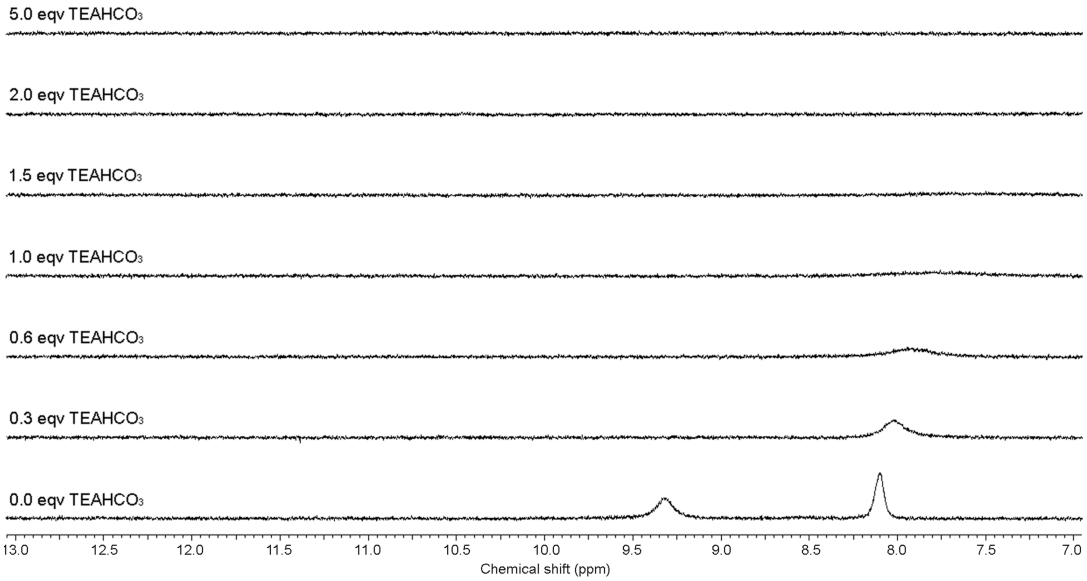

Figure S54. ^{1}H NMR titration of compound **8** with $TEAHCO_3$ in DMSO-d_6 with 0.5 % water at 298K. Stack plot. Peak broadening hindered determination of binding constants.

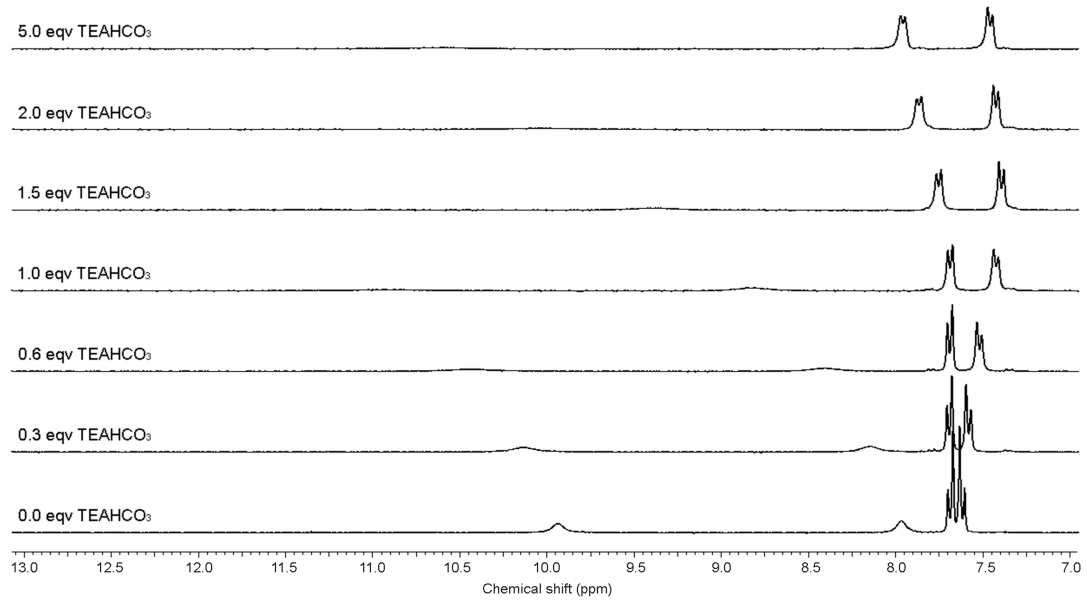

Figure S55. ^{1}H NMR titration of compound **9** with $TEAHCO_3$ in DMSO-d_6 with 0.5 % water at 298K. Stack plot. Peak broadening hindered determination of binding constants.

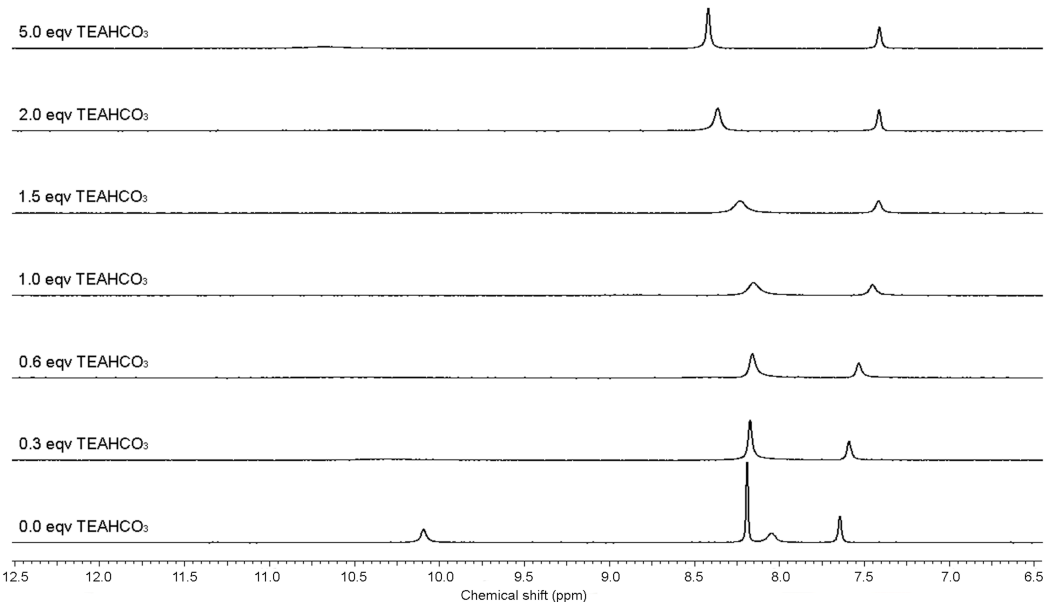

Figure S56. ^{1}H NMR titration of compound **10** with $TEAHCO_3$ in DMSO-d_6 with 0.5 % water at 298K. Stack plot. Peak broadening hindered determination of binding constants.

S4.8 Interaction with $TBANO_3$

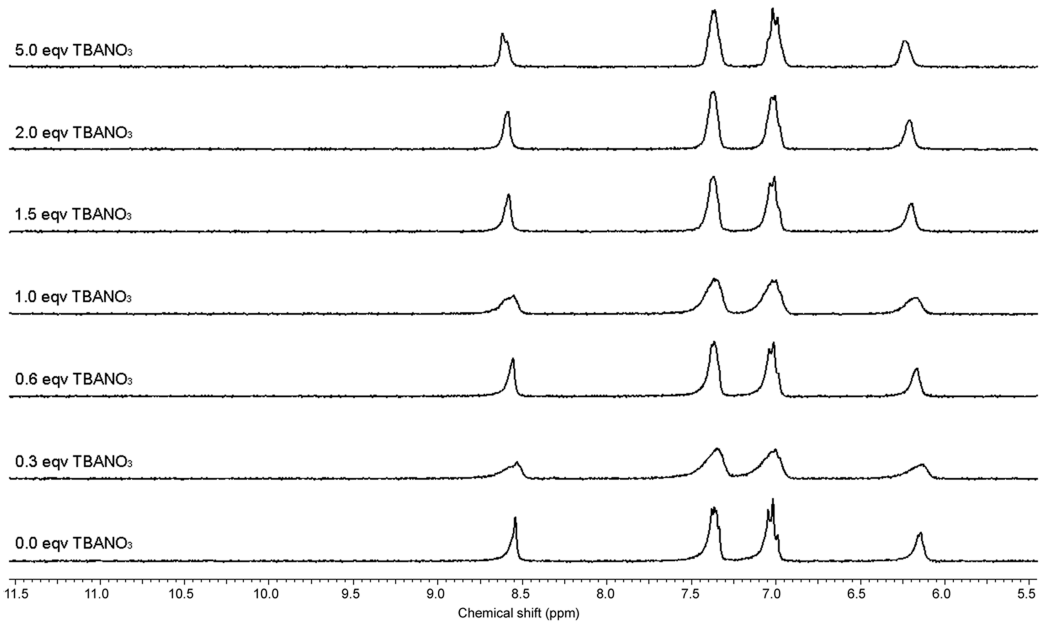

Figure S57. ^{1}H NMR titration of compound **2** with $TBANO_3$ in DMSO-d_6 with 0.5 % water at 298K. Stack plot. No binding detected.

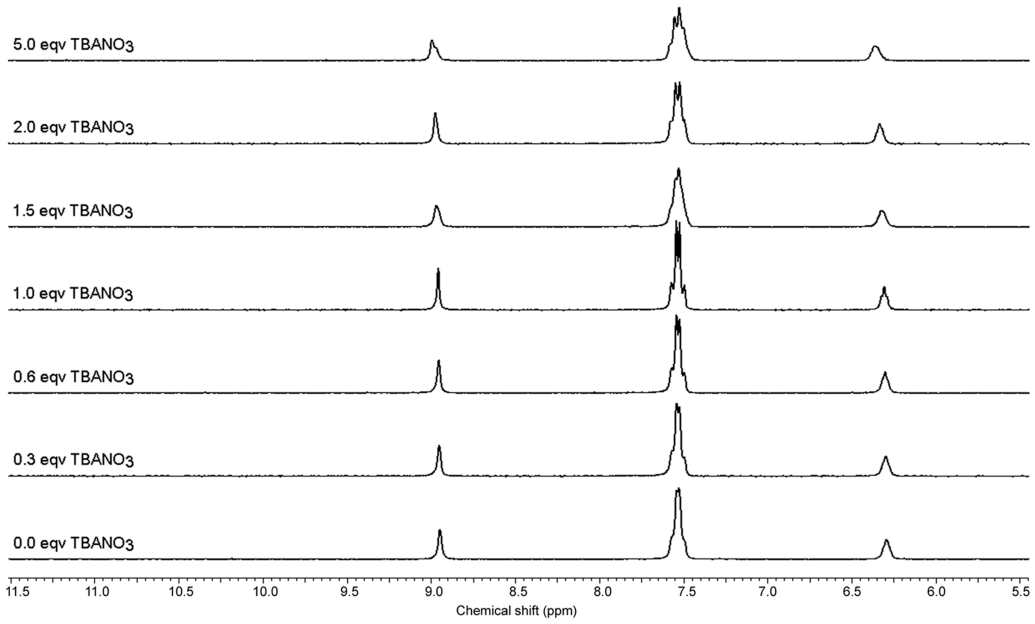

Figure S58. ^{1}H NMR titration of compound **4** with $TBANO_3$ in DMSO-d_6 with 0.5 % water at 298K. Stack plot. No binding detected.

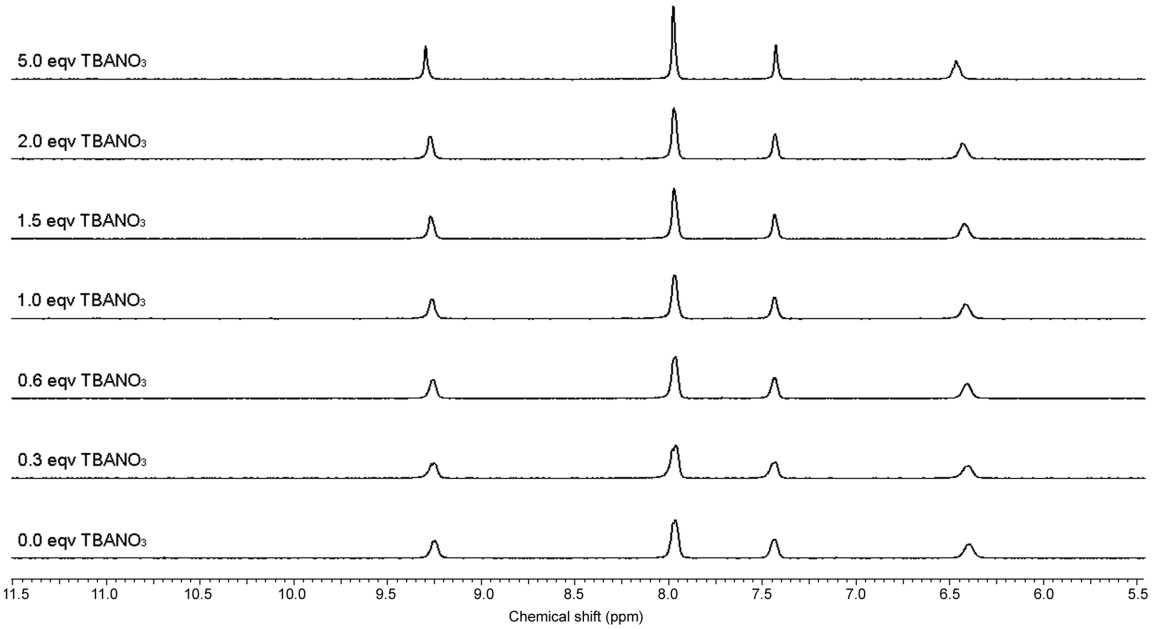

Figure S59. ^{1}H NMR titration of compound **5** with $TBANO_3$ in DMSO-d_6 with 0.5 % water at 298K. Stack plot. No binding detected.

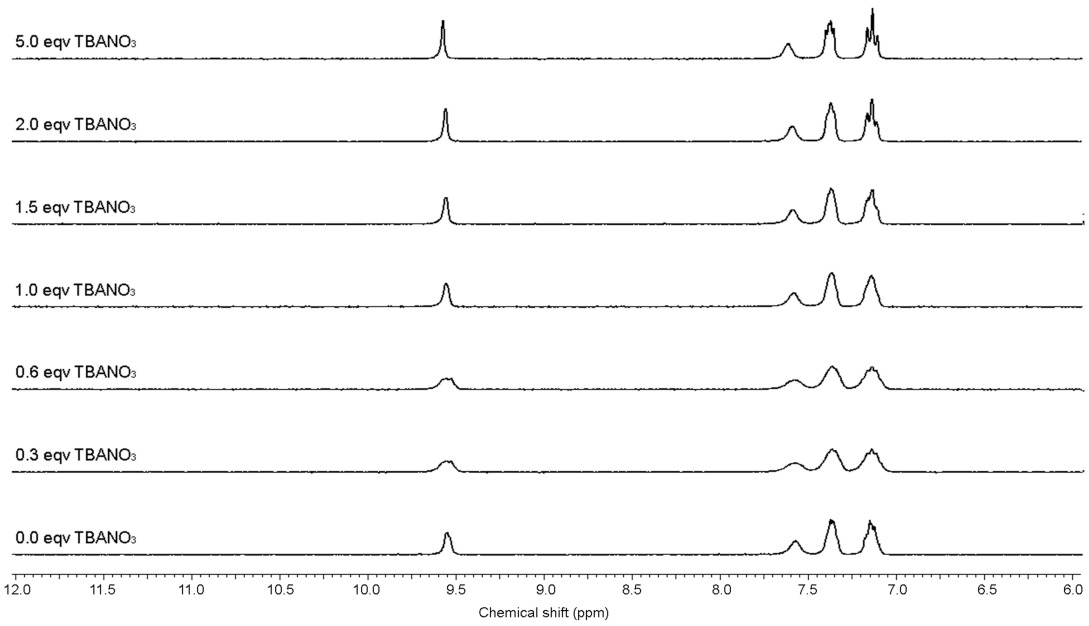

Figure S60. ^{1}H NMR titration of compound **7** with $TBANO_3$ in DMSO-d_6 with 0.5 % water at 298K. Stack plot. No binding detected.

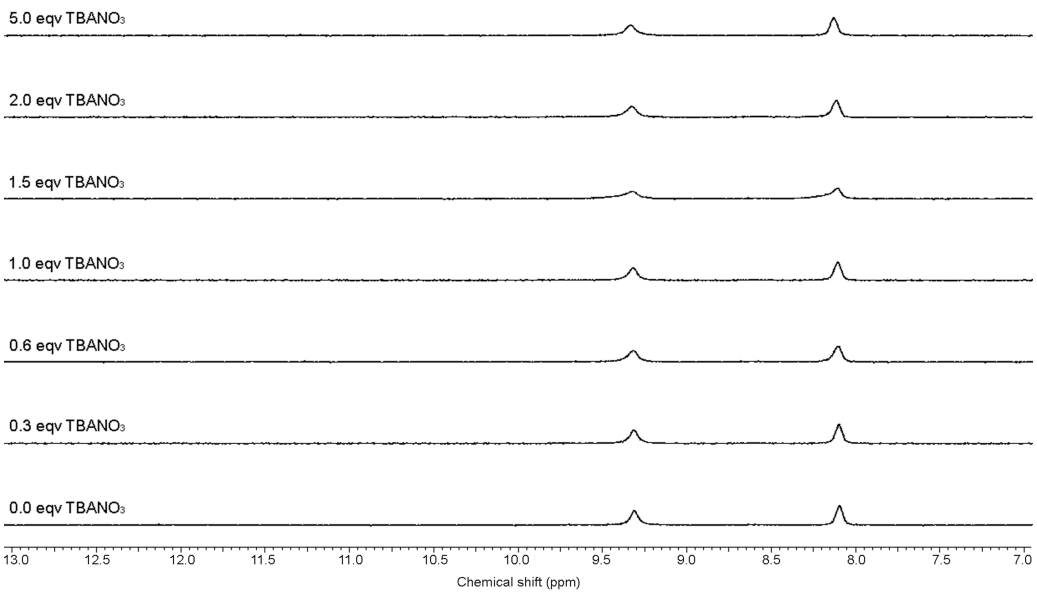

Figure S61. ^{1}H NMR titration of compound **8** with $TBANO_3$ in DMSO-d_6 with 0.5 % water at 298K. Stack plot. No binding detected.

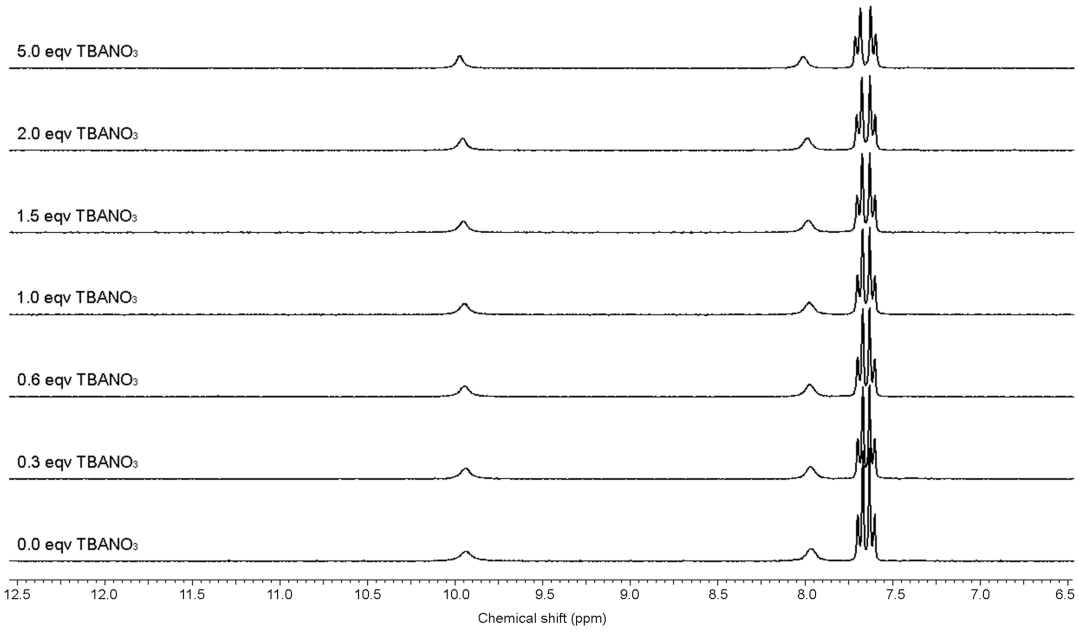

Figure S62. ^{1}H NMR titration of compound **9** with $TBANO_3$ in DMSO-d_6 with 0.5 % water at 298K. Stack plot. No binding detected.

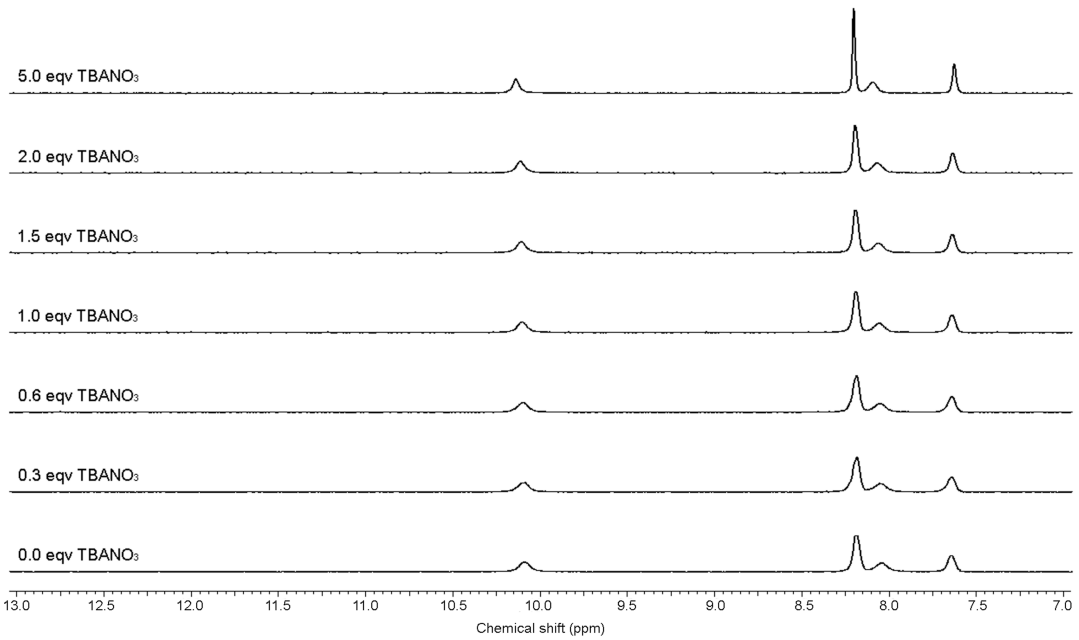

Figure S63. ^{1}H NMR titration of compound **10** with $TBANO_3$ in DMSO-d_6 with 0.5 % water at 298K. Stack plot. No binding detected.

S5. SINGLE CRYSTAL X-RAY DIFFRACTION

Data were collected on a Bruker Nonius KappaCCD with a Mo rotating anode generator. Original unit cell determination was performed using DirAx (Duisenberg, A.J.M.(1992). J. Appl. Cryst. 25, 92-96.).[6] Data collection was according to standard procedures (Data collection software, R. Hooft, Nonius B.V., 1998).[7] Lorentz and polarization corrections were applied during data reduction with DENZO (Z. Otwinowski & W. Minor, *Methods in Enzymology* (1997) Vol. **276**: *Macromolecular Crystallography*, part A, pp. 307−326; C. W. Carter, Jr. & R. M. Sweet, Eds., Academic Press)[8] and multi-scan absorption corrections were applied using SADABS (Sheldrick, G. M. SADABS - Bruker Nonius area detector scaling and absorption correction - V2.10).[9] The structures were solved using SHELXS-97 (G. M. Sheldrick, Acta Cryst. (1990) A**46** 467−473)[10] and refined on *F2* by the full-matrix least-squares technique using the SHELXL-97 program package (G. M. Sheldrick (1997), University of Göttingen, Germany).[11] Graphics are generated using ORTEP-III, MERCURY 1.3 or ViewerLite and Pov-Ray. In all cases the non-hydrogen atoms are refined anisotropically till convergence. Hydrogen atoms were stereochemically fixed at idealized positions and then refined isotropically. Hydrogen bonds are calculated using HTAB command in SHELXL-97.

X-ray data for compound 2 (free ligand), CCDC 830480

Compound **2** and 1.5 equivalents of $TEAHCO_3$ were dissolved in dichloromethane and the mixture was sonicated for 10 minutes. Single crystals suitable for X-ray diffraction were obtained by allowing diethylether to diffuse into this solution at room temperature. No complex with HCO_3^- was formed. Crystal data for compound **2**. $C_{27}H_{30}F_3N_7O_3$, M_r = 557.58, T = 120(2) K, colorless crystals, triclinic, space group P-1, a = 9.4003(3) Å, b = 12.4017(3) Å, c = 12.7967(4) Å, α = 85.417(2)°, β = 70.634(2) °, γ = 72.182(2)°, V = 1339.53(7) Å^3, ρ_c = 1.382 g cm^{-3}, μ = 0.107 m^{-1}, Z = 2, reflections collected: 23343, unique reflections: 6133 (R_{int} = 0.0333), 362 parameters, R indices (all data): R_1 = 0.0662, wR_2 = 0.1065, final R indices [$I > 2\sigma I$]: R_1 = 0.0507, wR_2 = 0.0978, $GOOF$ = 1.076

Table S2. Hydrogen bond properties for **2**

Donor--H···Acceptor	D-H (Å)	H···A (Å)	D···A (Å)	D-H···A (°)	Remark
N2--H2···O2	0.86	2.10	2.9112(18)	156.4	Intra
N3--H3···O2	0.86	2.20	2.9674(18)	148.4	Intra
N4--H4···O3	0.86	2.02	2.8427(18)	159.4	
N5--H5···O3	0.86	2.32	3.0913(18)	148.6	
N7--H7···O1	0.86	2.11	2.8843(18)	149.1	
N6--H6···O1	0.86	2.12	2.8768(18)	146.4	

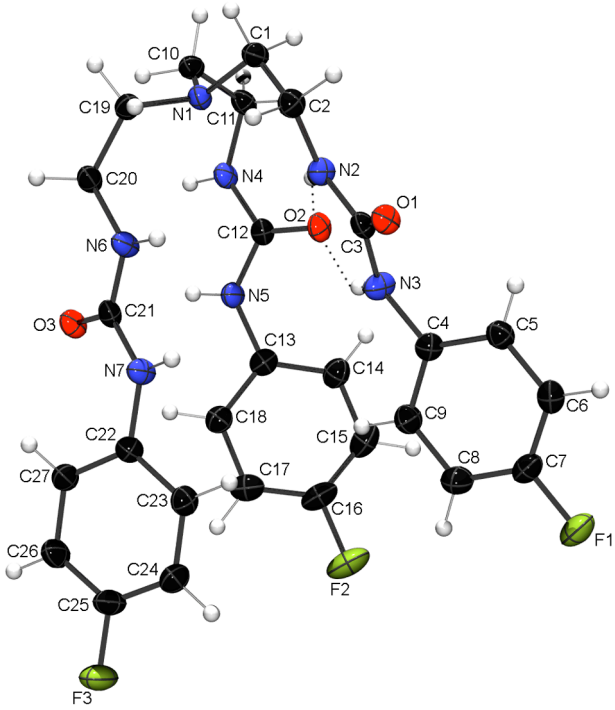

Figure S64. ORTEP diagram of **2** with atom numbering, showing 50 % probability factor for the thermal ellipsoids. Intramolecular hydrogen bonds are represented by dashed lines.

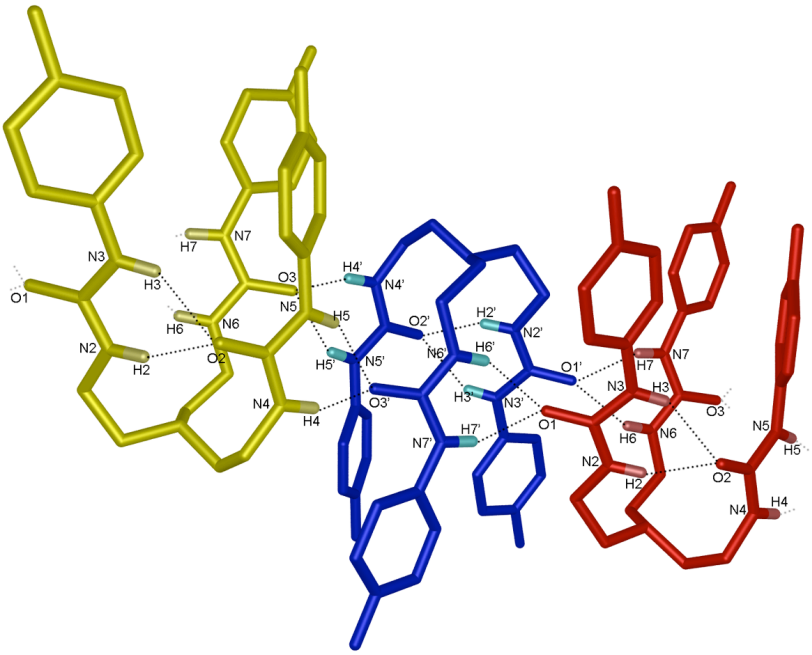

Figure S65. Schematic representation of the intra- and intermolecular hydrogen bonds in the crystal of **2**. For clarity, non-acidic hydrogens are omitted and only atoms involved in hydrogen bonding are labeled.

X-ray data for compound 7 (free ligand), CCDC 830485

Compound **7** was dissolved in 1:1 dichloromethane:diethylether with 10 % methanol. Single crystals suitable for X-ray diffraction were obtained by slow evaporation at room temperature. Crystal data for compound **7**. $C_{27}H_{30}F_3N_7S_3$, M_r = 605.79, T = 120(2) K, colorless crystals, triclinic, space group P-1, a = 7.7351(15) Å, b = 18.620(4) Å, c = 20.778(4) Å, α = 108.11(3)°, β = 90.13(3) °, γ = 95.55(3)°, V = 2829.4(11) Å^3, ρ_c = 1.422 g cm^{-3}, μ = 0.313 m^{-1}, Z = 4, reflections collected: 9528, unique reflections: 9528 (R_{int} = 0.0435), 723 parameters, R indices (all data): R_1 = 0.0846, wR_2 = 0.1559, final R indices [$I > 2\sigma I$]: R_1 = 0.0638, wR_2 = 0.1414, $GOOF$ = 1.083. Two non-merohedral twin components were identified and modeled appropriately (see CIF file).

Table S3. Hydrogen bond properties for **7**

Donor--H···Acceptor	D-H (Å)	H···A (Å)	D···A (Å)	D-H···A (°)	Remark
N10--H10···N2	0.86	2.60	3.452(5)	172.9	Intra
N11--H11···S1	0.86	2.59	3.403(4)	158.2	Intra
N12--H12···N4	0.86	2.64	3.491(5)	172.8	Intra
N13--H13···S2	0.86	2.60	3.410(4)	157.0	Intra
N2--H2···S4	0.86	2.45	3.267(4)	160.0	Intra
N3--H3···S4	0.86	2.47	3.300(4)	161.7	Intra
N4--H4···S3	0.86	2.45	3.269(4)	160.3	Intra
N5--H5A···S3	0.86	2.46	3.289(4)	162.1	Intra
N6--H6A···S2	0.86	2.53	3.339(4)	156.4	
N7--H7···S2	0.86	2.69	3.502(4)	158.1	
N8--H8A···S1	0.86	2.59	3.370(4)	152.0	
N9--H9A···S1	0.86	2.57	3.398(4)	161.7	

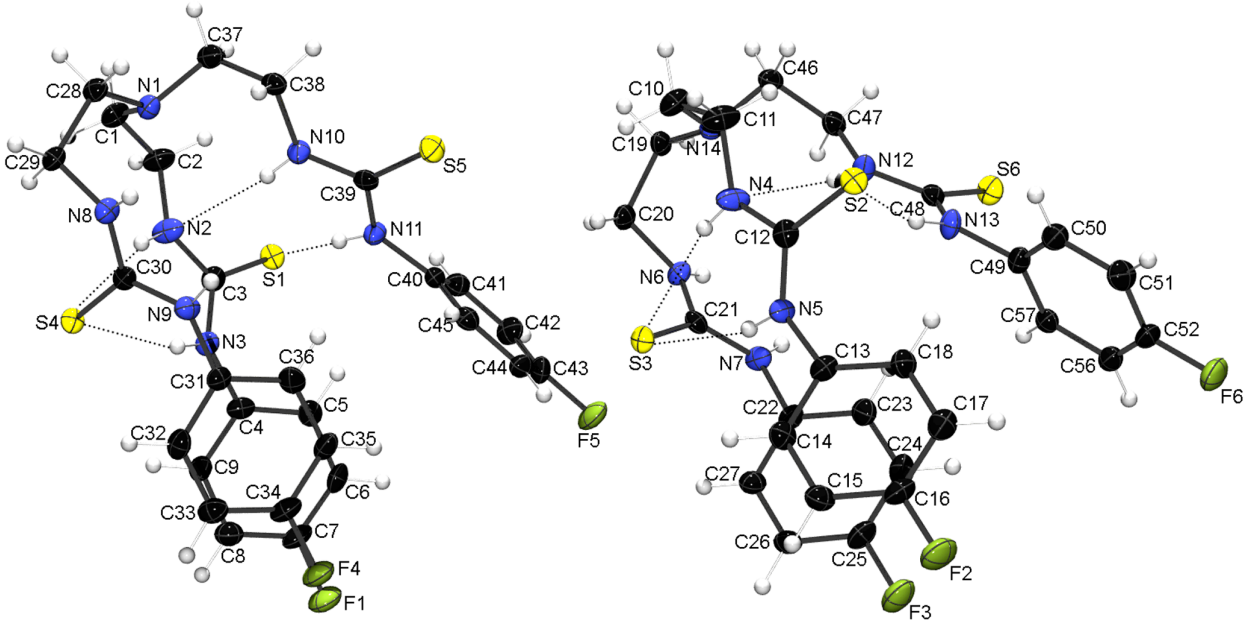

Figure S66. ORTEP diagram of **7** with atom numbering, showing 50 % probability factor for the thermal ellipsoids. Intramolecular hydrogen bonds are represented by dashed lines.

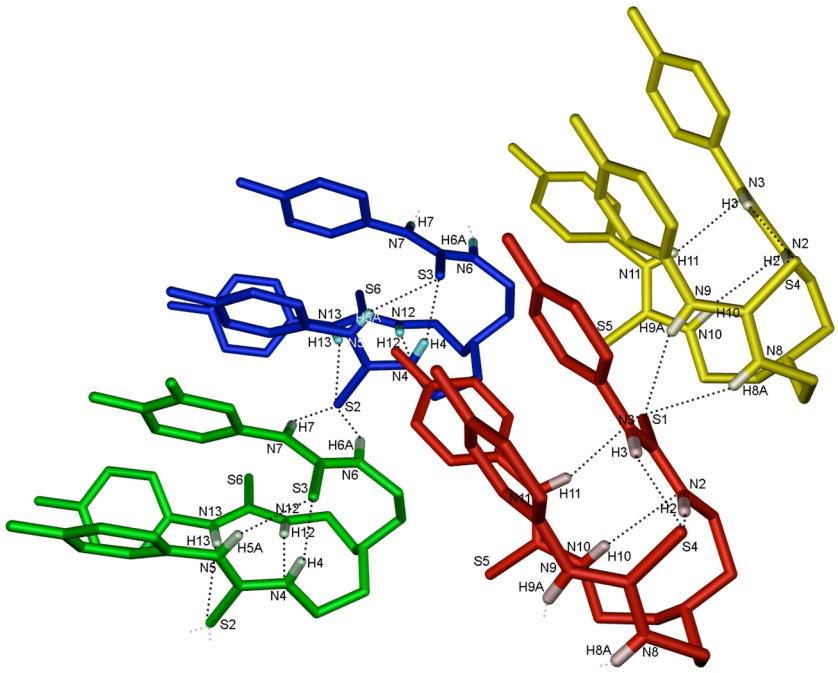

Figure S67. Schematic representation of the intra- and intermolecular hydrogen bonds in the crystal of **7**. For clarity, non-acidic hydrogens are omitted and only atoms involved in hydrogen bonding are labeled.

X-ray data for compound 9 (free receptor), CCDC 830478

Single crystals suitable for X-ray diffraction were obtained by allowing a solution of compound **9** in a 2:1 mixture of ethanol:DCM to slowly evaporate at room temperature. Crystal data for compound (**9**·EtOH). $C_{32}H_{36}F_9N_7OS_3$, M_r = 801.89, T = 120(2) K, colorless crystals, monoclinic, space group P 21/c, a = 9.4376(1) Å, b = 24.6470(2) Å, c = 15.5593(2) Å, α = 90.00º, β = 91.717(1)º, γ = 90.00º, V = 3617.60(7) Å^3, ρ_c = 1.472 g cm^{-3}, μ = 0.290 m^{-1}, Z = 4, reflections collected: 47520, unique reflections: 8287 (R_{int} = 0.0413), 471 parameters, R indices (all data): R_1 = 0.0537, wR_2 = 0.1178, final R indices [$I > 2\sigma I$]: R_1 = 0.0444, wR_2 = 0.1120, $GOOF$ = 1.062

Table S4. Hydrogen bond properties for (**9**·EtOH).

Donor--H···Acceptor	D-H (Å)	H···A (Å)	D···A (Å)	D-H···A (°)	Remark
O1--H10···S2	0.82	2.43	3.2378(14)	171.1	
N3--H3···S3	0.86	2.64	3.4210(16)	150.8	Intra
N4--H4···S1	0.86	2.84	3.5209(15)	137.5	Intra
N5--H5···S1	0.86	2.48	3.3234(15)	168.6	Intra
N6--H6···O1	0.86	2.12	2.929(2)	157.7	
N7--H7···O1	0.86	2.11	2.927(2)	158.3	
N2--H2···S2	0.86	2.79	3.5017(16)	141.3	

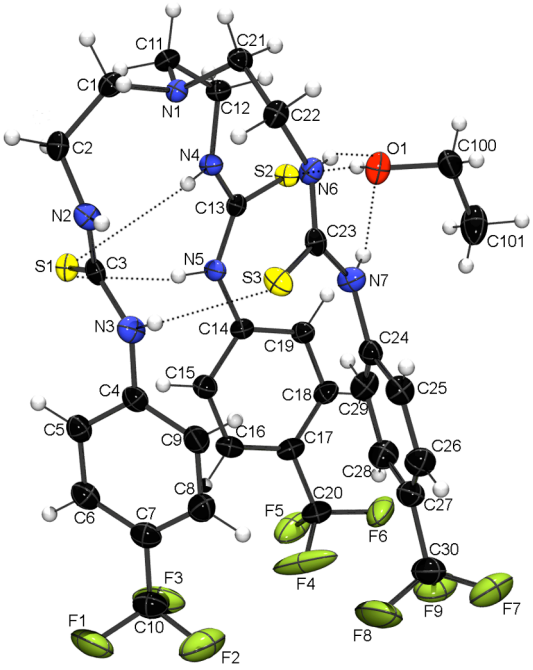

Figure S68. ORTEP diagram of (**9**·EtOH) with atom numbering, showing 50 % probability factor for the thermal ellipsoids. Hydrogen bonds are represented by dashed lines.

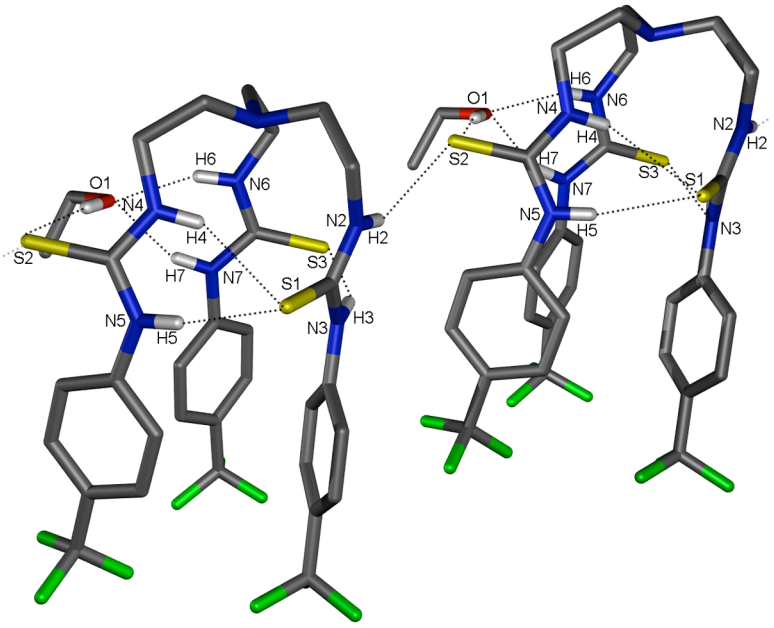

Figure S69. Schematic representation of the intra- and intermolecular hydrogen bonds in the crystal of (**9**·EtOH). For clarity, non-acidic hydrogens are omitted and only atoms involved in hydrogen bonding are labeled.

X-ray data for complex of 2 with chloride, CCDC 830486

Compound **2** and 1.5 equivalents of TBACl were dissolved in dichloromethane and the mixture was sonicated for 10 minutes. Single crystals suitable for X-ray diffraction were obtained by allowing diethylether to diffuse into this solution at room temperature. Crystal data for compound ((**2**⊃Cl·(TBA))$_2$). $C_{43}H_{66}F_3N_8O_3Cl$, M_r = 835.49, T = 120(2) K, colorless crystals, monoclinic, space group P 21, a = 14.296(3) Å, b = 13.337(3) Å, c = 24.209(3) Å, α = 90.00º, β = 103.24(3)º, γ = 90.00º, V = 4493.1(18) Å^3, ρ_c = 1.235 g cm^{-3}, μ = 0.144 m^{-1}, Z = 4, reflections collected: 61699, unique reflections: 18752 (R_{int} = 0.0361), 1047 parameters, R indices (all data): R_1 = 0.0546, wR_2 = 0.1142, final R indices [$I > 2\sigma I$]: R_1 = 0.0484, wR_2 = 0.1111, *GOOF* = 1.154. structure was refined as a racemic twin with Flack parameter = 0.56(3).

Table S5. Hydrogen bond properties for (**2**⊃Cl·(TBA))$_2$.

Donor--H···Acceptor	D-H (Å)	H···A (Å)	D···A (Å)	D-H···A (°)
N2--H2···Cl1	0.86	2.55	3.3568(19)	157.7
N3--H3···Cl1	0.86	2.51	3.3314(18)	160.1
N4--H4···Cl1	0.86	2.62	3.398(2)	151.9
N5--H5A···Cl1	0.86	2.43	3.2681(18)	165.4
N6--H6A···Cl1	0.86	2.78	3.565(2)	152.6
N7--H7···Cl1	0.86	2.40	3.247(2)	170.7
N9--H9A···Cl2	0.86	2.63	3.424(2)	154.1
N10--H10···Cl2	0.86	2.44	3.2447(19)	155.8
N11--H11···Cl2	0.86	2.59	3.392(2)	156.5
N12--H12···Cl2	0.86	2.47	3.308(2)	164.7
N13--H13···Cl2	0.86	2.84	3.600(2)	148.1
N14--H14A···Cl2	0.86	2.35	3.2002(19)	169.6

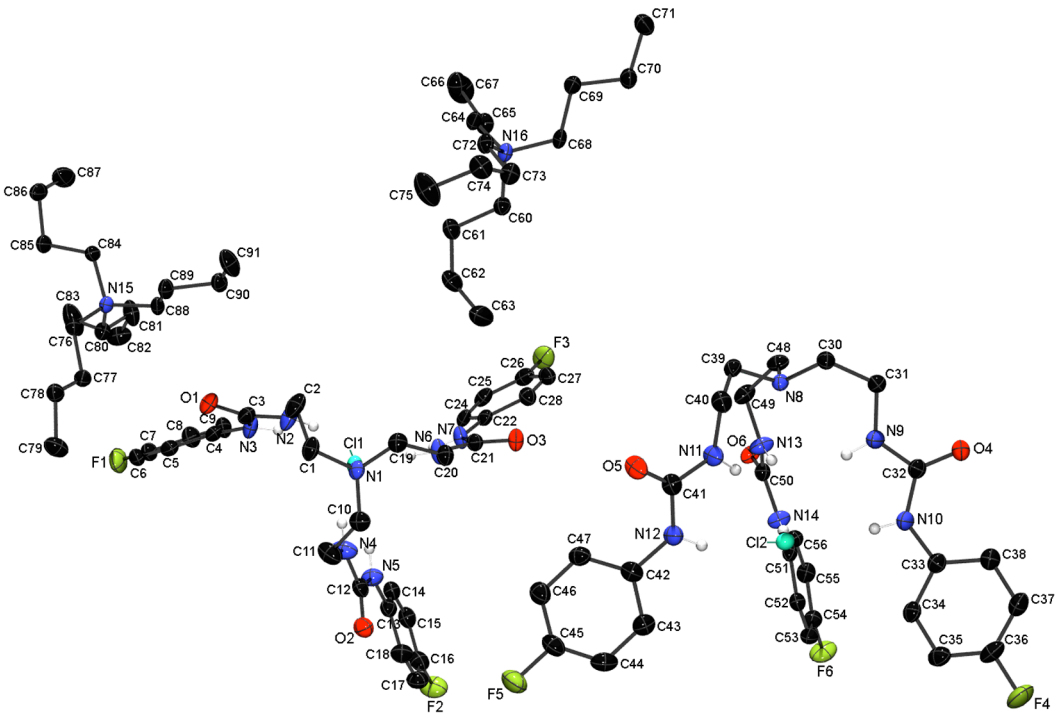

Figure S70. ORTEP diagram of (**2**⊃Cl·(TBA))$_2$ with atom numbering, showing 50 % probability factor for the thermal ellipsoids. Non-acidic hydrogens are omitted for clarity.

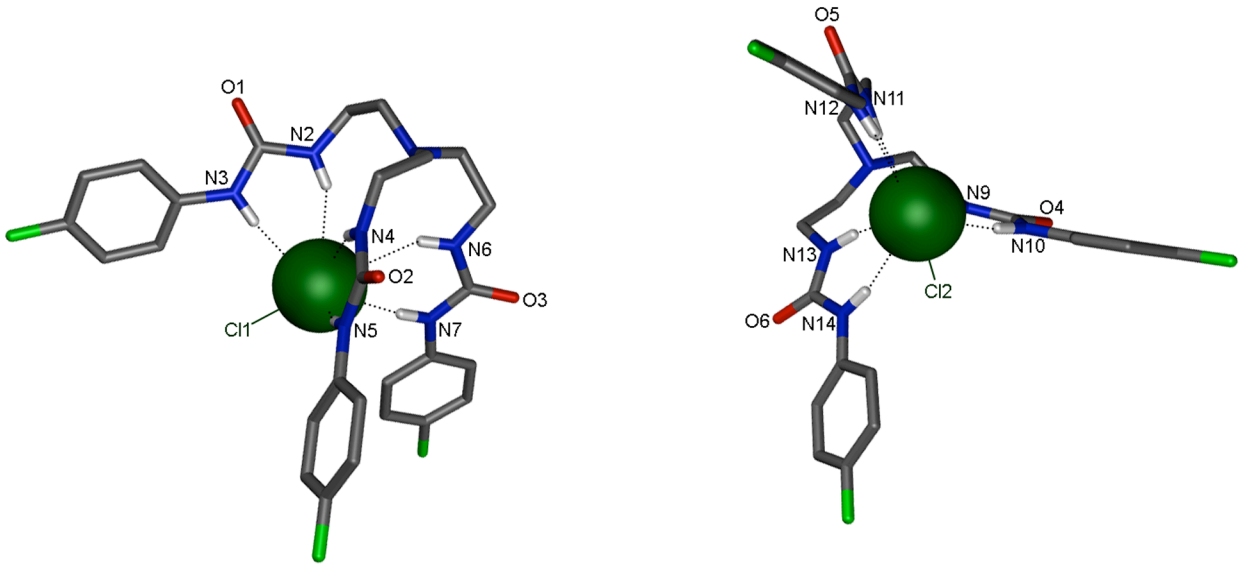

Figure S71. Schematic representation of the hydrogen bonds in the crystal of (**2**⊃Cl·(TBA))$_2$. For clarity, non-acidic hydrogens and TBA counterions are omitted and only atoms involved in hydrogen bonding are labeled. Hydrogen bonds are represented by dashed lines.

X-ray data for complex of 7 with chloride, CCDC 830481

Compound **7** and 1.5 equivalents of TBACl were dissolved in dichloromethane and the mixture was sonicated for 10 minutes. Single crystals suitable for X-ray diffraction were obtained by allowing diethylether to diffuse into this solution at room temperature. Crystal data for compound (**7**⊃Cl·(TBA)). $C_{43}H_{66}F_3N_8S_3Cl$, M_r = 883.70, T = 120(2) K, colorless plates, monoclinic, space group P 21/n, a = 15.5466(2) Å, b = 12.5639(2) Å, c = 24.0788(4) Å, α = 90.00º, β = 98.139(1)º, γ = 90.00º, V = 4655.8(1) Å^3, ρ_c = 1.261 g cm^{-3}, μ = 0.268 m^{-1}, Z = 4, reflections collected: 410699, unique reflections: 7126 (R_{int} = 0.0333), 534 parameters, R indices (all data): R_1 = 0.1058, wR_2 = 0.2449, final R indices [$I > 2\sigma I$]: R_1 = 0.0895, wR_2 = 0.2271, $GOOF$ = 1.013. Disorder present in each arm of tetrabutylammonium (TBA) counterion and in one aromatic ring, atoms have been split over two positions with near equal occupancy.

Table S6. Hydrogen bond properties for (**7**⊃Cl·(TBA)).

Donor--H···Acceptor	D-H (Å)	H···A (Å)	D···A (Å)	D-H···A (°)
N2--H2···Cl1	0.88	2.62	3.438(3)	154.6
N3--H3···Cl1	0.88	2.40	3.255(3)	162.6
N4--H4···Cl1	0.88	2.66	3.456(2)	151.5
N6--H6···Cl1	0.88	2.59	3.391(3)	151.9
N7--H7···Cl1	0.88	2.45	3.250(3)	151.9
N5A--H5A···Cl1	0.88	2.35	3.229(2)	172.5
N5B--H5B···Cl1	0.88	2.36	3.229(2)	172.0

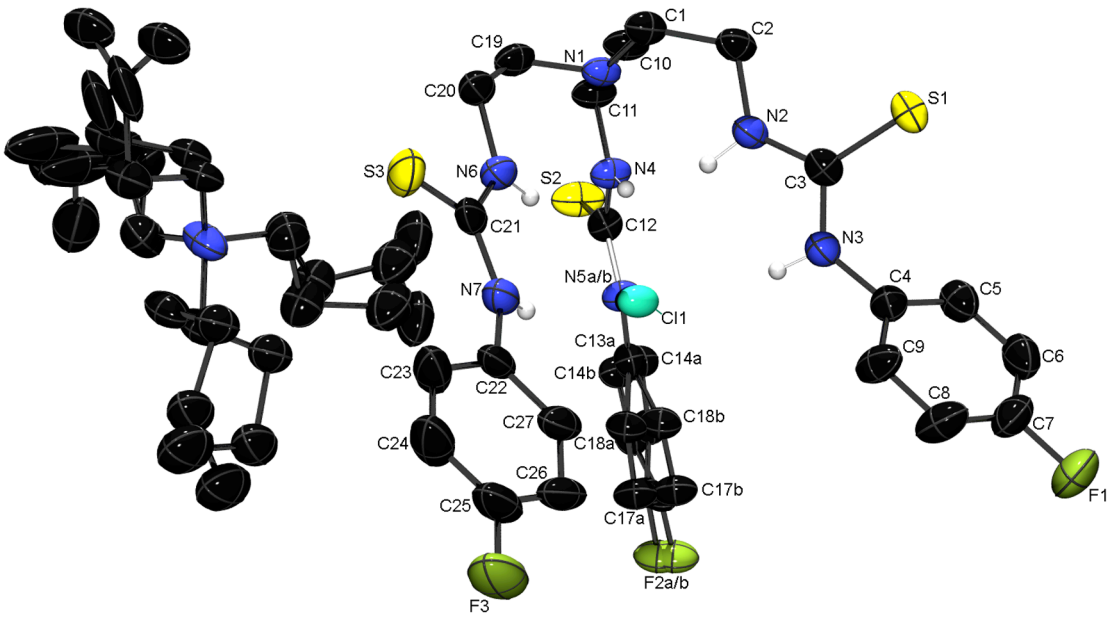

Figure S72. ORTEP diagram of (**7**⊃Cl·(TBA)) with atom numbering, showing 50 % probability factor for the thermal ellipsoids. Non-acidic hydrogens are omitted for clarity. Atoms in TBA counterion (disordered) are not labeled for clarity.

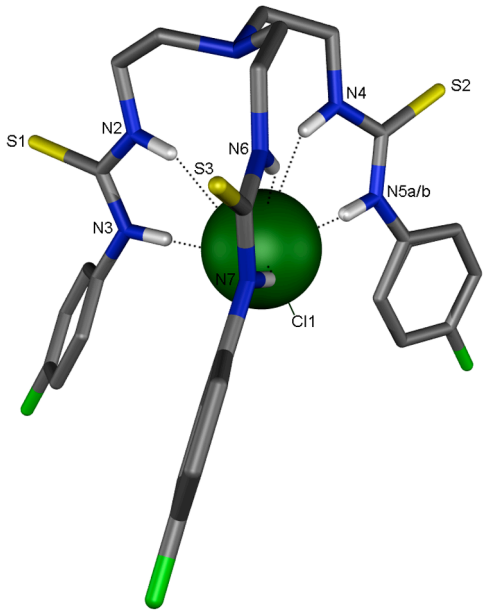

Figure S73. Schematic representation of the hydrogen bonds in the crystal of (**7**⊃Cl·(TBA)). For clarity, non-acidic hydrogens, TBA counterions and disorder are omitted and only atoms involved in hydrogen bonding are labeled. Hydrogen bonds are represented by dashed lines.

X-ray data for complex of 8 with chloride, CCDC 830473

Compound **8** and 1 equivalent of TBACl were dissolved in methanol, heated and stirred for 10 minutes at 40 ºC and than the solvent was evaporated. The oily residue was redissoleved in 1:1:1 DCM/hexane/Et_2O. Single crystals suitable for X-ray diffraction were obtained upon slow evaporation of the solvent mixture. Crystal data for structure (**8**⊃Cl·(TBA)). $C_{43}H_{54}F_{15}N_8S_3Cl$, M_r = 1099.60, T = 120(2) K, colorless crystals, triclinic, space group P -1, a = 11.8830(2) Å, b = 14.0770(2) Å, c = 16.0453(1) Å, α = 80.918(1)º, β = 81.677(1)º, γ = 80.137(1)º, V = 2592.00(6) Å^3, ρ_c = 1.409 g cm^{-3}, μ = 0.288 m^{-1}, Z = 2, reflections collected: 52814, unique reflections: 11615 (R_{int} = 0.0405), 631 parameters, R indices (all data): R_1 = 0.0510, wR_2 = 0.1331, final R indices [$I > 2\sigma I$]: R_1 = 0.0425, wR_2 = 0.1268, $GOOF$ = 1.142

Table S7. Hydrogen bond properties for (**8**⊃Cl·(TBA)).

Donor--H···Acceptor	D-H (Å)	H···A (Å)	D···A (Å)	D-H···A (°)
N2--H2···Cl1	0.86	2.53	3.3293(15)	154.2
N4--H4···Cl1	0.86	2.59	3.3929(15)	155.5
N7--H7···Cl1	0.86	2.44	3.2543(15)	159.2
N6--H6···Cl1	0.86	2.56	3.3506(15)	153.2
N3--H3···Cl1	0.86	2.43	3.2256(16)	153.3
N5--H5···Cl1	0.86	2.42	3.2378(15)	159.0

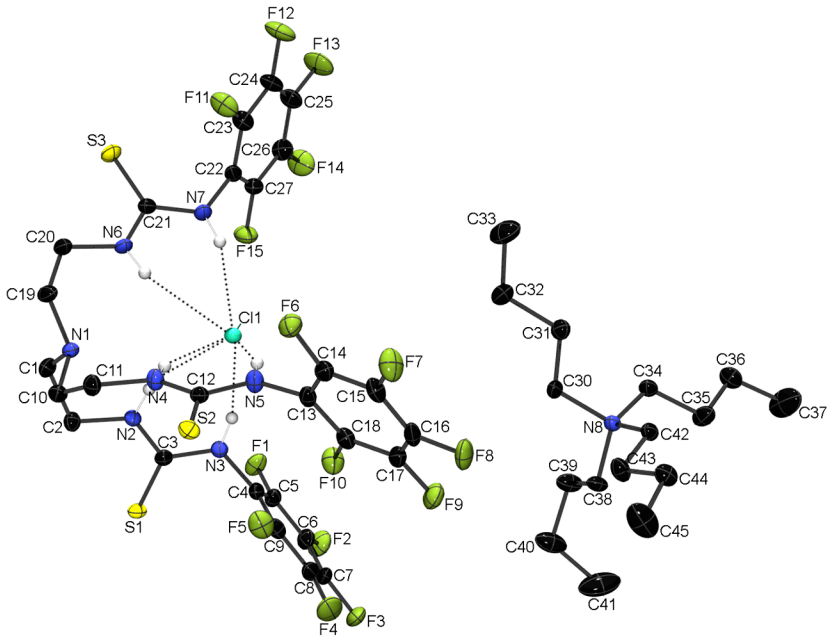

Figure S74. ORTEP diagram of (**8**⊃Cl·(TBA)) with atom numbering, showing 50 % probability factor for the thermal ellipsoids. Non-acidic hydrogens are omitted for clarity. Hydrogen bonds are represented by dashed lines.

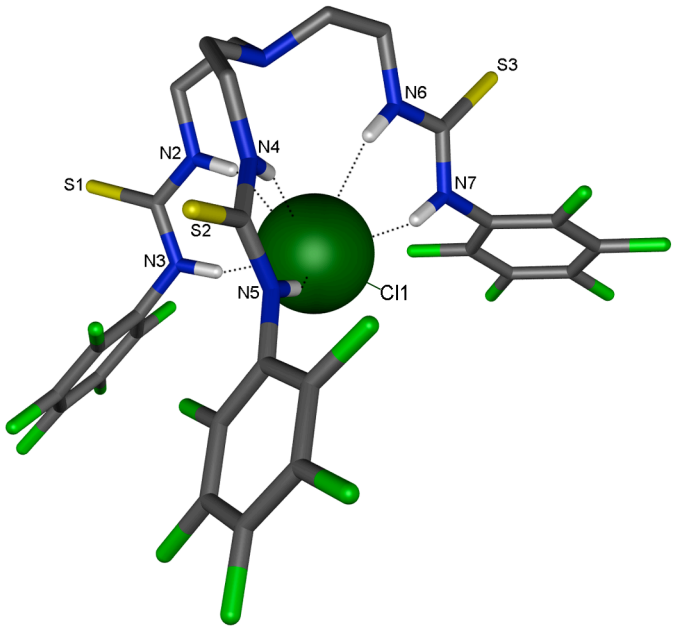

Figure S75. Schematic representation of the hydrogen bonds in the crystal of (**8**⊃Cl·(TBA)). For clarity, non-acidic hydrogens and TBA counterions are omitted and only atoms involved in hydrogen bonding are labeled. Hydrogen bonds are represented by dashed lines.

X-ray data for complex of 7 with sulfate, CCDC 830482

Compound **7** and 1.5 equivalents of TBA_2SO_4 (50 % aqueous solution) were dissolved in dichloromethane and the mixture was sonicated for 10 minutes. The solvents were removed by reduced pressure until all water was removed. After redissolving the residue in dichloromethane, single crystals suitable for X-ray diffraction could be obtained by allowing diethylether to diffuse into this solution at room temperature. Crystal data for structure $((\mathbf{7})_2 \supset SO_4 \cdot (TBA)_2 \cdot (Et_2O)_2)$. $C_{94}H_{152}F_6N_{16}S_7O_6$, M_r = 1940.81, T = 120(2) K, colorless crystal, triclinic, space group P -1, a = 13.3402(2) Å, b = 13.9433(3) Å, c = 16.0351(3) Å, α = 110.739(1)°, β = 108.838(1)°, γ = 97.067(1)°, V = 2543.25(9) Å^3, ρ_c = 1.267 g cm^{-3}, μ = 0.225 m^{-1}, Z = 1, reflections collected: 57930, unique reflections: 11670 (R_{int} = 0.0539), 602 parameters, R indices (all data): R_1 = 0.0789, wR_2 = 0.1606, final R indices [$I > 2\sigma I$]: R_1 = 0.0598, wR_2 = 0.1475, $GOOF$ = 1.040. Oxygen atoms in sulfate are disordered and were split over two equivalent positions (half occupancy for each position).

Table S8. Hydrogen bond properties for $((\mathbf{7})_2 \supset SO_4 \cdot (TBA)_2 \cdot (Et_2O)_2)$.

Donor--H···Acceptor	D-H (Å)	H···A (Å)	D···A (Å)	D-H···A (°)
N2--H2···O4	0.86	2.15	2.917(4)	148.2
N2--H2···O3	0.86	2.24	3.077(4)	164.2
N3--H3···O2	0.86	2.03	2.840(4)	155.9
N3--H3···O1	0.86	2.16	2.965(4)	155.7
N4--H4···O4	0.86	2.15	2.918(4)	149.1
N4--H4···O2	0.86	2.18	3.018(4)	164.5
N5--H5A···O3	0.86	2.25	3.091(4)	165.1
N5--H5A···O1	0.86	2.34	3.082(4)	144.6
N6--H6A···O4	0.86	2.20	2.977(4)	149.8
N6--H6A···O1	0.86	2.43	3.210(4)	151.9
N7--H7···O2	0.86	2.25	3.016(4)	149.1
N7--H7···O1	0.86	2.27	3.051(4)	150.9
N7--H7···O3	0.86	2.46	3.222(4)	147.5
N7--H7···O4	0.86	2.52	3.295(4)	150.4

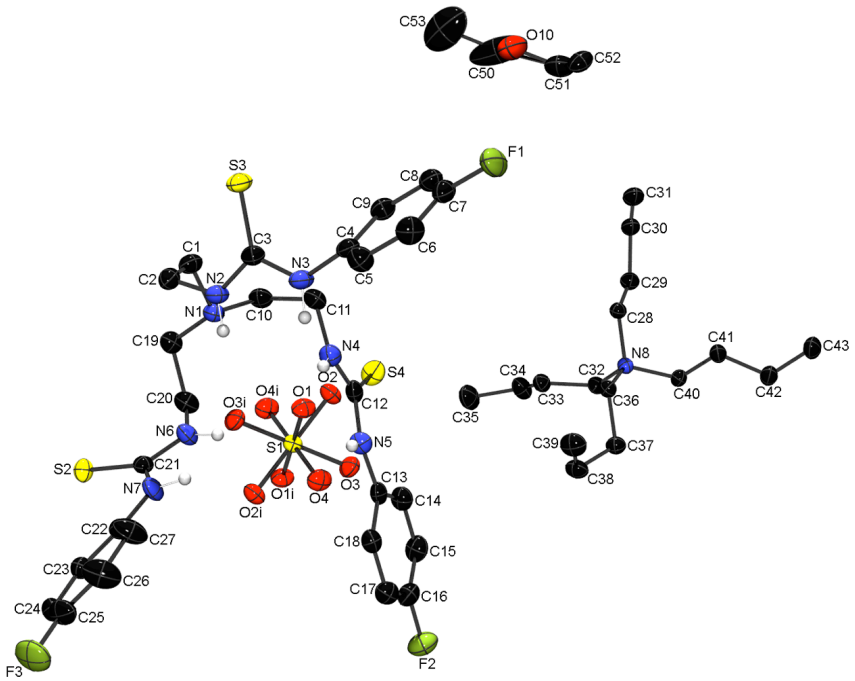

Figure S76. ORTEP diagram of asymmetric unit of ½(($\mathbf{7}$)$_2$⊃SO_4·(TBA)$_2$·(Et$_2$O)$_2$) with atom numbering, showing 50 % probability factor for the thermal ellipsoids. Non-acidic hydrogens are omitted for clarity.

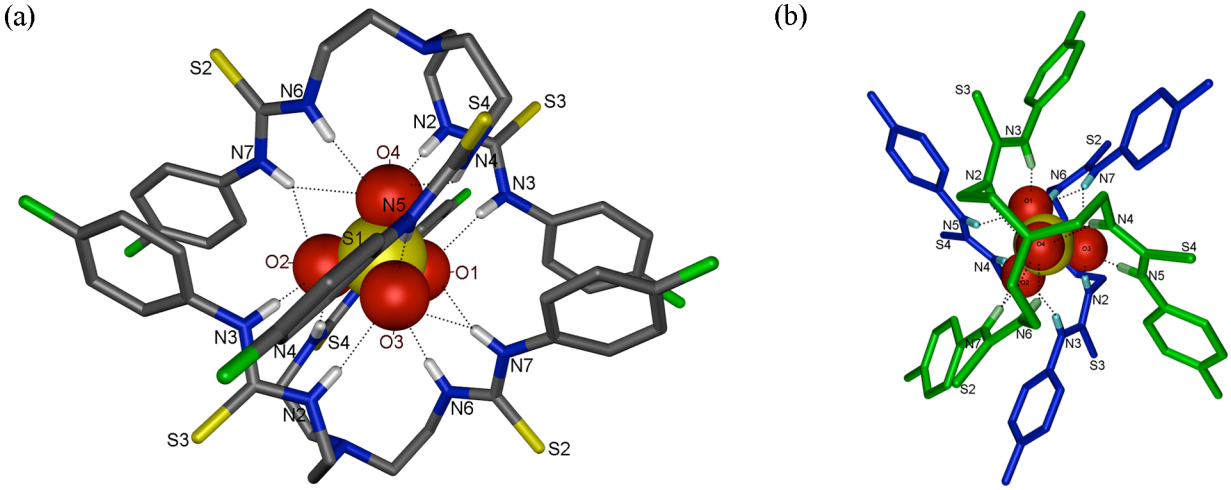

Figure S77. Two views of the hydrogen bonds in the complex of ($\mathbf{7}$)$_2$⊃SO_4. For clarity, non-acidic hydrogens, solvent and TBA counterions are omitted and only atoms involved in hydrogen bonding are labeled. Hydrogen bonds are represented by dashed lines. Disorder in sulfate is omitted (equivalent positions of oxygen are obtained by inversion with sulfur as centre of inversion).

X-ray data for complex of 8 with sulfate, CCDC 830474

Compound **8** and 1 equivalent of TBA_2SO_4 were dissolved in methanol and stirred for 3 hours. After removal of methanol under reduced pressure, the white solid was redissolved in 1:1:1 DCM/hexane/Et_2O. Single crystals suitable for X-ray diffraction were obtained upon slow evaporation of the solvent mixture. Crystal data for structure (**8**⊃SO_4·$(TBA)_2$·(C_6H_{14})). $C_{65}H_{104}F_{15}N_9S_4O_4$, M_r = 1488.85, T = 120(2) K, colorless crystals, monoclinic, space group P 2/n, a = 22.5108(2) Å, b = 12.6543(2) Å, c = 27.6850(4) Å, α = 90.00°, β = 103.915(1)°, γ = 90.00°, V = 7654.8(2) $Å^3$, ρ_c = 1.292 g cm^{-3}, μ = 0.210 m^{-1}, Z = 4, reflections collected: 115284, unique reflections: 13458 (R_{int} = 0.0701), 912 parameters, R indices (all data): R_1 = 0.0970, wR_2 = 0.2084, final R indices [$I > 2\sigma I$]: R_1 = 0.0782, wR_2 = 0.1888, $GOOF$ = 1.171. Disorder present in solvent (hexane) and tetrabutylammonium ions (atoms C48, C49, C56 and C57 were split over two equivalent positions).

Table S9. Hydrogen bond properties for (**8**⊃SO_4·$(TBA)_2$·(C_6H_{14})).

Donor--H···Acceptor	D-H (Å)	H···A (Å)	D···A (Å)	D-H···A (°)
N2--H2···O1	0.86	1.97	2.785(4)	158.3
N3--H3···O2	0.86	1.92	2.757(4)	163.4
N4--H4···O1	0.86	1.99	2.788(4)	153.3
N5--H5···O3	0.86	2.01	2.856(4)	169.0
N6--H6···O1	0.86	2.01	2.784(4)	148.7
N7--H7···O4	0.86	2.04	2.883(4)	166.3
C34--H34A···O4 [a)]	0.97	2.37	3.334(4)	170.7
C42--H42B···O3 [a)]	0.97	2.36	3.326(5)	172.1

[a)] Hydrogen bond / close contact found with PLATON

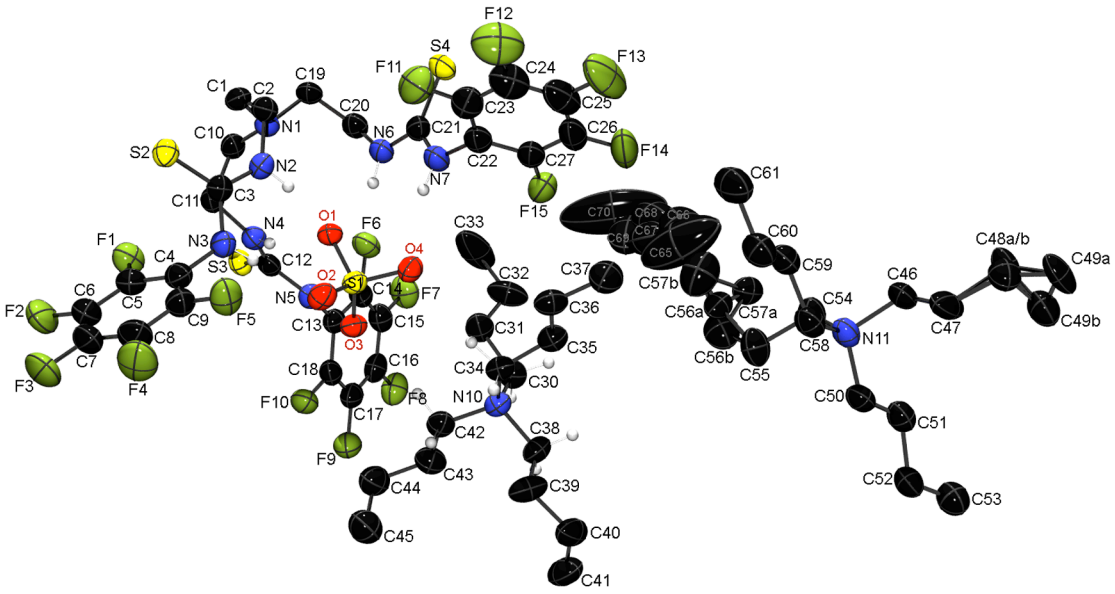

Figure S78. ORTEP diagram of ($\mathbf{8}\supset SO_4\cdot(TBA)_2\cdot(C_6H_{14})$) with atom numbering, showing 50 % probability factor for the thermal ellipsoids. Non-acidic hydrogens are omitted for clarity.

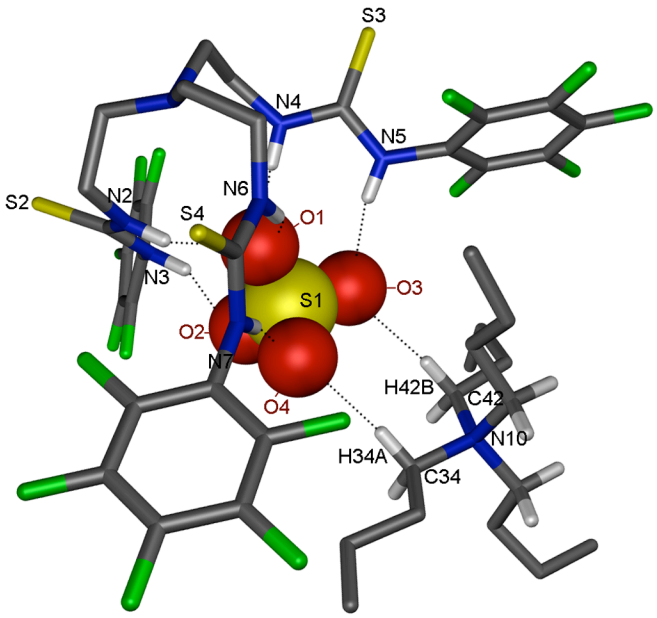

Figure S79. Schematic representation of the hydrogen bonds in the crystal of ($\mathbf{8}\supset SO_4\cdot(TBA)_2\cdot(C_6H_{14})$). For clarity, hexane and non-acidic hydrogens are omitted and only atoms involved in hydrogen bonding are labeled. Only TBA counterion in close contact with the sulfate complex is shown. Hydrogen bonds are represented by dashed lines.

X-ray data for complex of 5 with carbonate, CCDC 830479

Compound **5** and 15 equivalents of $TEAHCO_3$ were dissolved in DMSO with 0.5% water (sample of NMR titration experiment). Most of the solvent was allowed to slowly evaporate at 50 °C. Single crystals suitable for X-ray diffraction were obtained upon cooling down of the remaining mixture. Crystal data for structure ((**5**)$_2$⊃CO_3·$(TEA)_2$·$(DMSO)_2$). $C_{87}H_{106}F_{36}N_{16}O_{11}S_2$, M_r = 2300.02, T = 120(2) K, colorless crystals, monoclinic, space group C 2/c, a = 31.8754(2) Å, b = 17.8361(1) Å, c = 19.9633(1) Å, α = 90.00º, β = 117.6537(4)º, γ = 90.00º, V = 10053.29(11) Å^3, ρ_c = 1.520 g cm^{-3}, μ = 0.185 m^{-1}, Z = 4, reflections collected: 67431, unique reflections: 11481 (R_{int} = 0.0272), 715 parameters, R indices (all data): R_1 = 0.0744, wR_2 = 0.1740, final R indices [$I > 2\sigma I$]: R_1 = 0.0646, wR_2 = 0.1636, $GOOF$ = 1.068. Disorder is present in the -CF_3 substituents of the ligands. The fluorine atoms in –CF_3 group with F4, F5 and F6 have been spli into two positions (85 % and 15 % occupancy). The other –CF_3 groups could not be split properly and restrains were used to limit the size of the thermal ellipsoids.

Table S10. Hydrogen bond properties for ((**5**)$_2$⊃CO_3·$(TEA)_2$·$(DMSO)_2$).

Donor--H···Acceptor	D-H (Å)	H···A (Å)	D···A (Å)	D-H···A (°)
N2--H2···O1	0.86	2.55	3.297(3)	146.4
N3--H3···O2	0.86	1.98	2.8287(19)	170.8
N4--H4···O2	0.86	2.54	3.3918(18)	171.1
N5--H5···O1	0.86	1.99	2.835(2)	167.7
N6--H6···O1	0.86	2.21	3.033(3)	159.1
N7--H7···O1	0.86	2.01	2.863(3)	173.9

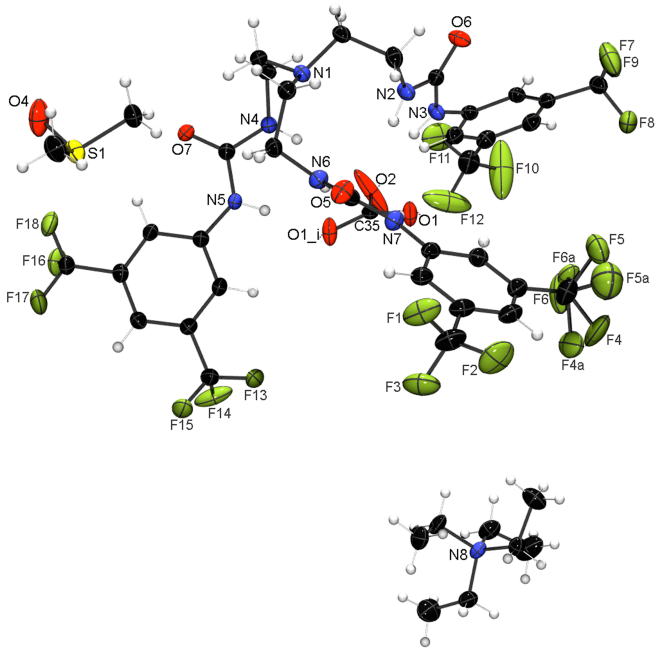

Figure S80. ORTEP diagram of asymmetric unit of $((\mathbf{5})_2 \supset CO_3 \cdot (TEA)_2 \cdot (DMSO)_2)$ with atom numbering, showing 50 % probability factor for the thermal ellipsoids. Non-acidic hydrogens are omitted for clarity.

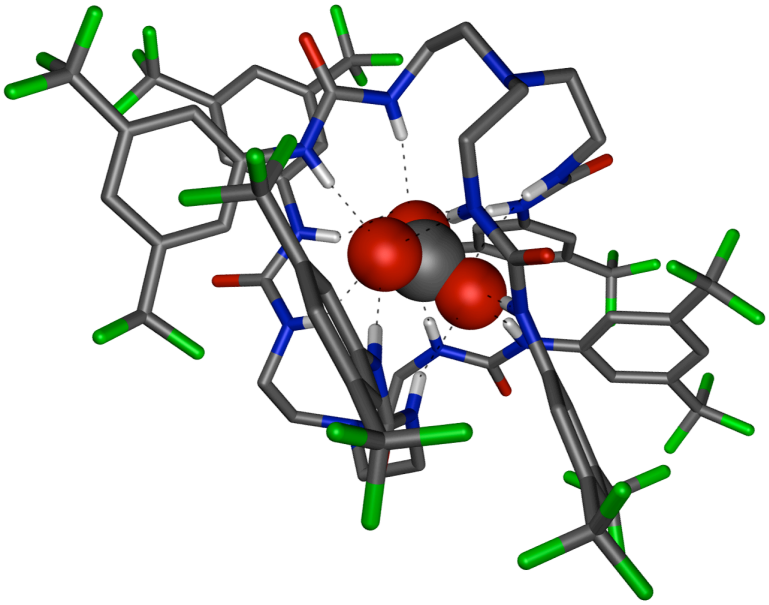

Figure S81. Schematic view of the hydrogen bonds in the crystal of $((\mathbf{5})_2 \supset CO_3 \cdot (TEA)_2 \cdot (DMSO)_2)$. For clarity, TEA counterions, DMSO and non-acidic hydrogens are omitted and only atoms involved in hydrogen bonding are labeled. Hydrogen bonds are represented by dashed lines.

X-ray data for deprotonated 8 (by bicarbonate), CCDC 830475

Compound **8** and 1 equivalent of $TEAHCO_3$ were dissolved in methanol, heated to 40 ºC and allowed to cool down to room temperature and stirred for another 24 hours. The solvent was removed under reduced pressure and the residue was redissolved in 1:1:1 DCM/hexane/Et_2O. Single crystals suitable for X-ray diffraction were obtained upon slow evaporation of the solvent mixture. Crystal data for structure ((**8**-H)$_2$·(TEA)$_2$·(CH_2Cl_2)$_2$). $C_{36}H_{39}F_{15}N_8S_3Cl_2$, M_r = 1035.86, T = 120(2) K, colorless plates, monoclinic, space group P 21/n, a = 23.0166(3) Å, b = 18.0997(2) Å, c = 23.5278(3) Å, α = 90.00º, β = 111.435(1)º, γ = 90.00º, V = 9123.6(2) Å^3, ρ_c = 1.508 g cm^{-3}, μ = 0.379 m^{-1}, Z = 8, reflections collected: 93879, unique reflections: 14907 (R_{int} = 0.0479), 1154 parameters, R indices (all data): R_1 = 0.1275, wR_2 = 0.2721, final R indices [$I > 2\sigma I$]: R_1 = 0.0960, wR_2 = 0.2420, $GOOF$ = 1.048. Disorder is present in TEA, dichloromethane and the aromatic rings of the ligand that could not be modeled by splitting the atom positions. Weak reflections were omitted and SADI and ISOR commands on atoms C101-C108 to model the structure.

Table S11. Hydrogen bond properties for ((**8**-H)$_2$·(TEA)$_2$·(CH_2Cl_2)$_2$). (found with PLATON)

Donor--H···Acceptor	D-H (Å)	H···A (Å)	D···A (Å)	D-H···A (°)
N2--H2···S6	0.86	2.54	3.390(4)	170
N4--H4···S6	0.86	2.70	3.442(5)	145
N5--H5···S6	0.86	2.59	3.357(7)	148
N6--H6···S6	0.86	2.62	3.431(6)	159
N7--H7···S6	0.86	2.54	3.361(7)	160
N9--H9···S1	0.86	2.72	3.440(5)	142
N10--H10···S1	0.86	2.62	3.325(5)	140
N11--H11···S1	0.86	2.71	3.451(5)	144
N12--H12···S1	0.86	2.53	3.337(5)	157
N13--H13···S1	0.86	2.45	3.274(4)	161

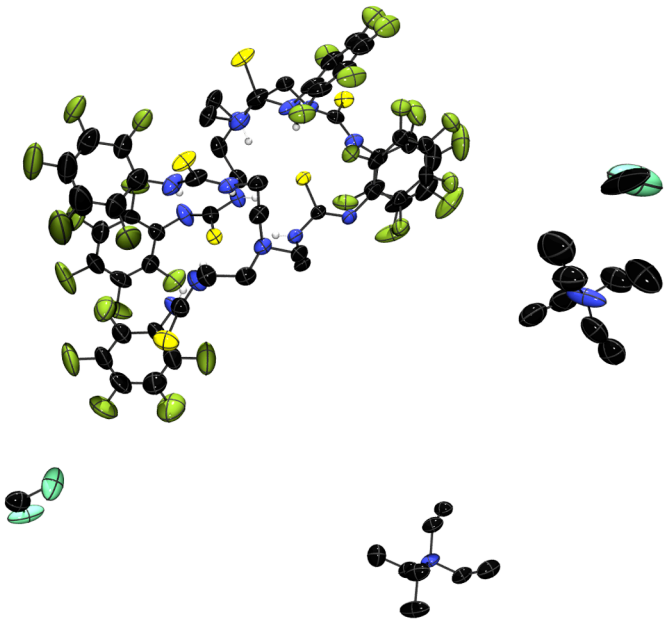

Figure S82. ORTEP diagram of asymmetric unit of ((**8**-H)$_2$·(TEA)$_2$·(CH_2Cl_2)$_2$) with atom numbering, showing 50 % probability factor for the thermal ellipsoids. Non-acidic hydrogens are omitted for clarity.

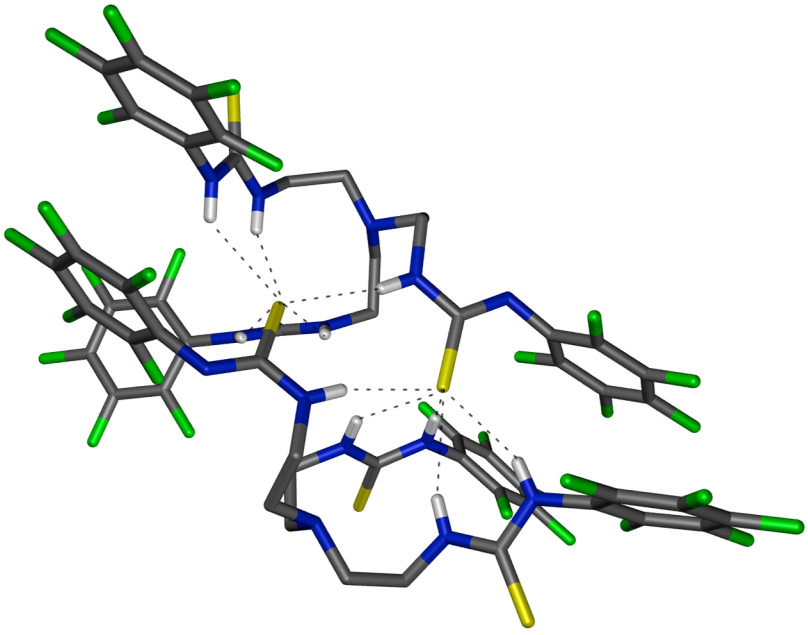

Figure S83. Schematic view of the hydrogen bonds in the crystal of ((**8**-H)$_2$·(TEA)$_2$·(CH_2Cl_2)$_2$). For clarity, TEA counterions, dichloromethane and non-acidic hydrogens are omitted and only atoms involved in hydrogen bonding are labeled. Hydrogen bonds are represented by dashed lines.

X-ray data for complex of 7 with hydrogen phosphate, CCDC 830484

Compound **7** and 2 equivalents of $TBAH_2PO_4$ were dissolved in 1:2:2 DCM/hexane/Et_2O with 10 % methanol. Single crystals suitable for X-ray diffraction were obtained upon slow evaporation of the solvent mixture. Crystal data for structure ((**7**)$_2$⊃HPO_4·$(TBA)_2$). $C_{86}H_{132}F_6N_{16}O_4PS_6$, M_r = 1791.47, T = 120(2) K, colorless crystals, triclinic, space group P -1, a = 13.3126(2) Å, b = 13.8595(2) Å, c = 16.0796(3) Å, α = 110.712(1)°, β = 109.217(1)°, γ = 96.384(1)°, V = 2531.92(20) Å^3, ρ_c = 1.175 g cm^{-3}, μ = 0.214 m^{-1}, Z = 1, reflections collected: 8913, unique reflections: 8913 (R_{int} = 0.0358), 556 parameters, R indices (all data): R_1 = 0.0653, wR_2 = 0.1470, final R indices [$I > 2\sigma I$]: R_1 = 0.0530, wR_2 = 0.1384, $GOOF$ = 1.082. A hydrogen atom is assumed on phosphate for charge balance, but could not be refined due to disorder in the phosphate anion (oxygen atoms are split in two equivalent positions). An attempt was made to model the disordered solvent, which is probably Et_2O, but the results were unsatisfactory. The situation was treated using the Squeeze algorithm.[12]

Table S12. Hydrogen bond properties for ((**7**)$_2$⊃HPO_4·$(TBA)_2$).

Donor--H···Acceptor	D-H (Å)	H···A (Å)	D···A (Å)	D-H···A (°)
N2--H2···O4	0.88	2.08	2.889(4)	152.2
N2--H2···O3	0.88	2.28	3.123(4)	159.6
N3--H3···O2	0.88	1.96	2.800(4)	158.7
N3--H3···O1	0.88	2.15	2.953(4)	150.8
N4--H4···O2	0.88	2.09	2.949(4)	165.0
N4--H4···O4	0.88	2.16	2.942(4)	148.1
N5--H5A···O3	0.88	2.21	3.062(4)	163.3
N5--H5A···O1	0.88	2.31	3.089(4)	147.2
N6--H6A···O4	0.88	2.14	2.922(4)	148.3
N6--H6A···O1	0.88	2.36	3.162(4)	151.2
N7--H7···O1	0.88	2.20	3.010(4)	152.1
N7--H7···O2	0.88	2.26	3.053(4)	149.1
N7--H7···O3	0.88	2.48	3.235(4)	144.4
N7--H7···O4	0.88	2.47	3.253(4)	148.0

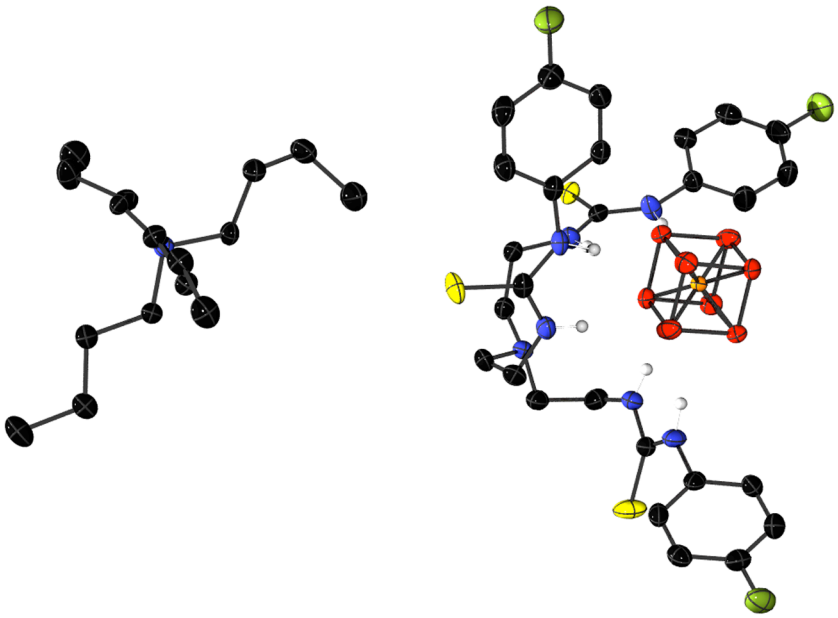

Figure S84. ORTEP diagram of asymmetric unit of ((**7**)$_2$⊃HPO_4·$(TBA)_2$) with atom numbering, showing 50 % probability factor for the thermal ellipsoids. Non-acidic hydrogens are omitted for clarity.

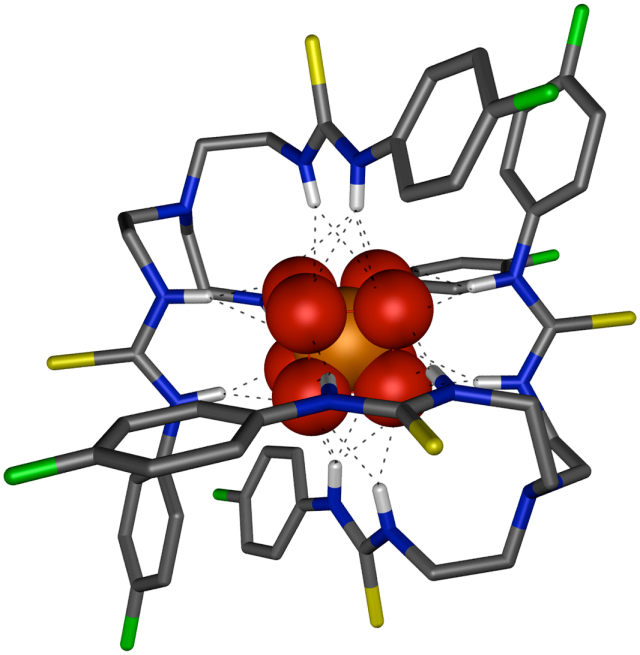

Figure S85. Schematic view of the hydrogen bonds in the crystal of ((**7**)$_2$⊃HPO_4·$(TBA)_2$). For clarity, TBA counterions and non-acidic hydrogens are omitted and only atoms involved in hydrogen bonding are labeled. Hydrogen bonds are represented by dashed lines.

X-ray data for complex of 8 with dihydrogen phosphate, CCDC 830476

Compound **7** and 1 equivalent of $TBAH_2PO_4$ were dissolved in 1:1:1 DCM/hexane/Et_2O and stirred for 30 minutes. Single crystals suitable for X-ray diffraction were obtained upon slow evaporation of the solvent mixture. Crystal data for structure ((**8**)$_2$⊃ $(H_2PO_4)_2$·$(TBA)_2$·$(Et_2O)_2$). $C_{47}H_{66}F_{15}N_8O_5PS_3$, M_r = 1235.26, T = 120(2) K, colorless crystals, triclinic, space group P -1, a = 12.0334(9) Å, b = 16.235(3) Å, c = 16.947(3) Å, α = 76.759(9)°, β = 74.367(11)°, γ = 77.746(10)°, V = 3063.3(10) Å^3, ρ_c = 1.339 g cm^{-3}, μ = 0.240 m^{-1}, Z = 2, reflections collected: 27731, unique reflections: 8755 (R_{int} = 0.120), 715 parameters, R indices (all data): R_1 = 0.1725, wR_2 = 0.3600, final R indices [$I > 2\sigma I$]: R_1 = 0.1323, wR_2 = 0.3319, $GOOF$ = 1.079. The observed reflections were diffuse with an intensity that dropped off quickly at higher angles. This has led to a lower quality refinement than would be desirable. An attempt was made to model the H_2O molecules, but the results were unsatisfactory. The situation was treated using the Squeeze algorithm.[12]

Table S13. Hydrogen bond properties for ((**8**)$_2$⊃ $(H_2PO_4)_2$·$(TBA)_2$·$(Et_2O)_2$).

Donor--H···Acceptor	D-H (Å)	H···A (Å)	D···A (Å)	D-H···A (°)
N2--H2···O1	0.86	2.05	2.881(9)	163.0
N3--H3···O2	0.86	2.00	2.776(10)	150.1
N4--H4···O1	0.86	2.06	2.844(8)	151.8
N5--H5···O4	0.86	2.24	3.057(9)	159.8
N5--H5···O1	0.86	2.56	3.218(8)	134.6
N6--H6···O1	0.86	2.07	2.838(9)	147.9
N7--H7···O3	0.86	2.22	3.067(9)	166.7
O3--H3A···O2	0.82	1.74	2.538(8)	162.2
O4--H4A···O10	0.82	1.81	2.570(9)	153.7

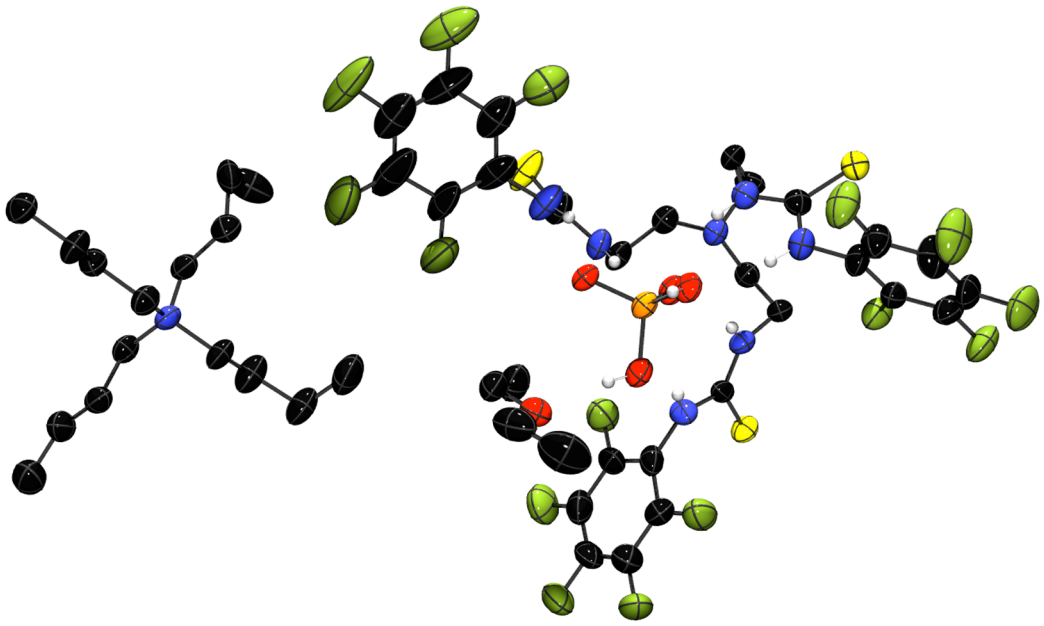

Figure S86. ORTEP diagram of asymmetric unit of $((\mathbf{8})_2\supset (H_2PO_4)_2\cdot(TBA)_2\cdot(Et_2O)_2)$ with atom numbering, showing 50 % probability factor for the thermal ellipsoids. Non-acidic hydrogens are omitted for clarity.

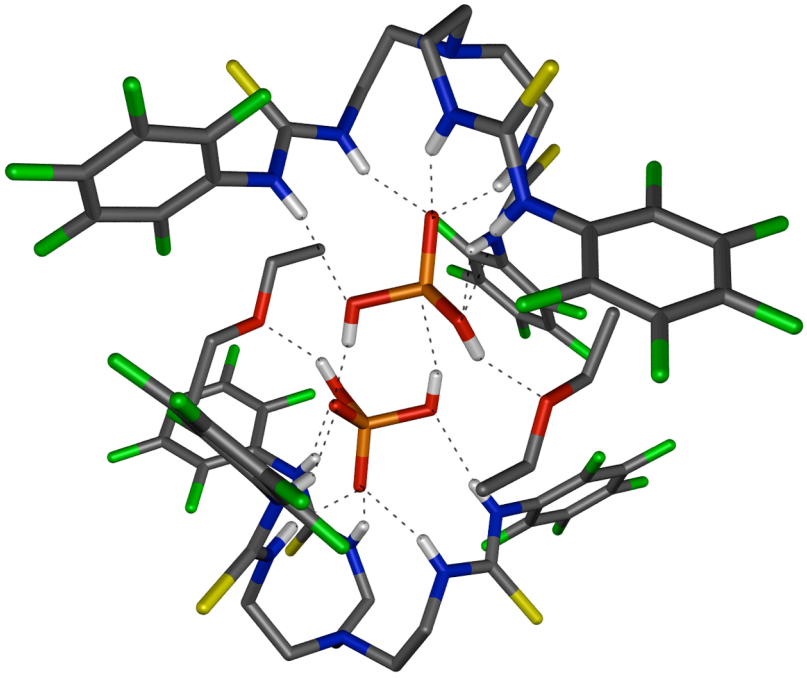

Figure S87. Two views of the hydrogen bonds in the crystal of $((\mathbf{8})_2\supset (H_2PO_4)_2\cdot(TBA)_2\cdot(Et_2O)_2)$. For clarity, TBA counterions and non-acidic hydrogens are omitted and only atoms involved in hydrogen bonding are labeled. Hydrogen bonds are represented by dashed lines.

X-ray data for complex of 10 with hydrogen phosphate, CCDC 830483

Compound **10** and 15 equivalents of $TBAH_2PO_4$ were dissolved in DMSO with 0.5% water (sample of NMR titration experiment) and 10 % methanol was added. Most of the solvent mixture was allowed to slowly evaporate at 50 °C. Single crystals suitable for X-ray diffraction were obtained upon cooling down of the remaining mixture. Crystal data for structure ((**10**)$_2$⊃HPO_4·$(TBA)_2$). $C_{98}H_{126}F_{36}N_{16}O_4PS_6$, M_r = 2499.54, T = 120(2) K, colorless crystals, monoclinic, space group $P21/c$, a = 17.8434(3) Å, b = 26.1975(5) Å, c = 26.2403(5) Å, α = 90.00°, β = 107.687(1)°, γ = 90.00°, V = 11686.3(4) Å^3, ρ_c = 1.421 g cm^{-3}, μ = 0.243 m^{-1}, Z = 4, reflections collected: 104545, unique reflections: 20537 (R_{int} = 0.0778), 1514 parameters, R indices (all data): R_1 = 0.1584, wR_2 = 0.1924, final R indices [$I > 2\sigma I$]: R_1 = 0.0900, wR_2 = 0.1581, *GOOF* = 1.074. A hydrogen is assumed on phosphate for charge balance, but could not be localized. Disorder is present in the –CF_3 groups. Fluorine atoms F4, F5, F6, F31, F32 and F33 were each split over two near equivalent positions (half occupancy), the other fluorine atoms were restrained using ISOR commands.

Table S14. Hydrogen bond properties for ((**10**)$_2$⊃HPO_4·$(TBA)_2$).

Donor--H···Acceptor	D-H (Å)	H···A (Å)	D···A (Å)	D-H···A (°)
N2--H2···O1	0.86	2.08	2.879(6)	153.4
N3--H3···O2	0.86	2.12	2.955(6)	162.8
N4--H4···O1	0.86	2.06	2.878(6)	158.3
N5--H5A···O3	0.86	2.06	2.898(6)	163.9
N6--H6···O1	0.86	2.03	2.881(6)	168.6
N7--H7A···O4	0.86	2.10	2.943(6)	167.0
N9--H9A···O2	0.86	2.28	3.047(6)	148.9
N10--H10···O2	0.86	2.06	2.864(6)	155.1
N11--H11···O3	0.86	2.26	3.029(6)	149.1
N12--H12···O3	0.86	1.99	2.829(6)	164.8
N13--H13···O4	0.86	2.26	3.034(6)	150.6
N14--H14···O4	0.86	2.03	2.870(6)	163.6

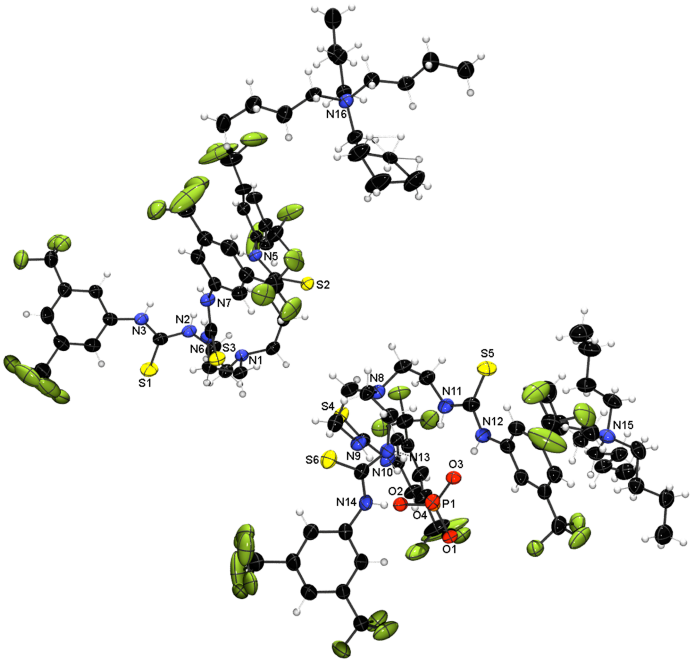

Figure S88. ORTEP diagram of asymmetric unit of ((**10**)$_2$⊃HPO_4·$(TBA)_2$) with atom numbering, showing 50 % probability factor for the thermal ellipsoids. Non-acidic hydrogens are omitted for clarity.

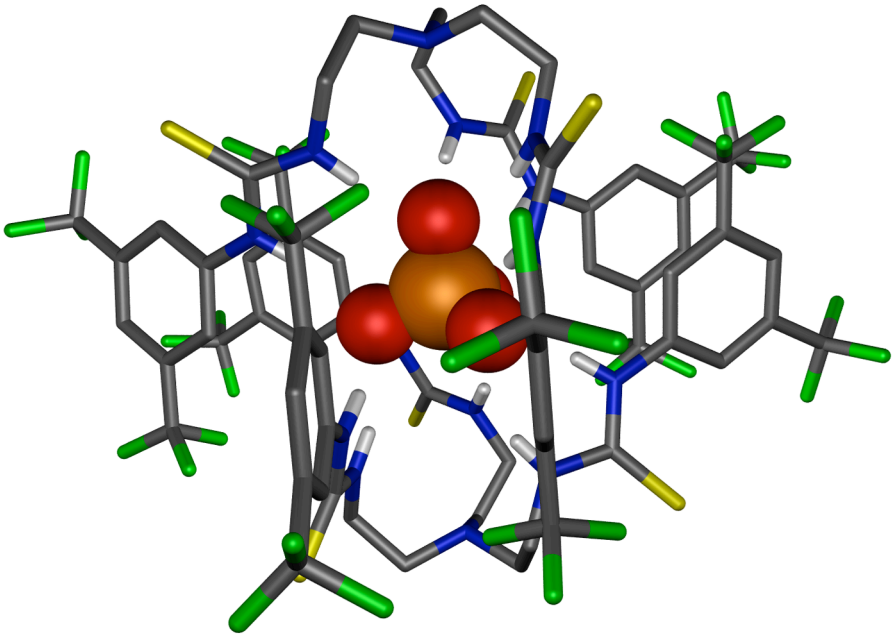

Figure S89. Schematic view of the hydrogen bonds in the crystal of ((**10**)$_2$⊃HPO_4·$(TBA)_2$). For clarity, TBA counterions and non-acidic hydrogens are omitted and only atoms involved in hydrogen bonding are labeled. Hydrogen bonds are represented by dashed lines.

X-ray data for complex of 8 with nitrate, CCDC 830477

Compound **8** and 1 equivalent of $TBANO_3$ were dissolved in methanol and stirred for 24 hours. The solvent was removed under reduced pressure and residue was redissolved in 1:1:1 DCM/hexane/Et_2O. Single crystals suitable for X-ray diffraction were obtained upon slow evaporation of the solvent mixture. Crystal data for structure (**8**⊃NO_3·TBA). $C_{43}H_{54}F_{15}N_9S_3O_3$, M_r = 1126.16, T = 120(2) K, colorless needle, monoclinic, space group P 21/n, a = 18.1581(2) Å, b = 15.6513(2) Å, c = 19.1011(2) Å, α = 90.00º, β = 107.0200º, γ = 90.00º, V = 5190.7(1) Å^3, ρ_c = 1.441 g cm^{-3}, μ = 0.244 m^{-1}, Z = 4, reflections collected: 44715, unique reflections: 9152 (R_{int} = 0.0399), 673 parameters, R indices (all data): R_1 = 0.1197, wR_2 = 0.2300, final R indices [$I > 2\sigma I$]: R_1 = 0.1073, wR_2 = 0.2222, $GOOF$ = 1.054. Disorder is present in the ligand structure that could not be modeled appropriately by splitting the atom positions. ISOR restrains on the fluorine atoms have been used to obtain the best possible result.

Table S15. Hydrogen bond properties for (**8**⊃NO_3·TBA). (found with PLATON)

Donor--H···Acceptor	D-H (Å)	H···A (Å)	D···A (Å)	D-H···A (°)
N2--H2···O2	0.88	2.06	2.921(6)	165
N3--H3···O1	0.88	2.24	2.903(6)	132
N4--H4···O1	0.88	2.08	2.942(7)	166
N5--H5···O3	0.88	2.48	3.005(7)	119
N6--H6···O3	0.88	2.19	3.049(8)	166
N7--H7···O2	0.88	2.25	2.884(6)	129
N7--H7···O3	0.88	2.58	3.366(7)	149

Table S16. Anion-π interactions for (**8**⊃NO_3^-·TBA). (found with PLATON)

Y--X(I)	Cg(J)	X..Cg (Å)	Y-X..Cg (°)	Y..Cg (Å)
C7--F3	Cg(2) [a]	3.275(4)	127.4(3)	4.226(6)
C18--F10	Cg(3) [b]	3.553(6)	109.2(4)	4.176(6)
N10--O2 [c]	Cg(2) [a]	3.013(4)	97.4(3)	3.415(6)

[a] Cg(2) = centre of gravity in 6-membered ring defined by C13, C14, C15, C16, C17 and C18
[b] Cg(3) = centre of gravity in 6-membered ring defined by C22, C23, C24, C25, C26 and C27
[c] Distance N10-C14 = 3.105(7) Å

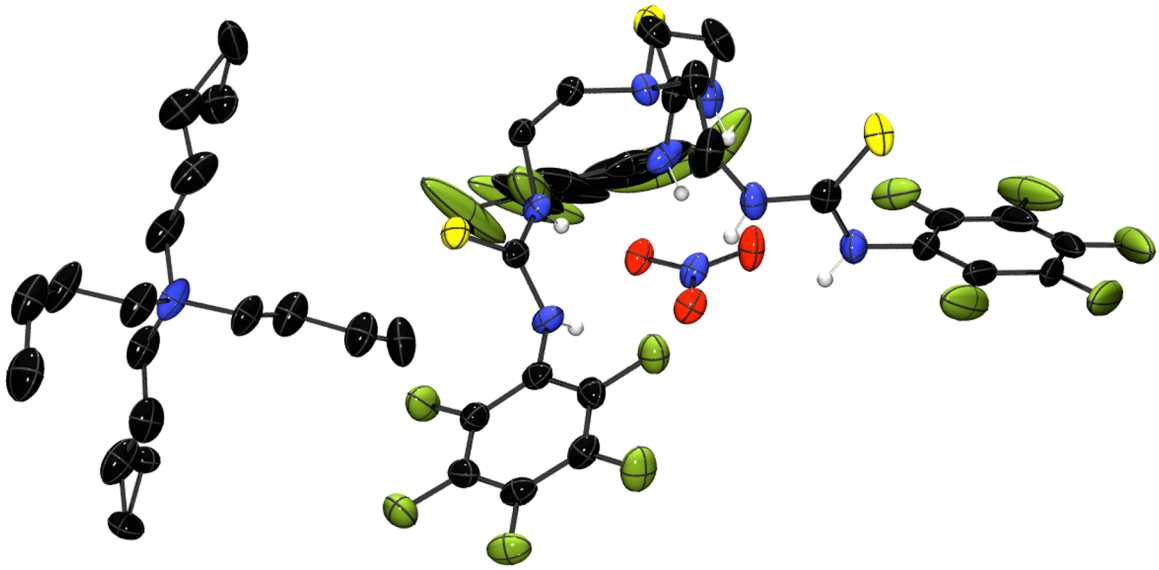

Figure S90. ORTEP diagram of asymmetric unit of (**8**⊃NO_3^-·TBA) with atom numbering, showing 50 % probability factor for the thermal ellipsoids. Non-acidic hydrogens are omitted for clarity.

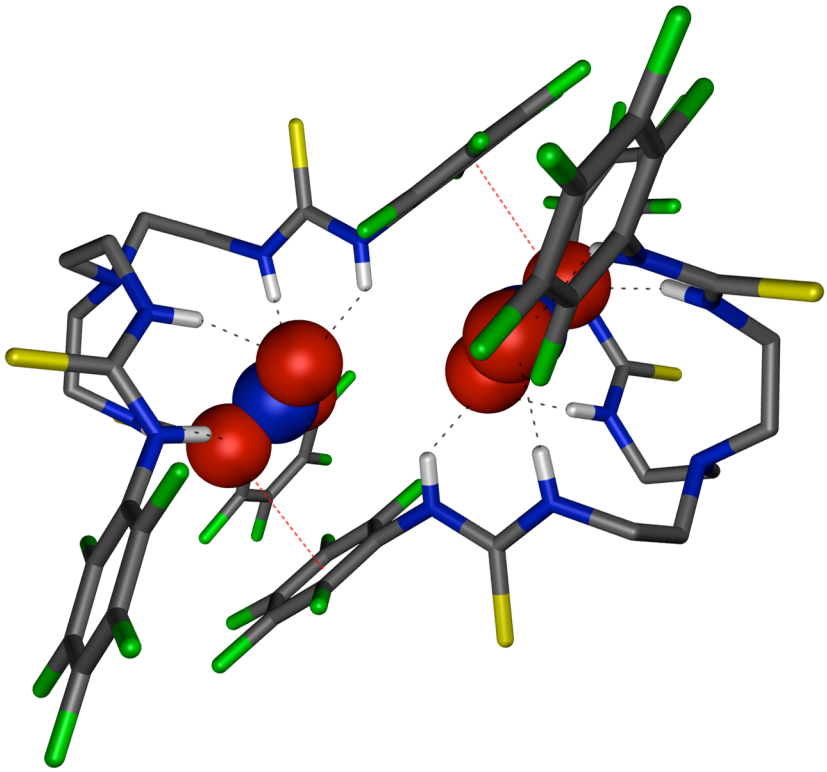

Figure S91. Schematic view of the hydrogen bonds in the crystal of dimeric (**8**⊃NO_3·TBA). For clarity, TBA counterions and non-acidic hydrogens are omitted and only atoms involved in hydrogen bonding are labeled. Hydrogen bonds are represented by dashed lines.

S6. TRANSPORT STUDIES

S6.1. Experimental procedures

These procedures describe typical membrane transport tests as referred to in the article. Internal and external solutions can vary (see caption of figures). Chloride concentrations during transport experiments were determined using an *Accumet* chloride-selective electrode. POPC (1-palmitoyl-2-oleoyl-*sn*-glycero-3-phosphocholine) was supplied by *Genzyme* and was stored at –20°C as a solution in chloroform (1 g POPC in 35 mL chloroform). Polyoxyethylene(8)lauryl ether was used as detergent and was supplied by *TCI*.

Preparation of Vesicles

A lipid film of POPC was formed from a chloroform solution under reduced pressure and dried under vacuum for at least 4 hours. The lipid film was rehydrated by vortexing with a metal chloride (MCl) salt solution (489 mM MCl, 5 mM phosphate buffer at pH 7.2). The lipid suspension was then subjected to nine freeze-thaw cycles, where the suspension was alternatingly allowed to freeze in a liquid nitrogen bath, followed by thawing in a water bath. The lipid suspension was allowed to age for 30 min at room temperature and was subsequently extruded 25 times through a 200 nm polycarbonate membrane. The resulting unilamellar vesicles were dialyzed against the external medium to remove unencapsulated MCl salts.

Chloride/Nitrate Transport Assay

Unilamellar POPC (with 0% or 30% cholesterol) vesicles containing NaCl, prepared as described above, were suspended in the external medium consisting of a 489 mM $NaNO_3$ solution buffered to pH 7.2 with sodium phosphate salts (5 mM buffer). The lipid concentration per sample was 1 mM. A DMSO solution of the carrier molecule was added to start the experiment and the chloride efflux was monitored using a chloride sensitive electrode. At 5 min, the vesicles were lysed with 50 μl of polyoxyethylene(8)lauryl ether (0.232 mM in 7:1 water:DMSO v/v) and a total chloride reading was taken at 7 min. The initial value was set at 0 % chloride efflux and the final chloride reading (at 7 minutes) was set as 100 % chloride efflux. All other data points were calibrated to these points.

Chloride/Bicarbonate Transport Assay

Unilamellar POPC vesicles containing 489 mM NaCl solution buffered to pH 7.2 with 20 mM sodium phosphate salts, prepared as described above, were suspended in the external medium consisting of a 162 mM Na_2SO_4 solution buffered to pH 7.2 with sodium phosphate salts (20 mM buffer). The lipid concentration per sample was 1 mM. A DMSO solution of the carrier molecule (10 mM) was added to start the experiment and chloride efflux was monitored using a chloride sensitive electrode. At 2 min, a $NaHCO_3$ solution (1 M in 162 mM Na_2SO_4 buffered to pH 7.2 with 20 mM sodium phosphate salts) was added so that the outer solution contained 40 mM $NaHCO_3$. At 7 min, the vesicles were lysed with 50 μl of polyoxyethylene(8)lauryl ether (0.232 mM in 7:1 water:DMSO v/v) and a total chloride reading was taken at 9 min. The initial value was set at 0 % chloride efflux and the final chloride reading (at 9 minutes) was set as 100 % chloride efflux. All other data points were calibrated to these points.

HPTS assays (HCl co-transport)

A lipid film of POPC was formed from a chloroform solution under reduced pressure and dried under vacuum for at least 6 hours. The lipid film was rehydrated by vortexing with a NaCl solution (1mM HPTS, 489 mM NaCl, 5 mM phosphate buffer at pH 7.2). The lipid suspension was then subjected to nine freeze-thaw cycles and allowed to age for 30 min at room temperature before extruding 25 times through a 200 nm polycarbonate membrane. The unincorporated HPTS was removed by size exclusion chromatography on a Sephadex G-25 column using a sodium sulfate solution as eluent (162 mM Na_2SO_4, 5 mM phosphate buffer at pH 7.2).

Unilamellar POPC vesicles containing NaCl, prepared as described above, were suspended in a Na_2SO_4 solution buffered to pH 7.2 with sodium phosphate salts. The lipid concentration per sample was 1 mM. A DMSO solution of the carrier molecule (10 mM) was added to start the experiment. The fluoresence of intravesicular HPTS was monitored by excitation at both 403 nm and 460 nm and recording the emission at 510 nm. After 300 s the vesicles were lysed with 30 μl of polyoxyethylene(8)lauryl ether (0.232 mM in 7:1 water:DMSO v/v). The internal pH was obtained by fitting the data to the following equation[1]:

$$pH = \frac{-1}{1.796} \cdot \ln\left(\frac{4.2055}{I_{460nm}/I_{403nm} - 1}\right) + 7.6142$$

Lucigenin assays (Cl^-/SO_4^{2-} antiport)

A lipid film of POPC was formed from a chloroform solution under reduced pressure and dried under vacuum for at least 6 hours. The lipid film was rehydrated by vortexing with a NaCl solution (2 mM lucigenin, 100 mM NaCl, 20 mM phosphate buffer at pH 7.2). The lipid suspension was then subjected to nine freeze-thaw cycles and allowed to age for 30 min at room temperature before extruding 25 times through a 200 nm polycarbonate membrane. The unincorporated lucigenin was removed by size exclusion chromatography on a Sephadex G-25 column using a sodium chloride solution as eluent (100 mM NaCl, 20 mM phosphate buffer at pH 7.2).

Unilamellar POPC vesicles containing NaCl and lucigenin, prepared as described above, were suspended in a NaCl solution buffered to pH 7.2 with sodium phosphate salts. The lipid concentration per sample was 0.5 mM. The internal chloride concentration could be monitored by the fluoresence of intravesicular lucigenin after excitation at 372 nm and recording the emission at 503 nm. At t = 30 s, a stock salt solution was added so that the outer concentration contained 40 mM of the new salt (stock solutions: 1 M $NaNO_3$, 1 M NaCl or 0.5 M Na_2SO_4). After 60 s, a methanol solution of the carrier molecule was added to start ion transport. After 240 s the vesicles were lysed with 30 µl of polyoxyethylene(8)lauryl ether (0.232 mM in 7:1 water:DMSO v/v).

S6.2. Evidence for antiport and co-transport mechanisms

Chloride/nitrate antiport

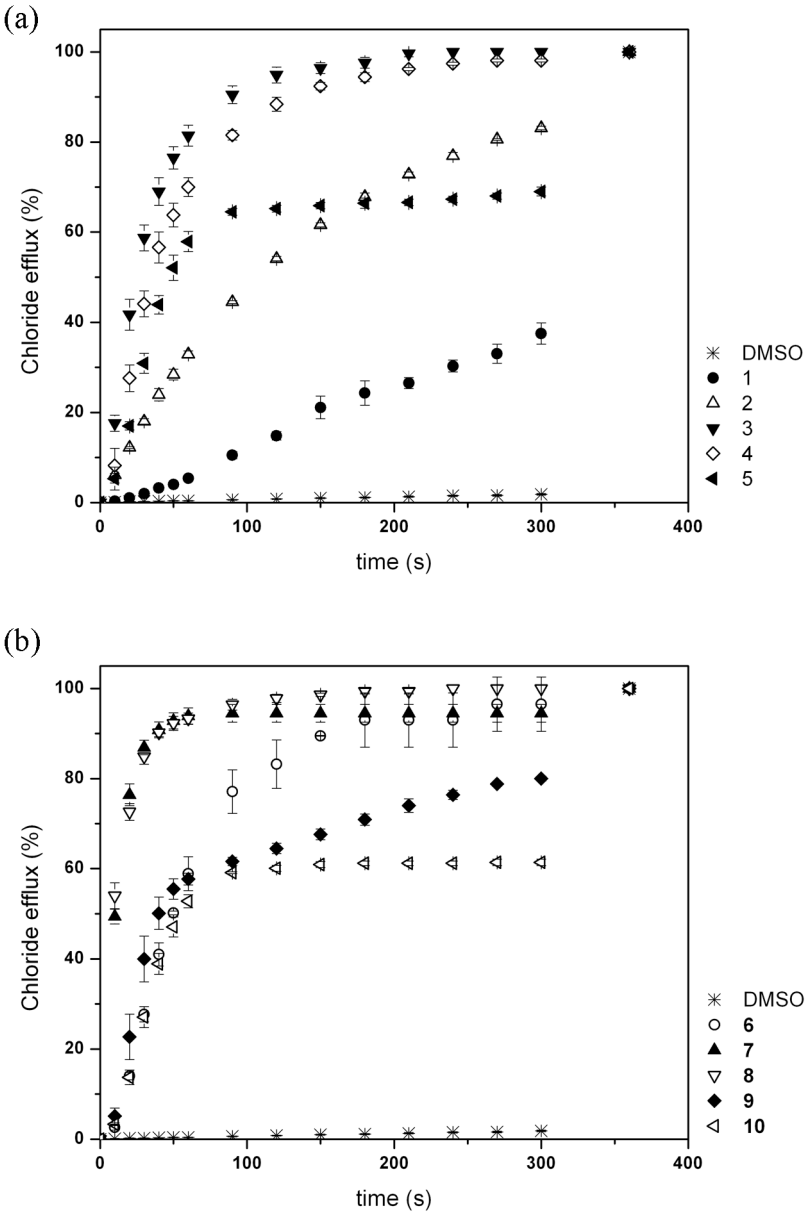

Figure S92. Chloride efflux promoted by **1-10** (2 % molar carrier to lipid) from unilamellar POPC vesicles loaded with 489 mM NaCl buffered to pH 7.2 with 5 mM sodium phosphate salts. The vesicles were dispersed in 489 mM NaNO3 buffered to pH 7.2 with 5 mM sodium phosphate salts. At the end of the experiment, detergent was added to lyse the vesicles and calibrate the ISE to 100 % chloride efflux. Each point represents the average of three trials. (a) urea compounds **1-5**. (b) thiourea compounds **6-10**.

Chloride/bicarbonate antiport

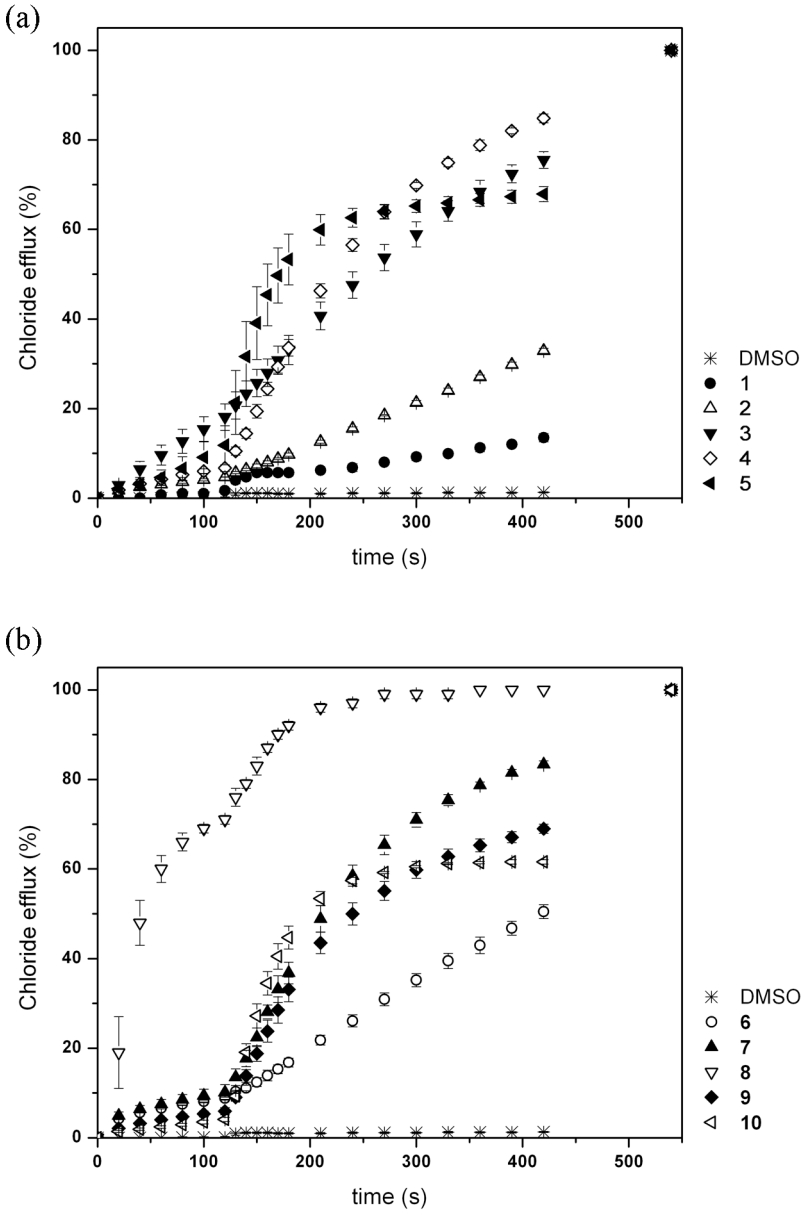

Figure S93. Chloride efflux promoted by **1-10** (2 % molar carrier to lipid) from unilamellar POPC vesicles loaded with 450 mM NaCl buffered to pH 7.2 with 20 mM sodium phosphate salts. The vesicles were dispersed in 162 mM Na_2SO_4 buffered to pH 7.2 with 20 mM sodium phosphate salts. At t = 120s, a solution of $NaHCO_3$ was added to give a 40 mM external concentration. At the end of the experiment, detergent was added to lyse the vesicles and calibrate the ISE to 100 % chloride efflux. Each point represents the average of three trials. (a) ureas **1-5**. (b) thioureas **6-10**.

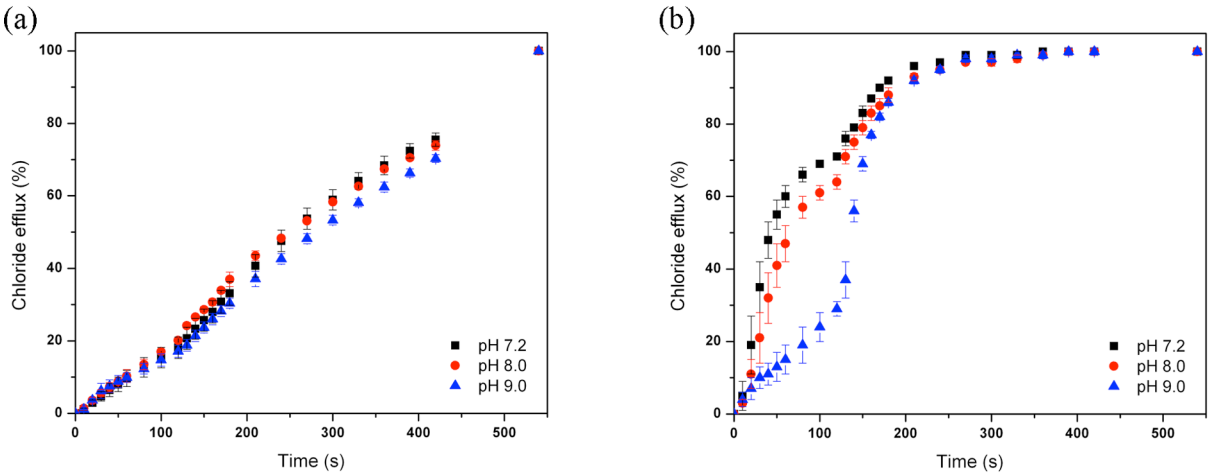

Figure S94. Chloride efflux promoted by **3** or **8** (2 % molar carrier to lipid) from unilamellar POPC vesicles loaded with 450 mM NaCl buffered to pH 7.2 with 20 mM sodium phosphate salts. The vesicles were dispersed in 162 mM Na_2SO_4 buffered to pH 7.2 with 20 mM sodium phosphate salts, or buffered to pH 8.0 or pH 9.0 with Tris buffer. At t = 120s, a solution of $NaHCO_3$ was added to give a 40 mM external concentration. At the end of the experiment, detergent was added to lyse the vesicles and calibrate the ISE to 100 % chloride efflux. Each point represents the average of three trials. (a) urea **3**. (b) thiourea **8**.

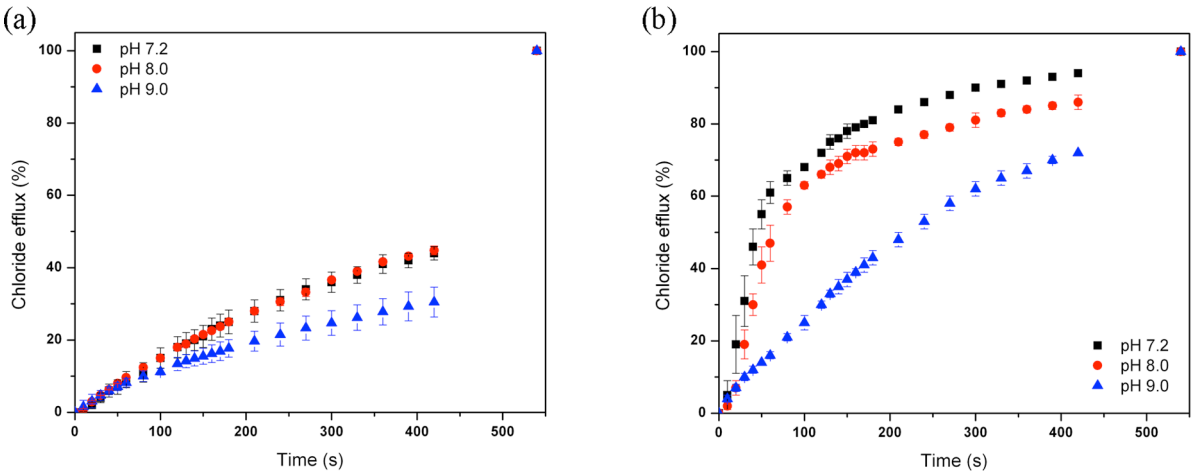

Figure S95. Chloride efflux promoted by **3** or **8** (2 % molar carrier to lipid) from unilamellar POPC vesicles loaded with 450 mM NaCl buffered to pH 7.2 with 20 mM sodium phosphate salts. The vesicles were dispersed in 162 mM Na_2SO_4 buffered to pH 7.2 with 20 mM sodium phosphate salts, or buffered to pH 8.0 or pH 9.0 with Tris buffer. At the end of the experiment, detergent was added to lyse the vesicles and calibrate the ISE to 100 % chloride efflux. Each point represents the average of three trials. (a) urea **3**. (b) thiourea **8**.

HCl co-transport

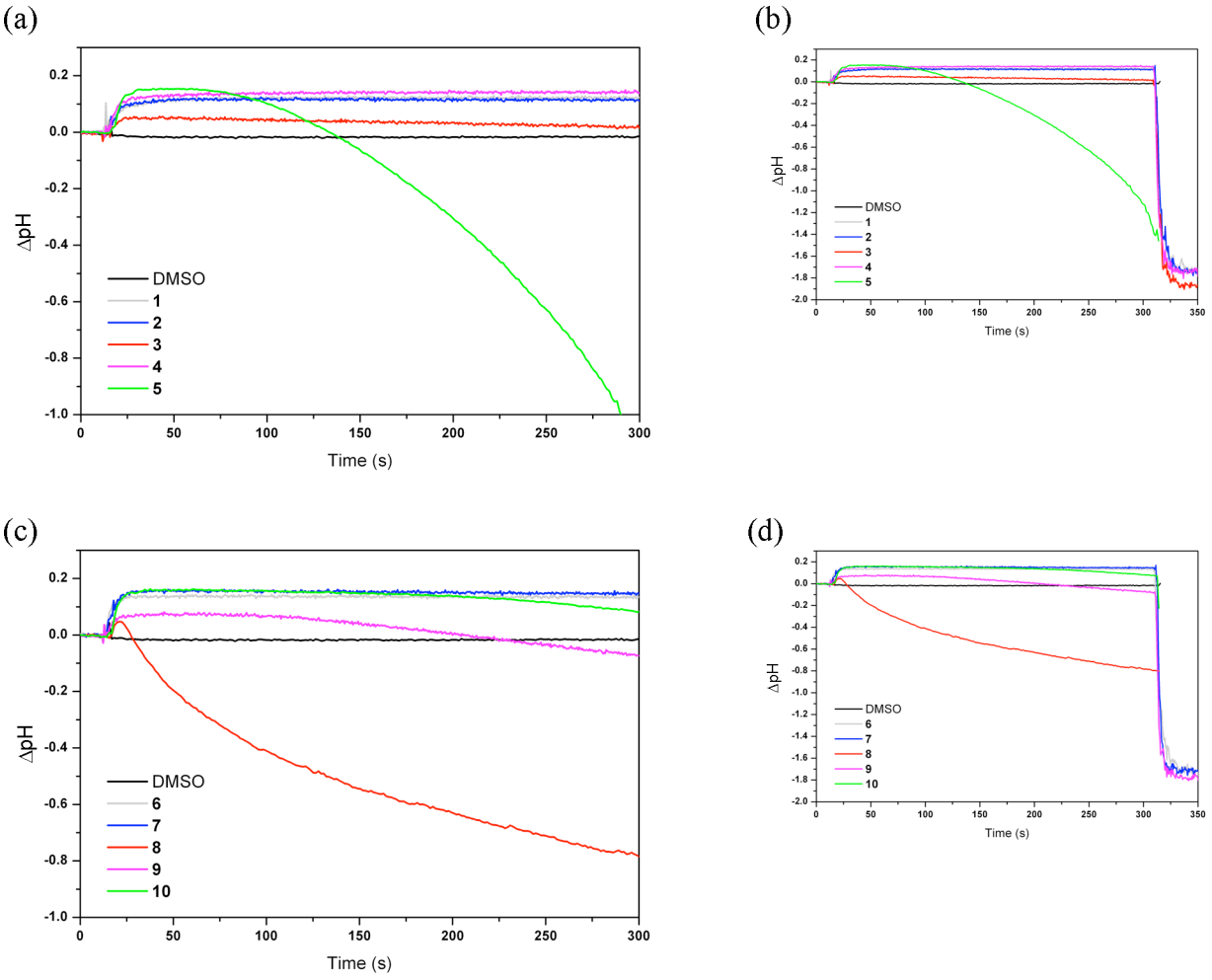

Figure S96. Intravesicular pH change promoted by **1-10** (2 % molar carrier to lipid) from unilamellar POPC vesicles loaded with 1 mM HPTS and 489 mM NaCl, buffered to pH 7.2 with 5 mM sodium phosphate salts. The vesicles were dispersed in 162 mM Na_2SO_4 buffered to pH 7.2 with 5 mM sodium phosphate salts. At t = 15 s, a DMSO solution of the putative transporters was added to start the experiment. At the end of the experiment (t = 300 s), detergent was added to lyse the vesicles. Each point represents the average of three trials. (a) ureas **1-5**, close-up view. (b) ureas **1**-**5**, total experiment. (c) thioureas **6-10**, close-up view. (d) thioureas **6**-**10**, total experiment.

Chloride/sulfate antiport

In this experiment, there is no chloride gradient or pH gradient and HCl co-transport becomes very unlikely. The transport mechanism that can occur is antiport of chloride with the anion that was spiked into the external solution at t = 30 s. Increase in fluorescence indicates that lucigenin is no longer quenched by chloride and hence that chloride is transported out of the vesicle.

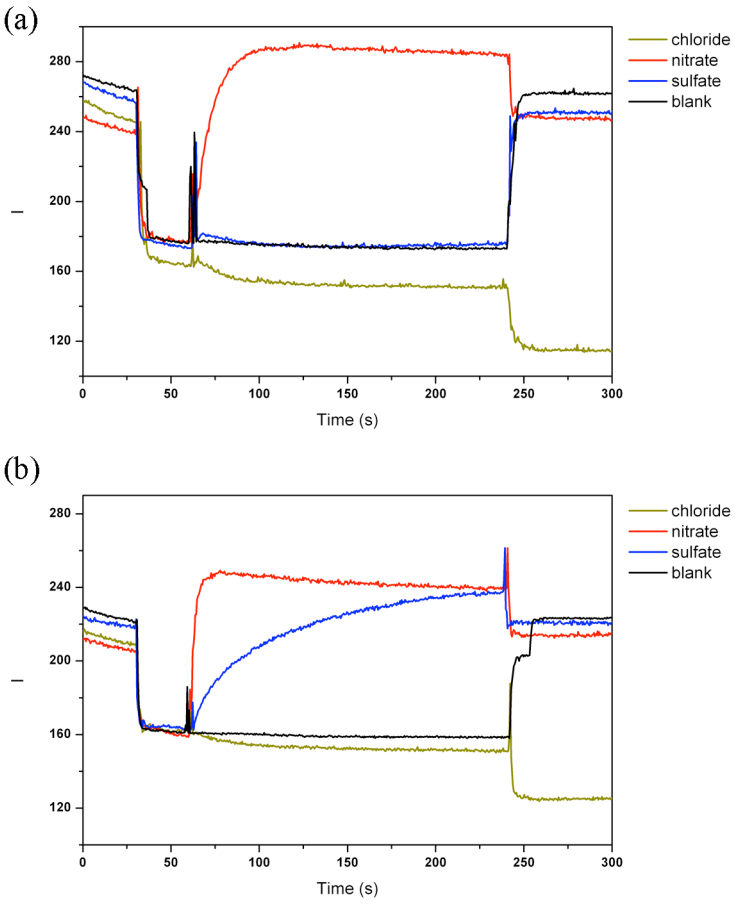

Figure S97. Unilamellar POPC vesicles were loaded with 100 mM NaCl and 2 mM lucigenin buffered to pH 7.2 with 20 mM sodium phosphate salts and dispersed in a 100 mM NaCl solution (buffered to pH 7.2). At t = 30 s, a solution of the appropriate anion was added (final concentration of 40 mM $NaNO_3$, 40 mM Na_2SO_4 or 40 mM NaCl). At t = 60 s, a methanol solution of the putative transport was added. At the end of the experiment (240 s), detergent was added to lyse the vesicles. The blank measurement refers to the addition of Na_2SO_4, followed by the addition of methanol. Each point represents the average of three trials; (a) compound **3** (2 % molar carrier to lipid). (b) compound **8** (4% molar carrier to lipid).

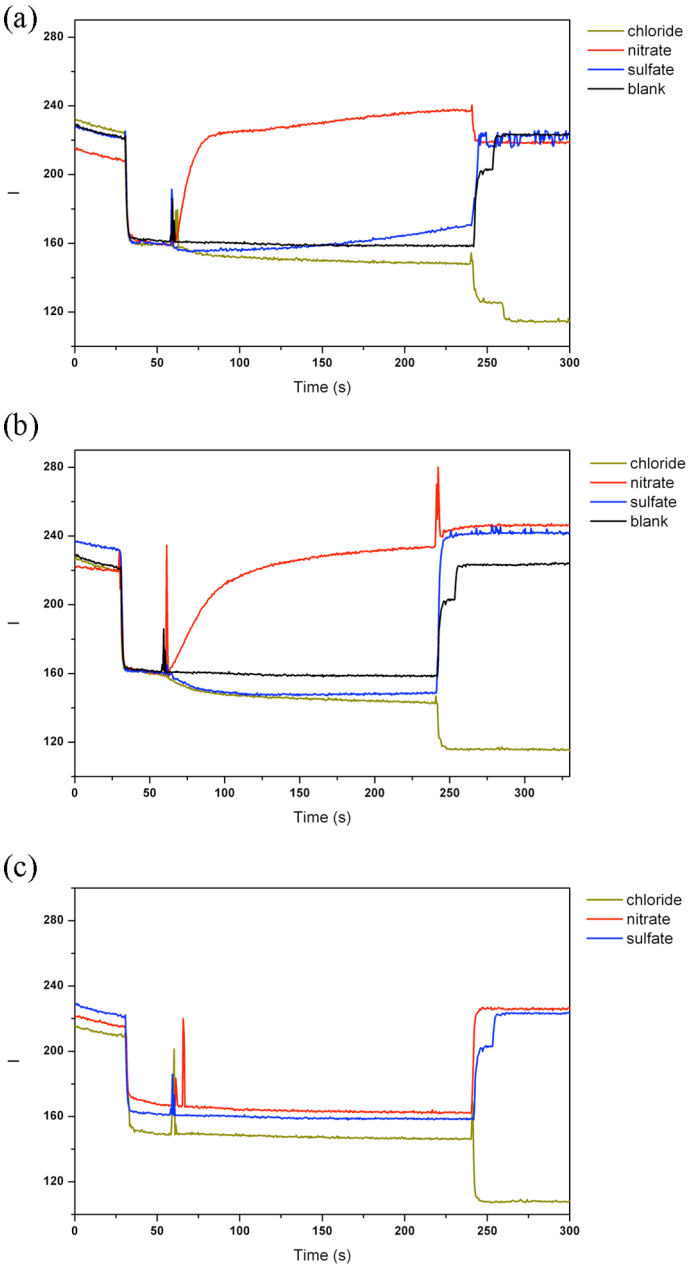

Figure S98. Unilamellar POPC vesicles were loaded with 100 mM NaCl and 2 mM lucigenin buffered to pH 7.2 with 20 mM sodium phosphate salts and dispersed in a 100 mM NaCl solution (buffered to pH 7.2). At t = 30 s, a solution of the appropriate anion was added (final concentration of 40 mM $NaNO_3$, 40 mM Na_2SO_4 or 40 mM NaCl). At t = 60 s, a methanol solution of the putative transport was added. At the end of the experiment (240 s), detergent was added to lyse the vesicles. The blank measurement refers to the addition of Na_2SO_4, followed by the addition of methanol. Each point represents the average of three trials; (a) compound **5** (4 % molar carrier to lipid). (b) compound **10** (4% molar carrier to lipid). (c) methanol (no carrier).

S6.3. Evidence for mobile carrier mechanism

Cholesterol test

Vesicles were prepared in the same way as described above (see section S5.1), but the lipid consisted of a 7:3 mixture of POPC and cholesterol. Cholesterol is believed to increase the viscosity of the membrane, hence slowing down diffusion in the lipid bilayer. This effect should be more pronounced in the case of a mobile carrier mechanism.

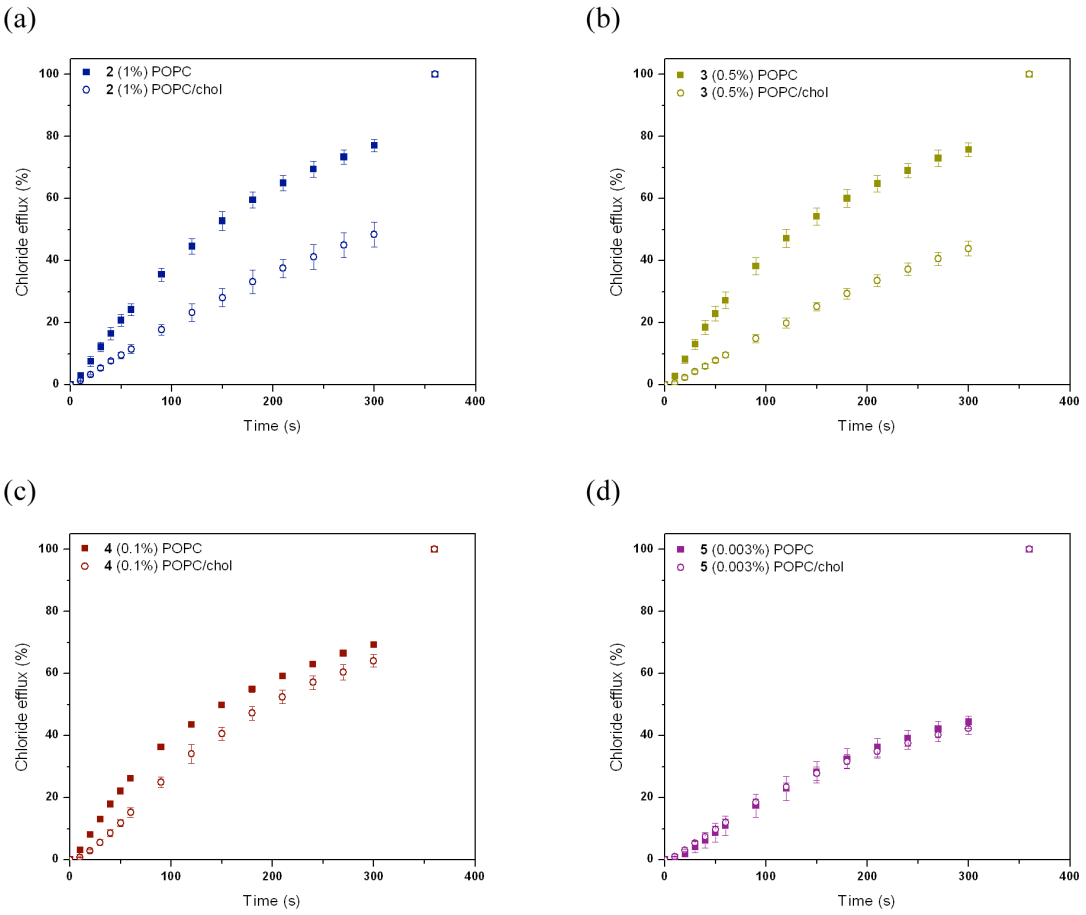

Figure S99. Chloride efflux promoted by ureas **2-5** from unilamellar POPC vesicles (filled symbols) or unilamellar 7:3 POPC:cholesterol vesicles (empty symbols) loaded with 489 mM NaCl buffered to pH 7.2 with 5 mM sodium phosphate salts. The vesicles were dispersed in 489 mM $NaNO_3$ buffered to pH 7.2 with 5 mM sodium phosphate salts. At the end of the experiment, detergent was added to lyse the vesicles and calibrate the ISE to 100% chloride efflux. Each point represents the average of three trials. (a) Compound **2**, 1 mol% carrier to lipid. (b) Compound **3**, 0.5 mol% carrier to lipid. (c) Compound **4**, 0.1 mol% carrier to lipid. (d) Compound **5**, 0.003 mol% carrier to lipid.

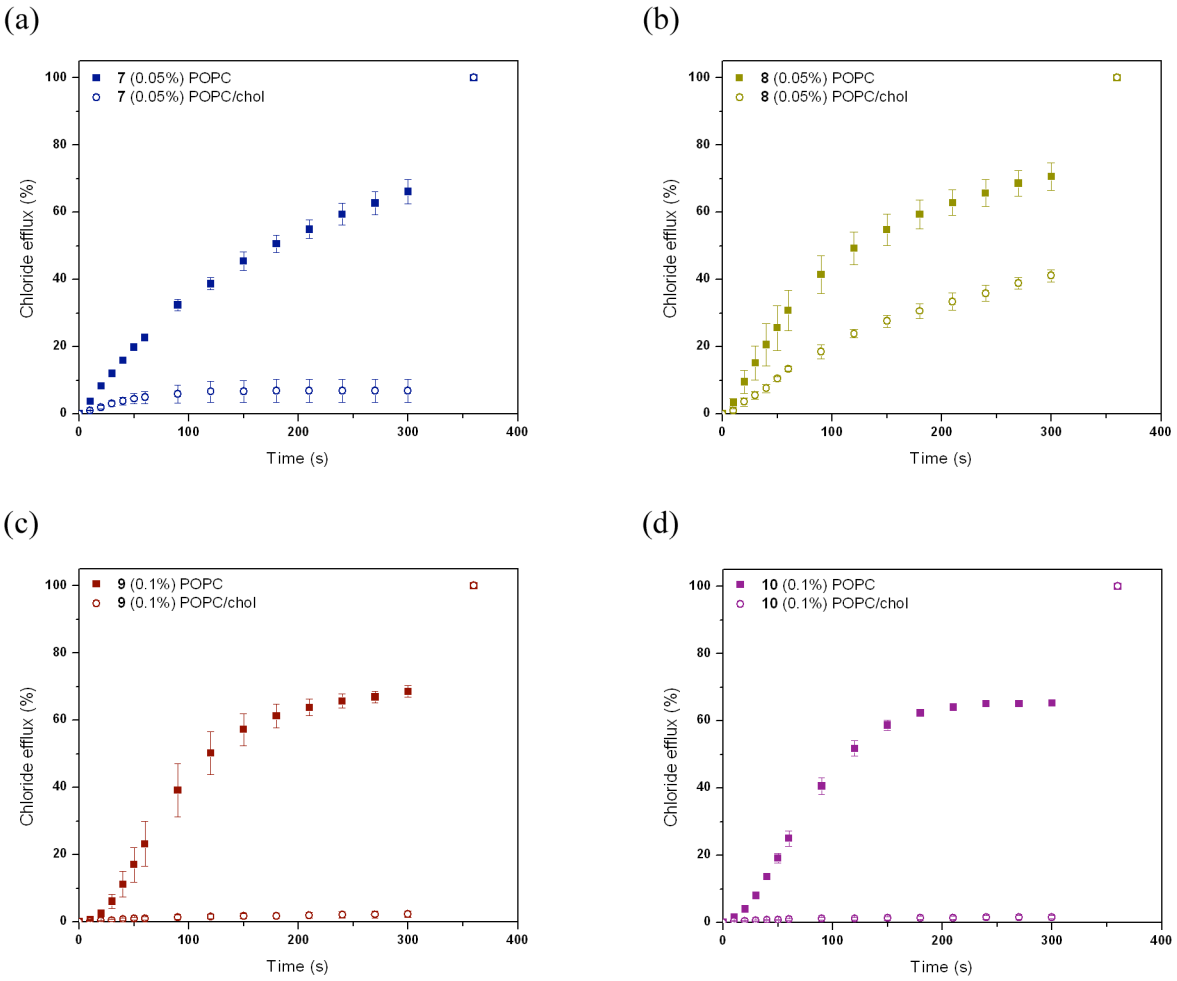

Figure S100. Chloride efflux promoted by thioureas **7-10** from unilamellar POPC vesicles (filled symbols) or unilamellar 7:3 POPC:cholesterol vesicles (empty symbols) loaded with 489 mM NaCl buffered to pH 7.2 with 5 mM sodium phosphate salts. The vesicles were dispersed in 489 mM $NaNO_3$ buffered to pH 7.2 with 5 mM sodium phosphate salts. At the end of the experiment, detergent was added to lyse the vesicles and calibrate the ISE to 100% chloride efflux. Each point represents the average of three trials. (a) Compound **7**, 0.05 mol% carrier to lipid. (b) Compound **8**, 0.05 mol% carrier to lipid. (c) Compound **9**, 0.1 mol% carrier to lipid. (d) Compound **10**, 0.1 mol% carrier to lipid.

U-tube experiment

In a U-tube experiment the lipid bilayer is substituted with a bulk organic phase. In these conditions ion channel formation is virtually impossible. The organic phase consisted of 20 mL nitrobenzene (for solubility reasons) and contained 1mM of carrier. A control experiment was executed with neat nitrobenzene (no carrier). The same aqueous phases were used as for the vesicle experiments. The donating phase contained 500 mM NaCl and was buffered to pH 7.2 with 5 mM phosphate salts (10 mL). The receiving phase contained 500 mM $NaNO_3$ and was buffered to pH 7.2 with 5 mM phosphate salts (10 mL). The change in chloride concentration of the receiving phase was monitored with a chloride-selective electrode 5the electrode was calibrated to convert the potential readings (mV) to chloride concentrations (M)). The experiments were conducted at room temperature and the results are shown in Figure S101.

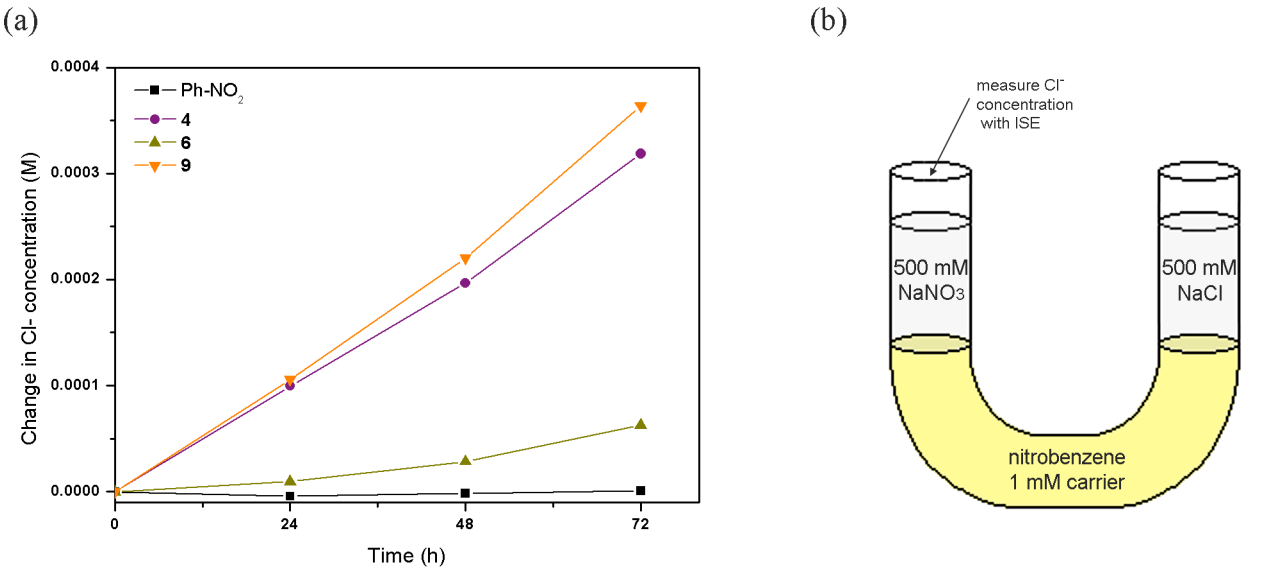

Figure S101. U-tube experiment in nitrobenzene. (a) Graph showing the change in the chloride concentration of the receiving aqueous phase as a function of time. (b) Experimental set-up.

S6.4. Stucture activity relationship

Initial rate of chloride efflux

(a)

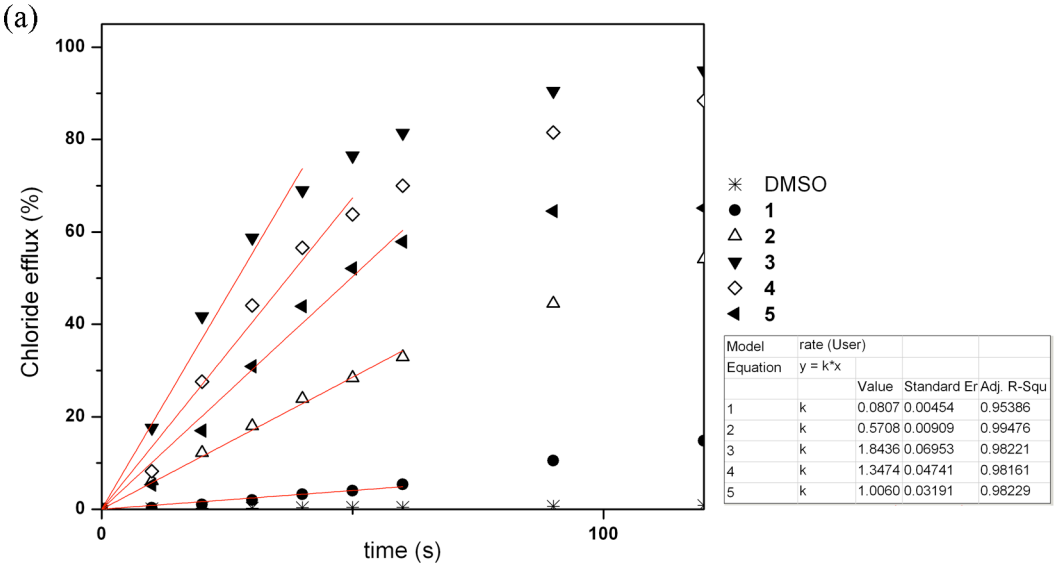

Model	rate (User)			
Equation	y = k*x			
		Value	Standard Er	Adj. R-Squ
1	k	0.0807	0.00454	0.95386
2	k	0.5708	0.00909	0.99476
3	k	1.8436	0.06953	0.98221
4	k	1.3474	0.04741	0.98161
5	k	1.0060	0.03191	0.98229

(b)

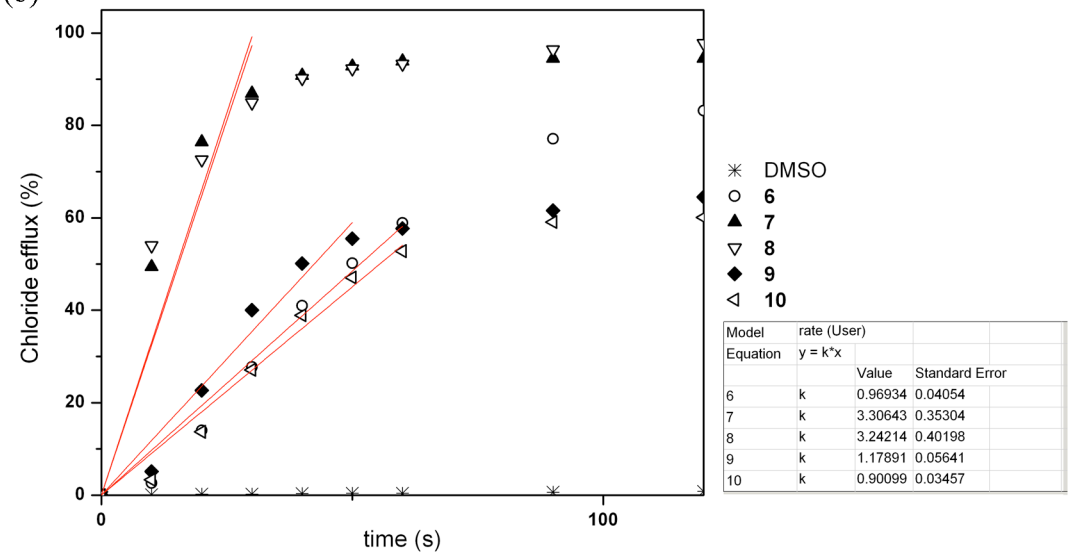

Model	rate (User)		
Equation	y = k*x		
		Value	Standard Error
6	k	0.96934	0.04054
7	k	3.30643	0.35304
8	k	3.24214	0.40198
9	k	1.17891	0.05641
10	k	0.90099	0.03457

Figure S102. Chloride efflux promoted by **1-10** (2% molar carrier to lipid) from unilamellar POPC vesicles loaded with 489 mM NaCl buffered to pH 7.2 with 5 mM sodium phosphate salts. The vesicles were dispersed in 489 mM NaNO3 buffered to pH 7.2 with 5 mM sodium phosphate salts. At the end of the experiment, detergent was added to lyse the vesicles and calibrate the ISE to 100% chloride efflux. Each point represents the average of three trials. The initial data points are fitted to a linear curve $y=k*x$, to obtain the initial transport rate k_{ini} (% s^{-1}). (a) urea compounds **1-5**. (b) thiourea compounds **6-10**.

(a)

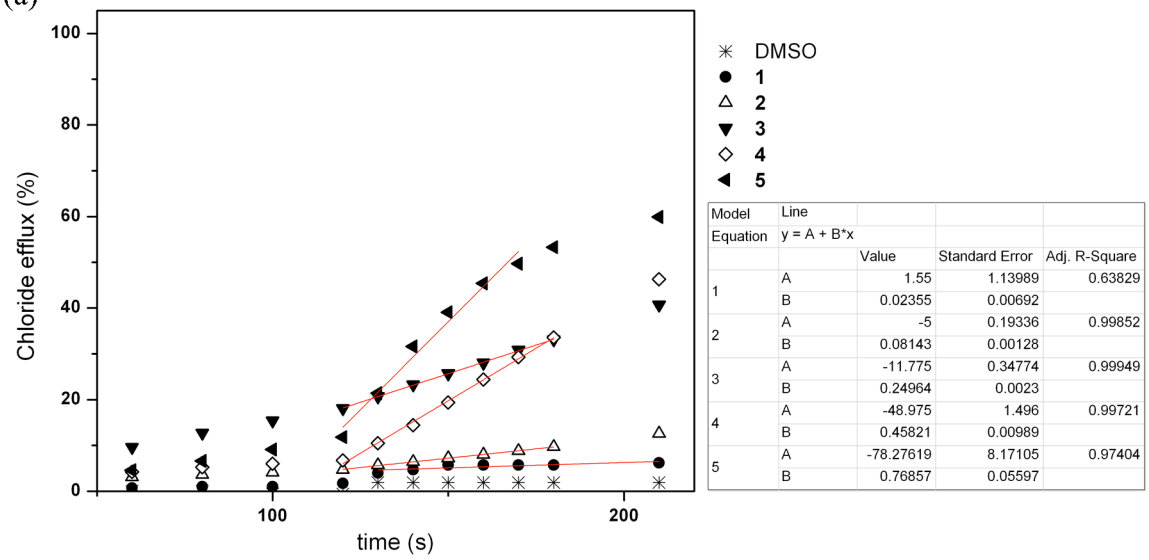

Model	Line			
Equation	y = A + B*x			
		Value	Standard Error	Adj. R-Square
1	A	1.55	1.13989	0.63829
	B	0.02355	0.00692	
2	A	-5	0.19336	0.99852
	B	0.08143	0.00128	
3	A	-11.775	0.34774	0.99949
	B	0.24964	0.0023	
4	A	-48.975	1.496	0.99721
	B	0.45821	0.00989	
5	A	-78.27619	8.17105	0.97404
	B	0.76857	0.05597	

(b)

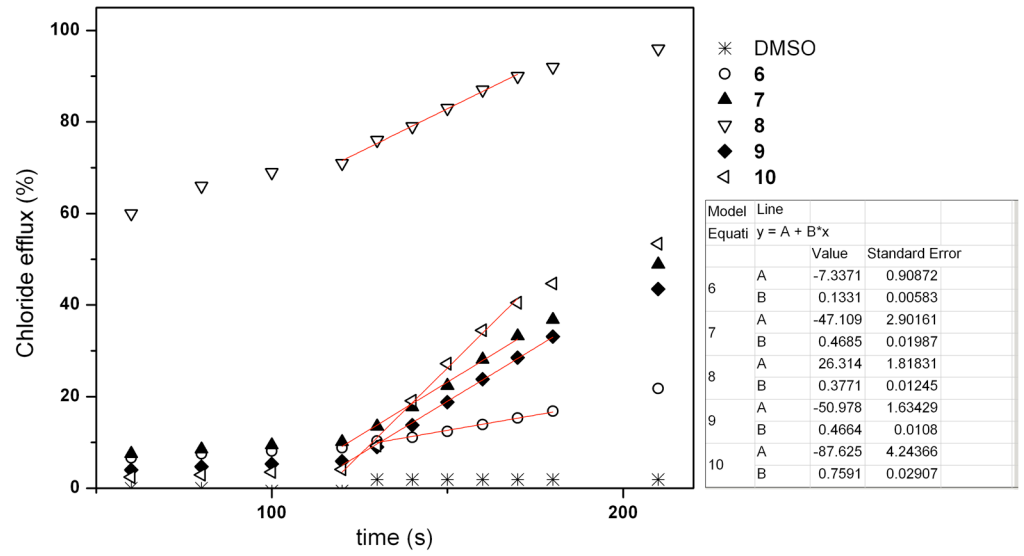

Model	Line		
Equati	y = A + B*x		
		Value	Standard Error
6	A	-7.3371	0.90872
	B	0.1331	0.00583
7	A	-47.109	2.90161
	B	0.4685	0.01987
8	A	26.314	1.81831
	B	0.3771	0.01245
9	A	-50.978	1.63429
	B	0.4664	0.0108
10	A	-87.625	4.24366
	B	0.7591	0.02907

Figure S103. Chloride efflux promoted by **1-10** (2 % molar carrier to lipid) from unilamellar POPC vesicles loaded with 450 mM NaCl buffered to pH 7.2 with 20 mM sodium phosphate salts. The vesicles were dispersed in 162 mM Na_2SO_4 buffered to pH 7.2 with 20 mM sodium phosphate salts. At t = 120s, a solution of $NaHCO_3$ was added to give a 40 mM external concentration. At the end of the experiment, detergent was added to lyse the vesicles and calibrate the ISE to 100 % chloride efflux. Each point represents the average of three trials. The initial data points after addition of $NaHCO_3$ are fitted to a linear curve $y=k*x+b$, to obtain the initial transport rate k_{ini} (% s^{-1}). (a) ureas **1-5**. (b) thioureas **6-10**.

Hill Plots

The chloride/nitrate or chloride/bicarbonate transport assays were performed as described above (see section S5.1) for various concentrations of carrier. The chloride efflux (%) 270 s after the addition of carrier (chloride/nitrate) or 270 s after the addition of $NaHCO_3$ (chloride/bicarbonate) was plotted as a function of the carrier concentration. Data points were fitted to the Hill equation:

$$y = V_{\max} \frac{x^n}{k^n + x^n}$$

where y is the chloride efflux at 270 s (%) and x is the carrier concentration (molar % carrier to lipid). V_{max}, k and n are the parameters to be fitted. V_{max} is the maximum efflux possible (usually 100%), n is the Hill coefficient and k is the carrier concentration needed to reach $V_{max}/2$. From the Hill plot $EC_{50,270s}$ values were calculated, defined as the carrier concentration (molar % carrier to lipid) needed to obtain 50 % chloride efflux after 270 s. An overview is given in Table S17 and Table S18.

Table S17. Overview of chloride/nitrate assays of compounds **1**-**10**. Errors are between brackets.

	k_{ini} [a)] (% s^{-1})	V_{max} [b)] (%)	k [b)] (% carrier:lipid)	n [b)]	$EC_{50,270s}$ [b)] (% carrier:lipid)
			Urea based compounds		
1	0.081 (0.004)	100[c)]	5.6 (0.1)[c)]	1.24 (0.03)[c)]	5.6[c)]
2	0.571 (0.009)	99 (3)	0.42 (0.04)	1.4 (0.1)	0.43
3	1.84 (0.07)	100	0.24 (0.01)	1.37 (0.08)	0.24
4	1.35 (0.05)	99.1 (0.4)	0.052 (0.002)	1.14 (0.03)	0.052
5	1.01 (0.03)	64.9 (0.2)	0.00211 (0.00005)	1.62 (0.05)	0.0044
			Thiourea based compounds		
6	0.97 (0.04)	100[c)]	0.308 (0.005)[c)]	1.93 (0.09)[c)]	0.31[c)]
7	3.3 (0.4)	100	0.0426 (0.0009)	2.9 (0.3)	0.042
8	3.2 (0.4)	90 (5)	0.029 (0.002)	2.4 (0.4)	0.032
9	1.18 (0.06)	79 (1)	0.069 (0.004)	4.8 (0.6)	0.077
10	0.90 (0.03)	64 (2)	0.03 (0.01)	5 (2)	0.042

[a)] initial rate of chloride efflux for 2% molar percentage carrier to lipid. [b)] parameters from Hill plot. [c)] previously published data.

Table S18. Overview of chloride/bicarbonate assays of compounds **1**-**10**. Errors are between brackets.

	k_{ini} [a] ($\% s^{-1}$)	V_{max} [b] (%)	k [b] (% carrier:lipid)	n [b]	$EC_{50,270s}$ [b] (% carrier:lipid)
			Urea based compounds		
1	0.024 (0.007)	-	-	-	>5 [c]
2	0.081 (0.001)	-	-	-	>5 [d]
3	0.250 (0.002)	- [e]	- [e]	- [e]	- [e]
4	0.46 (0.01)	81 (3)	0.16 (0.02)	1.2 (0.1)	0.24
5	0.77 (0.06)	66 (2)	0.017 (0.001)	1.5 (0.1)	0.036
			Thiourea based compounds		
6	0.186 (0.009)	73 (7)	1.1 (0.2)	1.00 (0.09)	2.3
7	0.47 (0.02)	84 (1)	0.26 (0.01)	1.2 (0.1)	0.35
8	0.38 (0.01)	- [e]	- [e]	- [e]	- [e]
9	0.47 (0.01)	68.7 (1.5)	0.092 (0.005)	4.8 (0.8)	0.11
10	0.76 (0.03)	60.7 (0.4)	0.093 (0.009)	3.8 (0.8)	0.14

[a] initial rate of chloride efflux (after addition of $NaHCO_3$) for 2% carrier to lipid. [b] parameters from Hill plot. [c] accurate Hill analysis could not be performed due to low activity, chloride efflux 270 s after the addition of $NaHCO_3$ was 20.9 % for 5 % loading of compound **1** (mol% carrier to lipid). [d] accurate Hill analysis could not be performed due to low activity, chloride efflux 270 s after the addition of $NaHCO_3$ was 36.2 % for 5 % loading of compound **2** (mol% carrier to lipid). [e] meaningful Hill analysis could not be performed due to significant background transport in the absence of $NaHCO_3$ (HCl symport and/or Cl^-/SO_4^{2-} antiport).

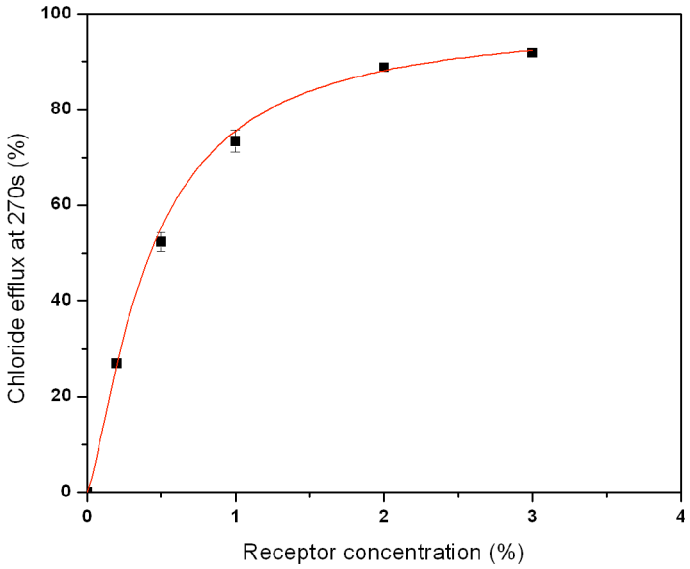

Model	Hill		
Equation	y=Vmax*x^n/(k^n+x^n)		
Reduced Chi-Sqr	3.09951		
Adj. R-Square	0.99813		
		Value	Standard Error
Chloride efflux at 270s	Vmax	98.76706	2.8688
Chloride efflux at 270s	k	0.41818	0.03762
Chloride efflux at 270s	n	1.35173	0.1238

Figure S104. Hill plot for chloride release mediated by receptor **2** from unilamellar POPC vesicles loaded with 489 mM NaCl buffered to pH 7.2 with 5 mM sodium phosphate salts. The vesicles were dispersed in 489 mM $NaNO_3$ buffered to pH 7.2 with 5 mM sodium phosphate salts. Chloride efflux was measured at 270 s.

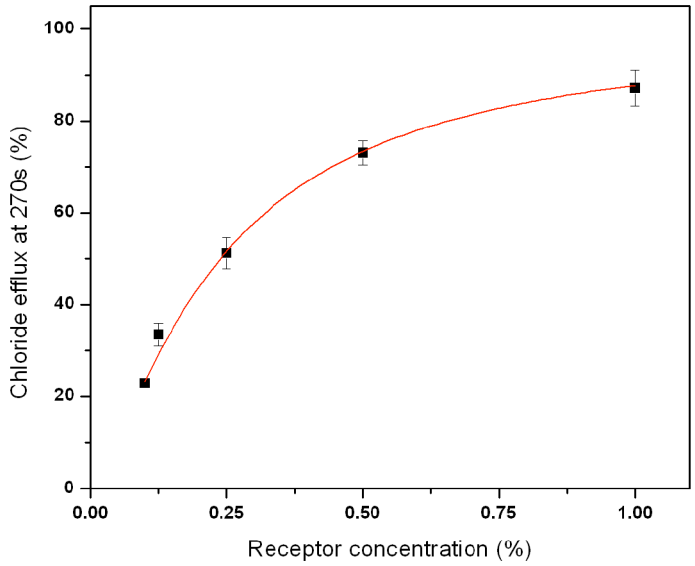

Model	Hill		
Equation	y=Vmax*x^n/(k^n+x^n)		
Reduced Chi-Sqr	1.14418		
Adj. R-Square	0.99253		
		Value	Standard Erro
Chloride efflux at 270s	Vmax	100	0
	k	0.2386	0.0109
	n	1.3686	0.07667

Figure S105. Hill plot for chloride release mediated by receptor **3** from unilamellar POPC vesicles loaded with 489 mM NaCl buffered to pH 7.2 with 5mM sodium phosphate salts. The vesicles were dispersed in 489 mM $NaNO_3$ buffered to pH 7.2 with 5 mM sodium phosphate salts. Chloride efflux was measured at 270 s.

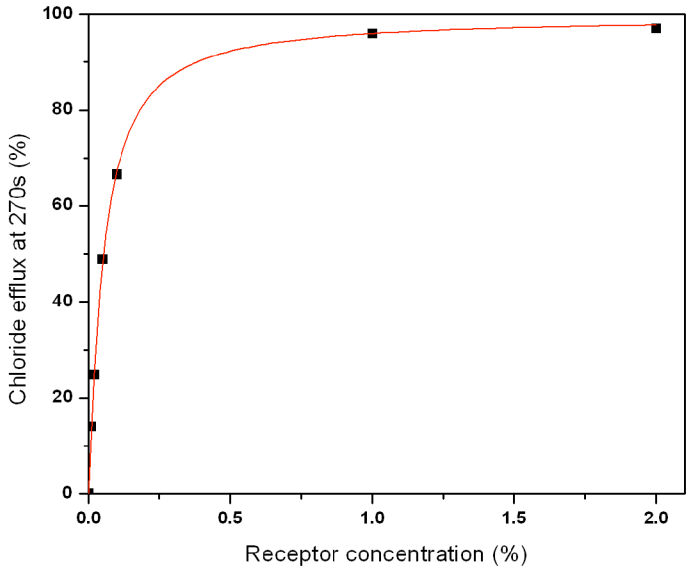

Model	Hill		
Equation	y=Vmax*x^n/(k^n+x^n)		
Reduced Chi-Sqr	2.46743		
Adj. R-Squar	0.99975		
		Value	Standard Err
Chloride efflux at 270s	Vmax	99.11481	0.43217
Chloride efflux at 270s	k	0.05171	0.0016
Chloride efflux at 270s	n	1.14595	0.03604

Figure S106. Hill plot for chloride release mediated by receptor **4** from unilamellar POPC vesicles loaded with 489 mM NaCl buffered to pH 7.2 with 5 mM sodium phosphate salts. The vesicles were dispersed in 489 mM $NaNO_3$ buffered to pH 7.2 with 5 mM sodium phosphate salts. Chloride efflux was measured at 270 s.

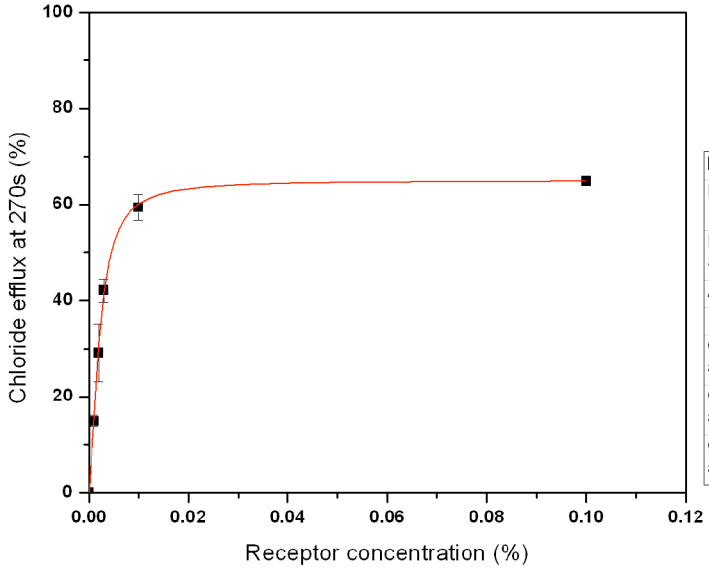

Model	Hill		
Equation	y=Vmax*x^n/(k^n+x^n)		
Reduced Chi-Sqr	0.11801		
Adj. R-Square	0.99968		
		Value	Standard Error
Chloride efflux at 270s	Vmax	64.90148	0.21494
Chloride efflux at 270s	k	0.00211	4.77272E-5
Chloride efflux at 270s	n	1.62424	0.05352

Figure S107. Hill plot for chloride release mediated by receptor **5** from unilamellar POPC vesicles loaded with 489 mM NaCl buffered to pH 7.2 with 5mM sodium phosphate salts. The vesicles were dispersed in 489 mM $NaNO_3$ buffered to pH 7.2 with 5 mM sodium phosphate salts. Chloride efflux was measured at 270 s.

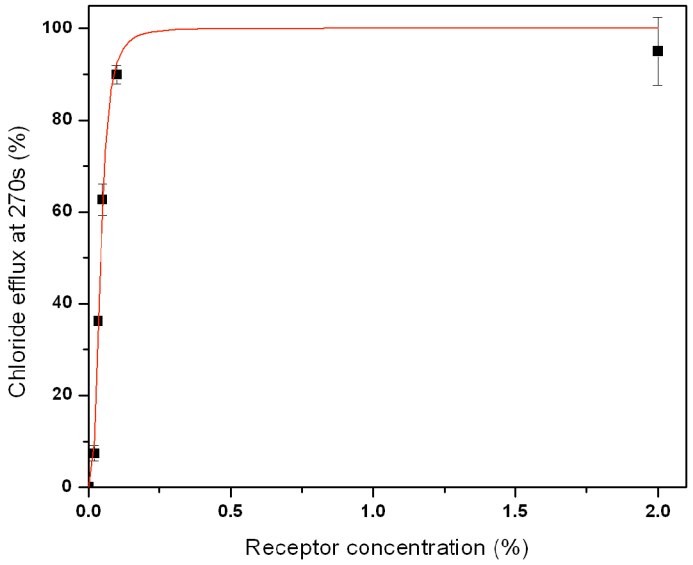

Model	Hill		
Equation	y=Vmax*x^n/(k^n+x^n)		
Reduced Chi-Sqr	1.41643		
Adj. R-Square	0.99487		
		Value	Standard Erro
Chloride efflux at 270s	Vmax	100	0
	k	0.04264	9.04329E-4
	n	2.9399	0.22669

Figure S108. Hill plot for chloride release mediated by receptor **7** from unilamellar POPC vesicles loaded with 489 mM NaCl buffered to pH 7.2 with 5 mM sodium phosphate salts. The vesicles were dispersed in 489 mM $NaNO_3$ buffered to pH 7.2 with 5 mM sodium phosphate salts. Chloride efflux was measured at 270 s.

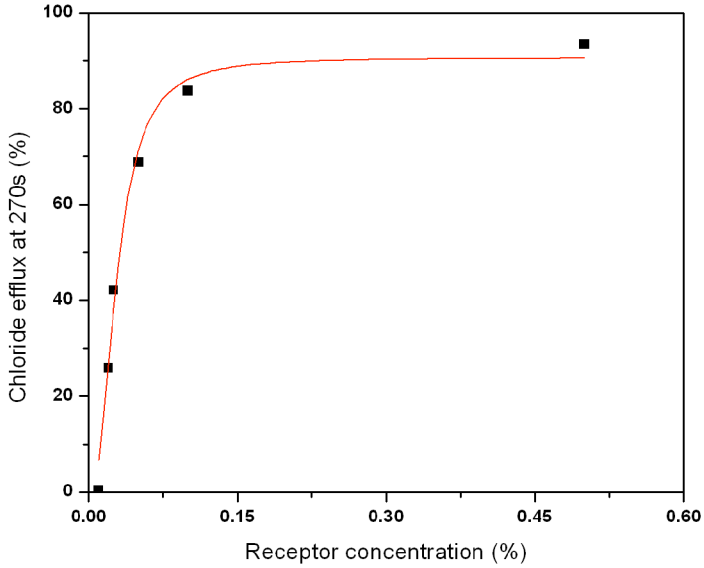

Model	Hill		
Equation	y=Vmax*x^n/(k^n+x^n)		
Reduced Chi-Sqr	27.59964		
Adj. R-Squar	0.9786		
		Value	Standard Err
Chloride efflux at 270s	Vmax	90.5878	4.55059
	k	0.02888	0.00263
	n	2.37895	0.45509

Figure S109. Hill plot for chloride release mediated by receptor **8** from unilamellar POPC vesicles loaded with 489 mM NaCl buffered to pH 7.2 with 5mM sodium phosphate salts. The vesicles were dispersed in 489 mM $NaNO_3$ buffered to pH 7.2 with 5 mM sodium phosphate salts. Chloride efflux was measured at 270 s.

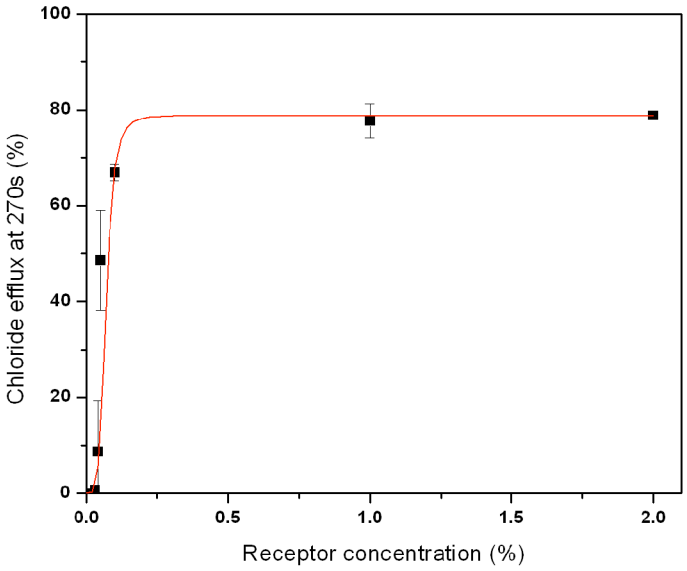

Model	Hill		
Equation	y=Vmax*x^n/(k^n+x^n)		
Reduced Chi-Sqr	3.67544		
Adj. R-Squa	0.99842		
		Value	Standard Er
Chloride efflux at 270s	Vmax	78.74101	0.98643
	k	0.06916	0.00433
	n	4.78897	0.58816

Figure S110. Hill plot for chloride release mediated by receptor **9** from unilamellar POPC vesicles loaded with 489 mM NaCl buffered to pH 7.2 with 5 mM sodium phosphate salts. The vesicles were dispersed in 489 mM $NaNO_3$ buffered to pH 7.2 with 5 mM sodium phosphate salts. Chloride efflux was measured at 270 s.

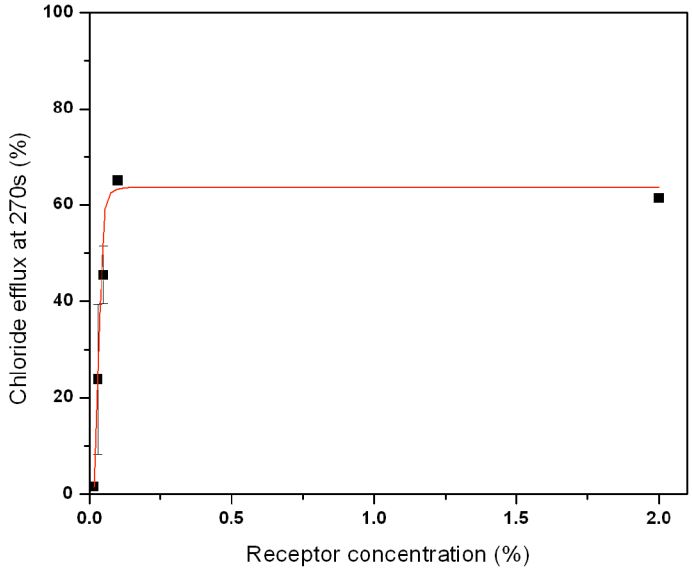

Model	Hill		
Equation	y=Vmax*x^n/(k^n+x^n)		
Reduced Chi-Sqr	11.15633		
Adj. R-Squa	0.99623		
		Value	Standard Er
Chloride efflux at 270s	Vmax	63.65606	1.68023
	k	0.03246	0.0118
	n	4.88597	2.39359

Figure S111. Hill plot for chloride release mediated by receptor **10** from unilamellar POPC vesicles loaded with 489 mM NaCl buffered to pH 7.2 with 5mM sodium phosphate salts. The vesicles were dispersed in 489 mM $NaNO_3$ buffered to pH 7.2 with 5 mM sodium phosphate salts. Chloride efflux was measured at 270 s.

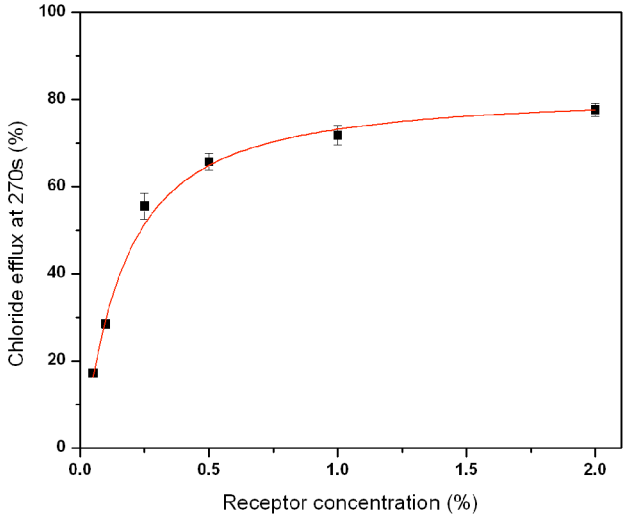

Model	Hill		
Equation	y=Vmax*x^n/(k^n+x^n)		
Reduced Chi-Sqr	1.50174		
Adj. R-Squa	0.99537		
		Value	Standard Er
Chloride efflux at 270s	Vmax	81.27917	2.83646
	k	0.15901	0.0163
	n	1.19968	0.11087

Figure S112. Hill plot for chloride release mediated by receptor **4** from unilamellar POPC vesicles loaded with 450 mM NaCl buffered to pH 7.2 with 20 mM sodium phosphate salts. The vesicles were dispersed in 162 mM Na_2SO_4 buffered to pH 7.2 with 20 mM sodium phosphate salts. At t = 120 s, a solution of $NaHCO_3$ was added to give a 40 mM external concentration. Chloride efflux was measured 270 s after the addition of $NaHCO_3$.

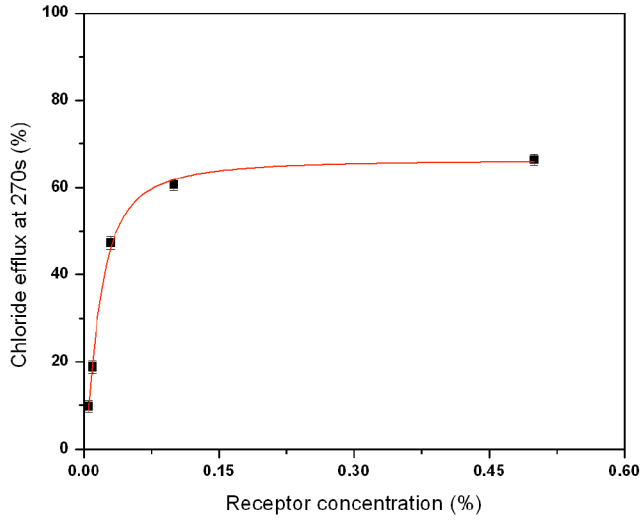

Model	Hill		
Equation	y=Vmax*x^n/(k^n+x^n)		
Reduced Chi-Sqr	1.49658		
Adj. R-Squa	0.99578		
		Value	Standard Er
Chloride efflux at 270s	Vmax	66.23445	1.50887
	k	0.01725	0.00123
	n	1.50761	0.12562

Figure S113. Hill plot for chloride release mediated by receptor **5** from unilamellar POPC vesicles loaded with 450 mM NaCl buffered to pH 7.2 with 20 mM sodium phosphate salts. The vesicles were dispersed in 162 mM Na_2SO_4 buffered to pH 7.2 with 20 mM sodium phosphate salts. At t = 120 s, a solution of $NaHCO_3$ was added to give a 40 mM external concentration. Chloride efflux was measured 270 s after the addition of $NaHCO_3$.

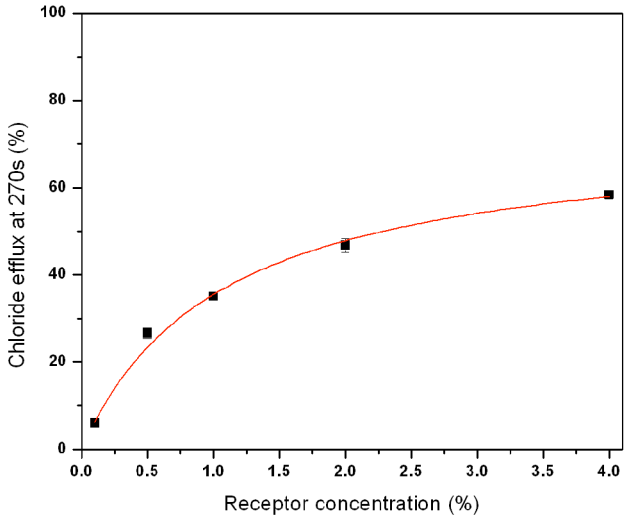

Model	Hill		
Equation	y=Vmax*x^n/(k^n+x^n)		
Reduced Chi-Sqr	4.03561		
Adj. R-Squa	0.99521		
		Value	Standard Er
Chloride efflux at 270s	Vmax	73.37666	6.92063
	k	1.06645	0.23725
	n	1.00041	0.09446

Figure S114. Hill plot for chloride release mediated by receptor **6** from unilamellar POPC vesicles loaded with 450 mM NaCl buffered to pH 7.2 with 20 mM sodium phosphate salts. The vesicles were dispersed in 162 mM Na_2SO_4 buffered to pH 7.2 with 20 mM sodium phosphate salts. At t = 120 s, a solution of $NaHCO_3$ was added to give a 40 mM external concentration. Chloride efflux was measured 270 s after the addition of $NaHCO_3$.

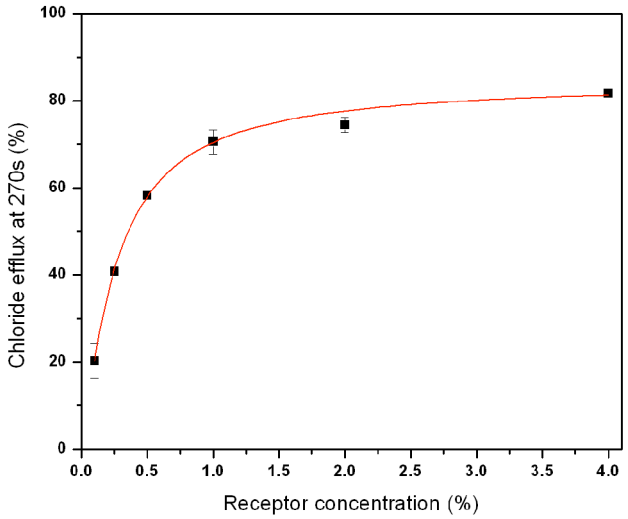

Model	Hill		
Equation	y=Vmax*x^n/(k^n+x^n)		
Reduced Chi-Sqr	1.37915		
Adj. R-Squa	0.99489		
		Value	Standard Er
Chloride efflux at 270s	Vmax	84.2743	1.44009
	k	0.25914	0.01042
	n	1.2071	0.1086

Figure S115. Hill plot for chloride release mediated by receptor **7** from unilamellar POPC vesicles loaded with 450 mM NaCl buffered to pH 7.2 with 20 mM sodium phosphate salts. The vesicles were dispersed in 162 mM Na_2SO_4 buffered to pH 7.2 with 20 mM sodium phosphate salts. At t = 120 s, a solution of $NaHCO_3$ was added to give a 40 mM external concentration. Chloride efflux was measured 270 s after the addition of $NaHCO_3$.

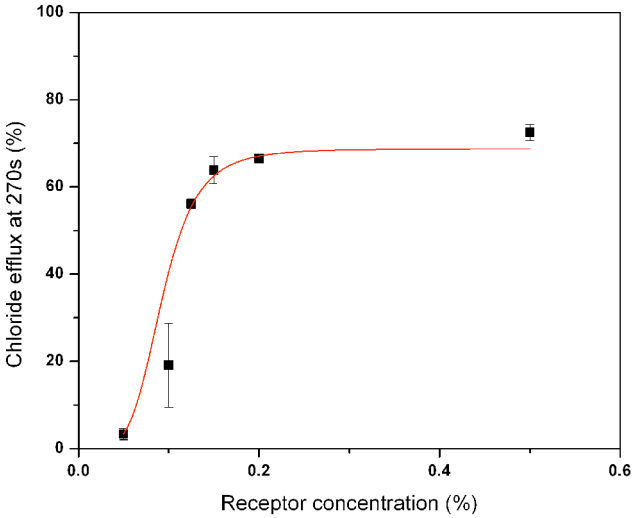

Model	Hill		
Equation	y=Vmax*x^n/(k^n+x^n)		
Reduced Chi-Sqr	3.52201		
Adj. R-Squar	0.99166		
		Value	Standard Err
Chloride efflux at 270s	Vmax	68.7278	1.52089
	k	0.09267	0.00501
	n	4.79253	0.85793

Figure S116. Hill plot for chloride release mediated by receptor **9** from unilamellar POPC vesicles loaded with 450 mM NaCl buffered to pH 7.2 with 20 mM sodium phosphate salts. The vesicles were dispersed in 162 mM Na_2SO_4 buffered to pH 7.2 with 20 mM sodium phosphate salts. At t = 120 s, a solution of $NaHCO_3$ was added to give a 40 mM external concentration. Chloride efflux was measured 270 s after the addition of $NaHCO_3$.

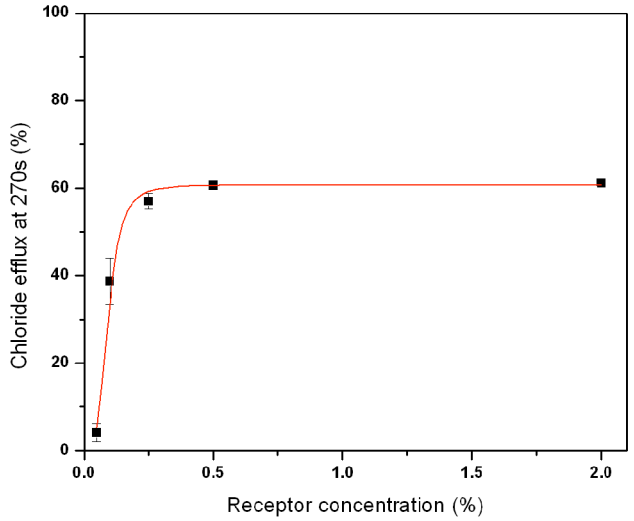

Model	Hill		
Equation	y=Vmax*x^n/(k^n+x^n)		
Reduced Chi-Sqr	1.42815		
Adj. R-Squa	0.99231		
		Value	Standard Er
Chloride efflux at 270s	Vmax	60.70712	0.39195
	k	0.09323	0.00867
	n	3.77434	0.79876

Figure S117. Hill plot for chloride release mediated by receptor **10** from unilamellar POPC vesicles loaded with 450 mM NaCl buffered to pH 7.2 with 20 mM sodium phosphate salts. The vesicles were dispersed in 162 mM Na_2SO_4 buffered to pH 7.2 with 20 mM sodium phosphate salts. At t = 120 s, a solution of $NaHCO_3$ was added to give a 40 mM external concentration. Chloride efflux was measured 270 s after the addition of $NaHCO_3$.

S6.5. Leveling out at 70%

Effect of buffer

Compounds **5**, **10** and to a lesser extent **9**, show a leveling out of chloride efflux after 1 minute and never reach chloride effluxes higher than 70 %. A possible explanation for this behavior might be competition of binding to the buffer anions (phosphate) in solution. To test this, the experiment was repeated with HEPES buffer instead of phosphate buffer (Figure S118) and no significant difference was observed. This suggests that binding to the buffer anions is unlikely.

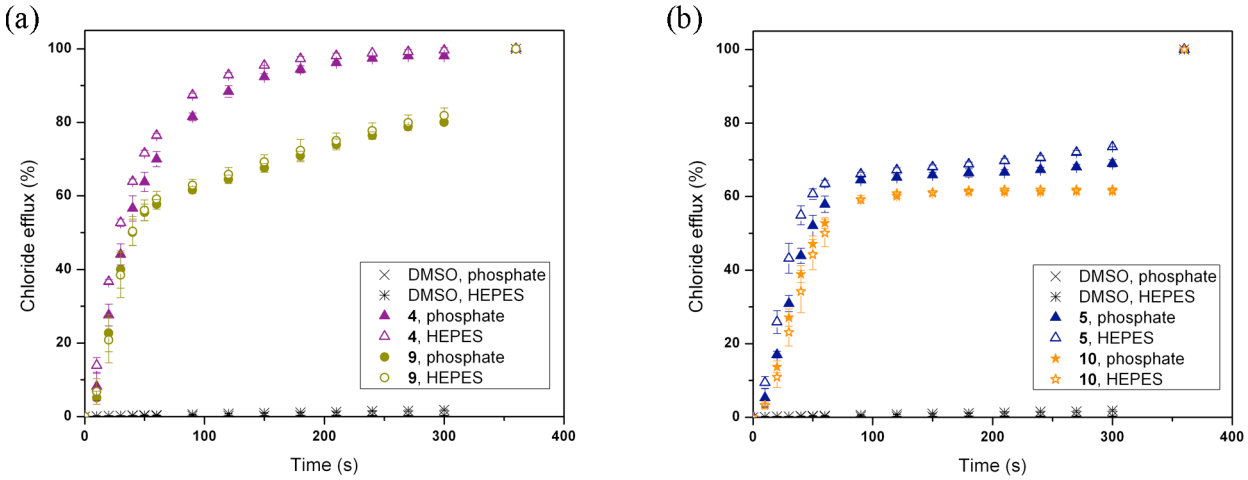

Figure S118. Chloride efflux promoted by **4**, **5**, **9** and **10** (2 % molar carrier to lipid) from unilamellar POPC vesicles loaded with 489 mM NaCl buffered to pH 7.2 with 5 mM sodium phosphate salts or with 5 mM HEPES buffer. The vesicles were dispersed in 489 mM $NaNO_3$ buffered to pH 7.2 with 5 mM sodium phosphate salts or with 5 mM HEPES buffer. At the end of the experiment, detergent was added to lyse the vesicles and calibrate the ISE to 100 % chloride efflux. Each point represents the average of three trials. Experiments with HEPES buffer are represented by empty symbols and the experiments with phosphate buffer are represented by filled symbols. (a) compounds **4** and **9**. (b) compounds **5** and **10**.

Effect of absolute ion concentrations

As more chloride is transported out of the vesicles, the ion gradient across the membrane becomes smaller and the thermodynamic driving force for transport decreases. To test if the

leveling out of chloride transport is due to the decrease in the ion gradient, the experiment was repeated by using a smaller initial gradient (200 mM instead of 500 mM ion concentrations). However, this resulted in the same behavior as observed for a larger initial gradient (Figure S119).

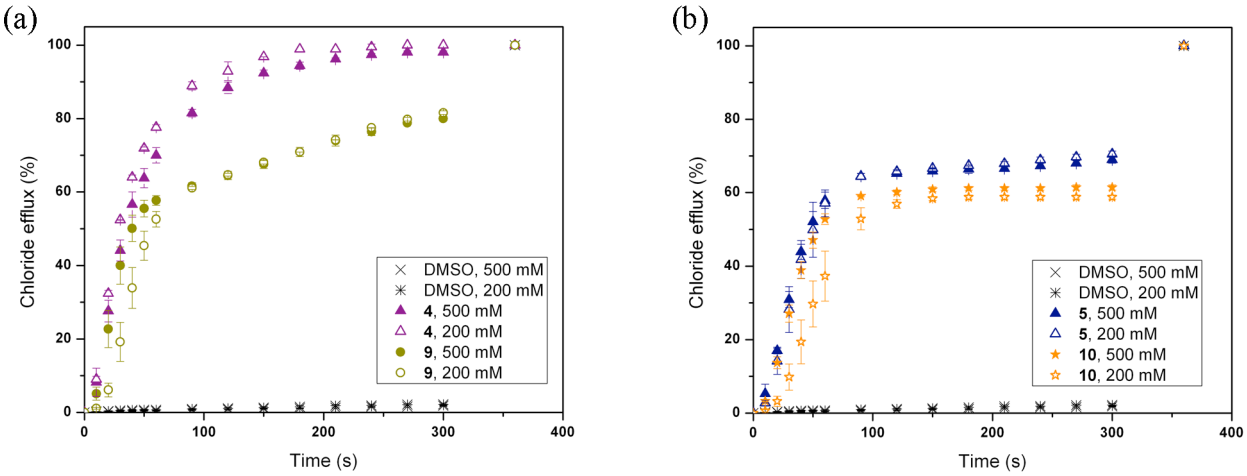

Figure S119. Chloride efflux promoted by **4**, **5**, **9** and **10** (2 % molar carrier to lipid) from unilamellar POPC vesicles loaded with 489 mM NaCl or 189 mM NaCl buffered to pH 7.2 with 5 mM sodium phosphate salts. The vesicles were dispersed in 489 mM $NaNO_3$ or 189 mM $NaNO_3$ buffered to pH 7.2 with 5 mM sodium phosphate salts. At the end of the experiment, detergent was added to lyse the vesicles and calibrate the ISE to 100 % chloride efflux. Each point represents the average of three trials. Experiments with 200 mM gradient are represented by empty symbols and the experiments with 500 mM gradient are represented by filled symbols. (a) compounds **4** and **9**. (b) compounds **5** and **10**.

Flippase activity

The leveling out behavior can also be the result of binding to the phospholipid headgroups in the lipid bilayer. This can result in so-called flippase activity. Flippase tests using NBD-labeled phospholipids were performed according to literature procedures,[13] but no significant flippase activity could be detected within the time scale of the Cl/NO_3 ISE experiments (first 5 minutes). The flippase activity that could be detected also seems to be of the same magnitude for both **2** (no leveling out) and **5** (leveling out), indicating that the flippase activity is not the reason for the observed platform at 70 % for compound **5**.

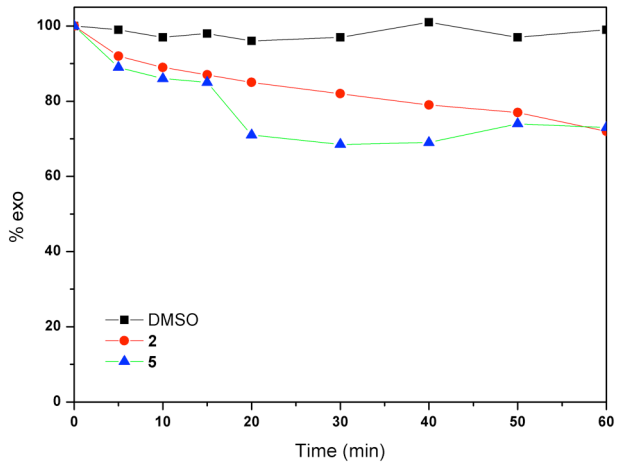

Figure S120. Change in the percent of NBD-lipid in the outer monolayer (% exo) promoted by **2** and **5** (2 % molar carrier to lipid) from unilamellar POPC vesicles loaded with 100 mM NaCl buffered to pH 7.2 with 5 mM sodium phosphate salts. The vesicles were dispersed in 100 mM $NaNO_3$ buffered to pH 7.2 with 5 mM sodium phosphate salts.

A lipid film of POPC was formed from a chloroform solution under reduced pressure and dried under vacuum for at least 6 hours. The lipid film was rehydrated by vortexing with a NaCl solution (100 mM NaCl, 5 mM phosphate buffer at pH 7.2). The lipid suspension was then subjected to nine freeze-thaw cycles and allowed to age for 30 min at room temperature before extruding 25 times through a 100 nm polycarbonate membrane.

Unilamellar POPC vesicles containing NaCl, prepared as described above, were suspended in a NaCl solution buffered to pH 7.2 with sodium phosphate salts (25 μM lipid, 35 mL total solution). Exo-labeled vesicles were prepared by slowly injecting a concentrated ethanolic solution of NBD-lipid into a stirring, room temperature solution of the unlabeled vesicles (final NBD-lipid concentration of 0.125 μM). A DMSO solution of the carrier molecule was added to start the experiment (2% molar carrier to lipid). Every few minutes, a 3 mL aliquot was removed and assayed for extend of translocation. The fluoresence of NBD-labeled phospholipids was monitored by excitation at 470 nm and recording the emission at 530 nm. The 200 s assay consisted of a dithionite injection at t = 50 s (60 mM) and the addition of detergent polyoxyethylene(8)lauryl ether (0.232 mM in 7:1 water:DMSO v/v) at t = 150 s. The percentage of exo NBD-labeled POPC lipid was calculated by $\%exo = 100*(F_i-F_f)/(F_i-F_d)$, where F_i is the intensity just prior to dithionite addition, F_f is the intensity just prior to the addition of detergent

and F_d is the intensity at the end of the experiment (50 s after the addition of detergent). The initial percentage of exo NBD-lipid was set at 100 %.

Dilution of vesicle concentration

Another reason why the chloride efflux does not reach levels higher than 70 % in the ISE experiments, might be due to the fact that the ISE experiments are bulk experiments. It is possible that the very lipophilic compounds redistribute in the membrane so fast that they cannot reach all of the vesicles. The observed chloride efflux then stops when the transport is finished in the vesicles containing the receptor, while the vesicle that do not contain the receptors account for the remaining 30 % chloride that was not transported. This might be tested by using pre-incorporation, but this was not possible due to poor solubility in dichloromethane and chloroform. One way to ensure a better distribution of the putative transporters over all of the vesicles is by using a lower vesicle concentration (0.25 mM instead of 1 mM), but no significant difference could be observed.

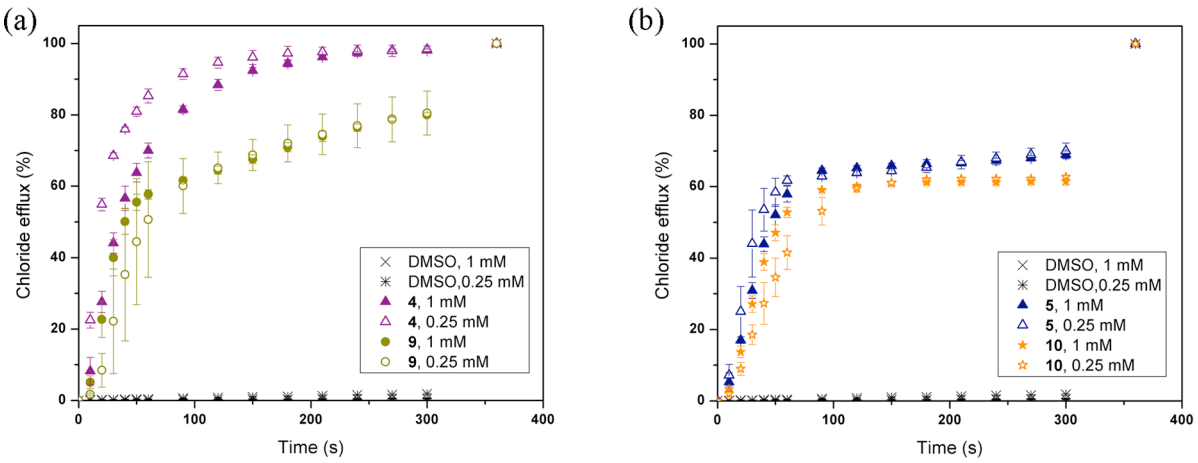

Figure S121. Chloride efflux promoted by **4**, **5**, **9** and **10** (2 % molar carrier to lipid) from unilamellar POPC vesicles loaded with 489 mM NaCl buffered to pH 7.2 with 5 mM sodium phosphate salts. The vesicles were dispersed in 489 mM $NaNO_3$ buffered to pH 7.2 with 5 mM sodium phosphate salts. The lipid concentration used was either 1 mM (filled symbols) or 0.25 mM (empty symbols). At the end of the experiment, detergent was added to lyse the vesicles and calibrate the ISE to 100 % chloride efflux. Each point represents the average of three trials. (a) compounds **4** and **9**. (b) compounds **5** and **10**.

Stepwise addition

Another way to test if the distribution of the carriers to all of the vesicles causes a problem, is by adding the carrier in several discrete steps. We therefore repeated the ISE experiment while adding the receptor to the vesicle solution in 8 discrete steps. As a comparison the test was also performed by adding the receptor in one step, followed by the addition of seven blank DMSO samples to eliminate the effect of using more organic solvents. However, the stepwise addition only led to a negligible increase in the overall chloride efflux. These tests suggest that distribution to the vesicles is not a major problem in the transport studies.

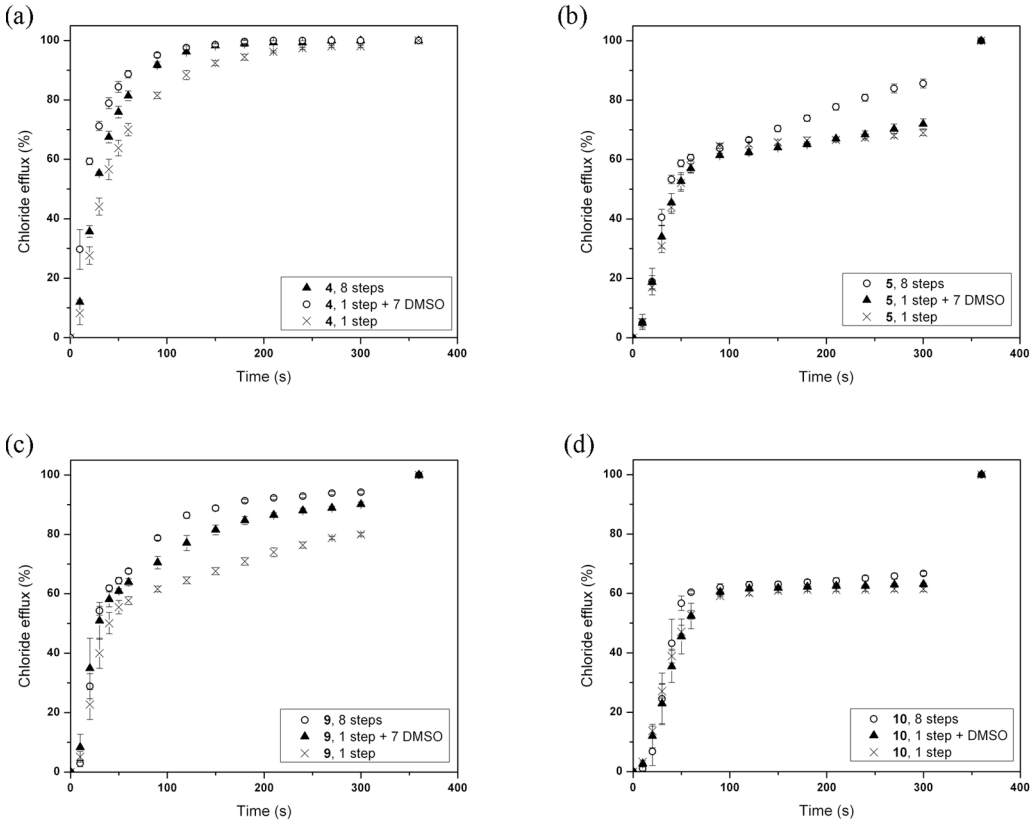

Figure S122. Chloride efflux promoted by **4**, **5**, **9** and **10** (2 % molar carrier to lipid) from unilamellar POPC vesicles loaded with 489 mM NaCl buffered to pH 7.2 with 5 mM sodium phosphate salts. The vesicles were dispersed in 489 mM $NaNO_3$ buffered to pH 7.2 with 5 mM sodium phosphate salts. To start the experiment, a DMSO solution of the carrier was added either in 1 step of 10 μL (2 %), 1 step (2 %) followed by 7 addition of 10 μL DMSO, or in 8 steps of 10 μL (0.25 % each, 2 % loading in total). At the end of the experiment, detergent was added to lyse the vesicles and calibrate the ISE to 100 % chloride efflux. Each point represents the average of three trials. (a) compound **4**. (b) compound **5**. (c) compound **9**. (d) compound **10**.

S7. IN VITRO STUDIES

S7.1. Cell Culture

Human small-cell lung carcinoma (SCLC) cell line (GLC4), human colon adenocarcinoma cell line (DLD-1) was purchased from the American Type Culture Collection (Rockville, MD), were cultured in RPMI 1640 medium (Biological Industries, Beit Haemek, Israel); human colon adenocarcinoma HT29 (mutated p53 in *Ala* 273 codon) cell line was derived from a sigmoid colon cancer of stage B1, human colon adenocarcinoma from lymph node metastasis cell line (SW-620), squamous cell carcinoma from tongue (HN4 cell line) and from mouth floor (CAL27 cell line) were cultured in DMEM. Both medium were supplemented with 10% FBS, 100 U/ml penicillin, 100 µg/ml streptomycin (all from GIBCO BRL, Paisley, UK), and 2 mM L-glutamine (Sigma Chemicals Co, St Louis, MO, USA), at 37 ºC, 5% CO_2 in air.

S7.2. Cell viability assay

Cell viability was determined by the MTT assay (Hansen et al., 1989). Briefly, $20x10^3$ cells were incubated in 96-well microtiter cell culture plates, in the absence (control cells) or in the presence 10 µM (single dose) or 1 to 16 µM (dose-response) of the 10 synthetic receptors in a final volume of 100 µl. After 24 hours incubation, 10 mM of MTT (diluted in PBS) was added to each well for an additional 4 hours. The blue MTT formazan precipitate was dissolved in 100 µl of isopropanol: 1N HCl (24:1) and the absorbance at 570 nm was measured on a multiwell plate reader. Cell viability was expressed as a percentage of control. IC_{50} values at 24 h of drug exposure were calculated as (drug concentration induced death, in %)-(spontaneous death, in %). For calculation IC_{50} values, a non linear equation was used. Data are shown as the mean value s.e.m. of triplicate cultures.

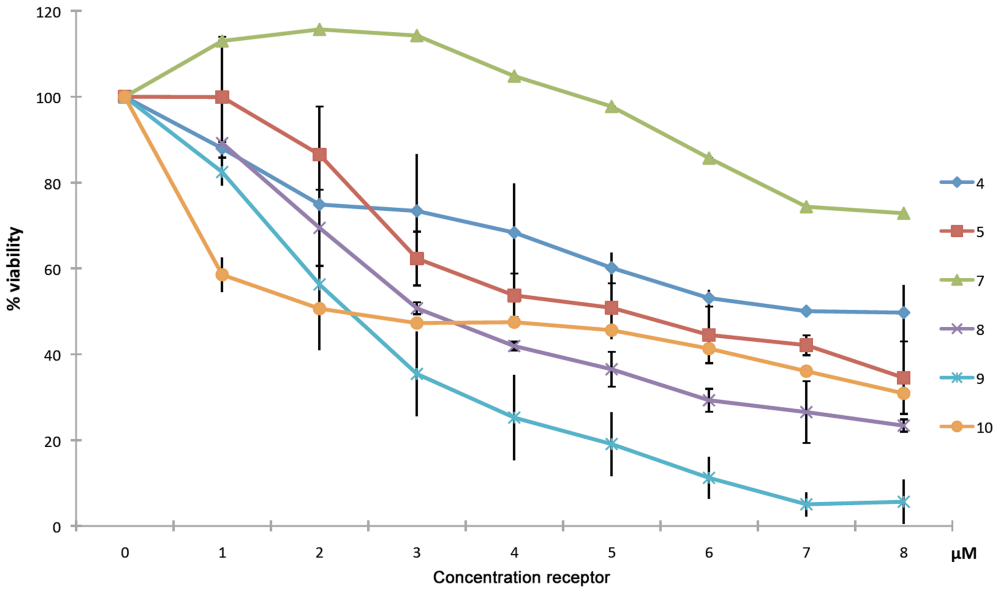

Figure S123. Dose–response curves (DRC) for receptors **4**, **5**, **7**, **8**, **9** and **10** on the viability of GLC4 cell line**.** The results are mean ±S.E.M. for three independent experiments in both cases and are expressed as % viability compared to control. Error bars represent standard deviation.

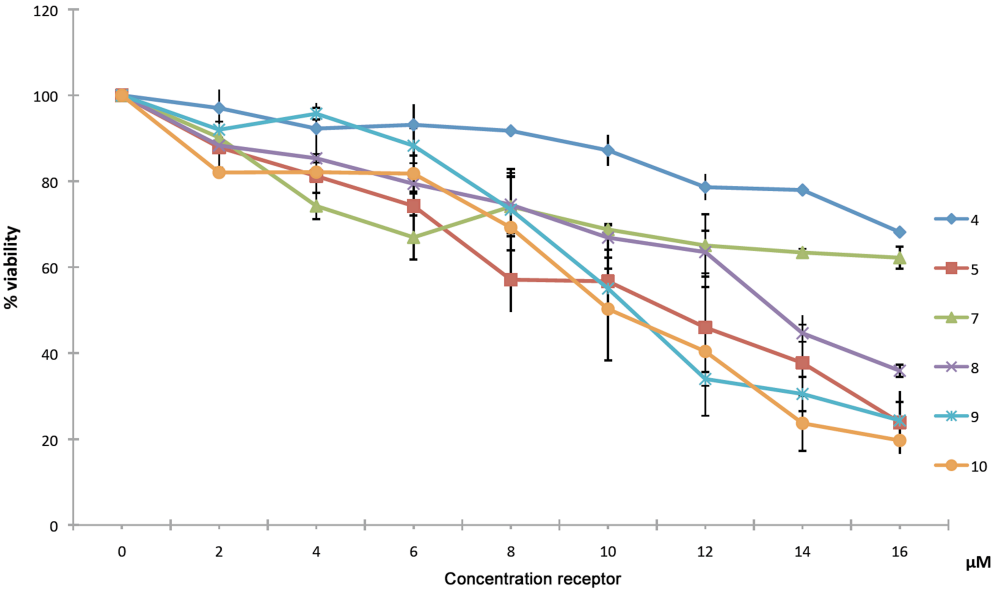

Figure S124. Dose–response curves (DRC) for receptors **4**, **5**, **7**, **8**, **9** and **10** on the viability of NH4 cell line**.** The results are mean ±S.E.M. for three independent experiments in both cases and are expressed as % viability compared to control. Error bars represent standard deviation.

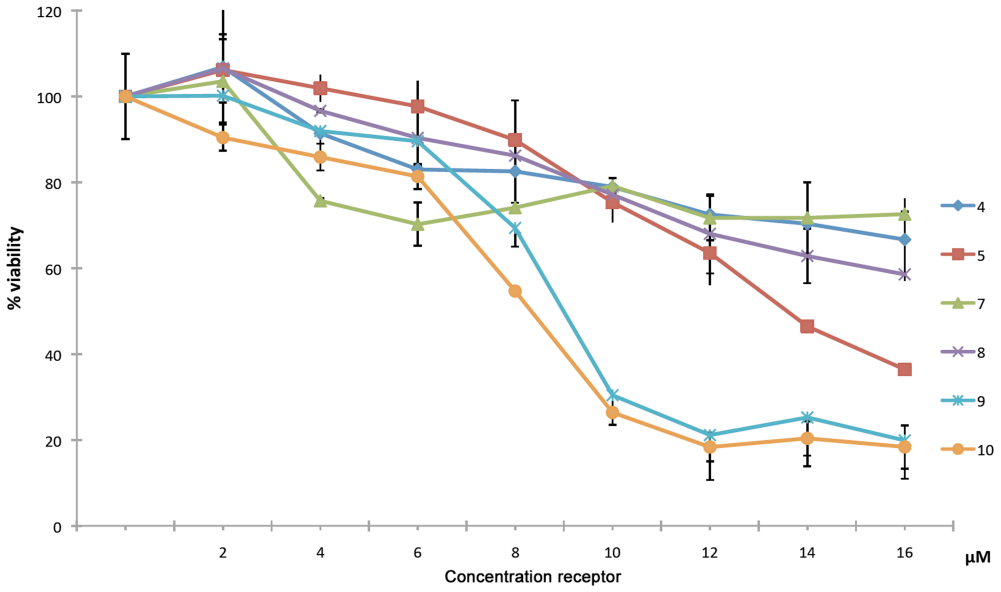

Figure S125. Dose–response curves (DRC) for receptors **4**, **5**, **7**, **8**, **9** and **10** on the viability of CAL27 cell line**.** The results are mean ±S.E.M. for three independent experiments in both cases and are expressed as % viability compared to control. Error bars represent standard deviation.

S7.3. Vital fluorescence microscopy (Acridine Orange staining)

The living cultured cells were stained with acridine orange (AO) (Holtzman, 1989). Briefly, GLC4 cells ($20x10^3$) on a chamber slide were incubated without and with 10 µM (receptors **1**, **2**, **3**, **6** and **7**) or the IC_{50} dose (receptors **4**, **5**, **8**, **9** and **10**) in RPMI supplemented with 10 % FBS at 37 ºC for 1 h. After 3 washes with PBS, cells were incubated with 5 µg/ml AO in PBS for 30 minutes. The chamber slides were washed 3 times with a PBS solution supplemented with 10% FBS and then examined with a Nikon microscope (E800) and photographed with diagnostic instruments photo automat system (Spot JR).

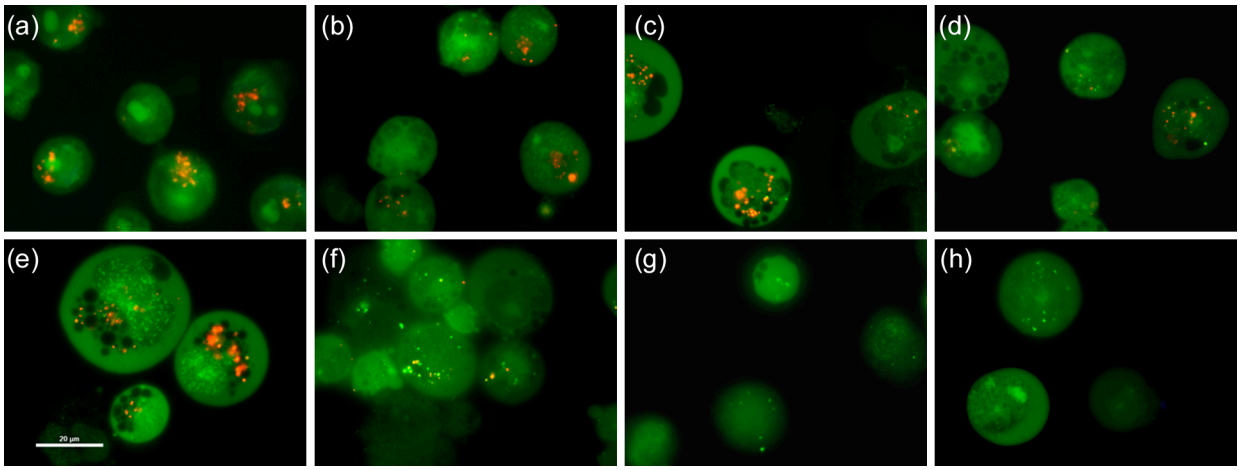

Figure S126. Acridine orange staining of GLC4 cell line after 1 h exposure at different receptors; (a) Untreated cells (control). (b) Cells treated with receptor **2**. (c) Cells treated with receptor **3**. (d) Cells treated with receptor **4**. (e) Cells treated with receptor **6**. (f) Cells treated with receptor **7**. (g) Cells treated with receptor **8**. (h) Cells treated with receptor **9**. In the case of (a), (b), (c) and (e) cells show granular orange fluorescence in the cytoplasm, while for (d), (f), (g) and (h) cells show complete disappearance of orange fluorescence cytoplasm granules.

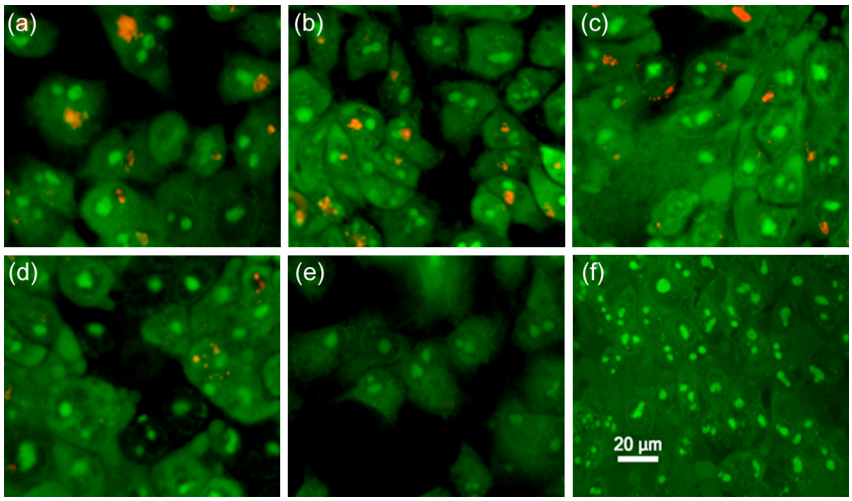

Figure S127. Acridine orange staining of CAL27cell line after 1 h exposure at different receptors (a) Untreated cells (control). (b) Cells treated with receptor **1**. (c) Cells treated with receptor **6**. (d) Cells treated with receptor **10**. (e) Cells treated with receptor **9**. (f) Cells treated with receptor **8**. In the case of (a), (b) and (c) cells show granular orange fluorescence in the cytoplasm, while for (d), (e) and (f) cells show disappearance of orange fluorescence cytoplasm granules.

S7.4. Hoechst staining

Cells were stained with the intercalating DNA dye Hoechst 33342 (Sigma) to reveal their nuclear morphology. GLC4 cells ($5x10^5$/ml) were incubated in the absence (control cells) or in the presence of 10 μM (receptors **1**, **2**, **3**, **6** and **7**) or the IC_{50} dose (receptors **4**, **5**, **8**, **9** and **10**) for 24 h. Cells were then washed in PBS and resuspended in PBS and Hoechst 33342 to a final concentration of 2 μg/ml and incubated for 30 min at 37ºC in the dark. After incubation, cells were washed in PBS and the sections were examined fluorometrically (emission above 420 nm, excitation 330-385 nm) with a Nikon microscope (E800) and photographed with diagnostic instruments photo automat system (Spot JR).

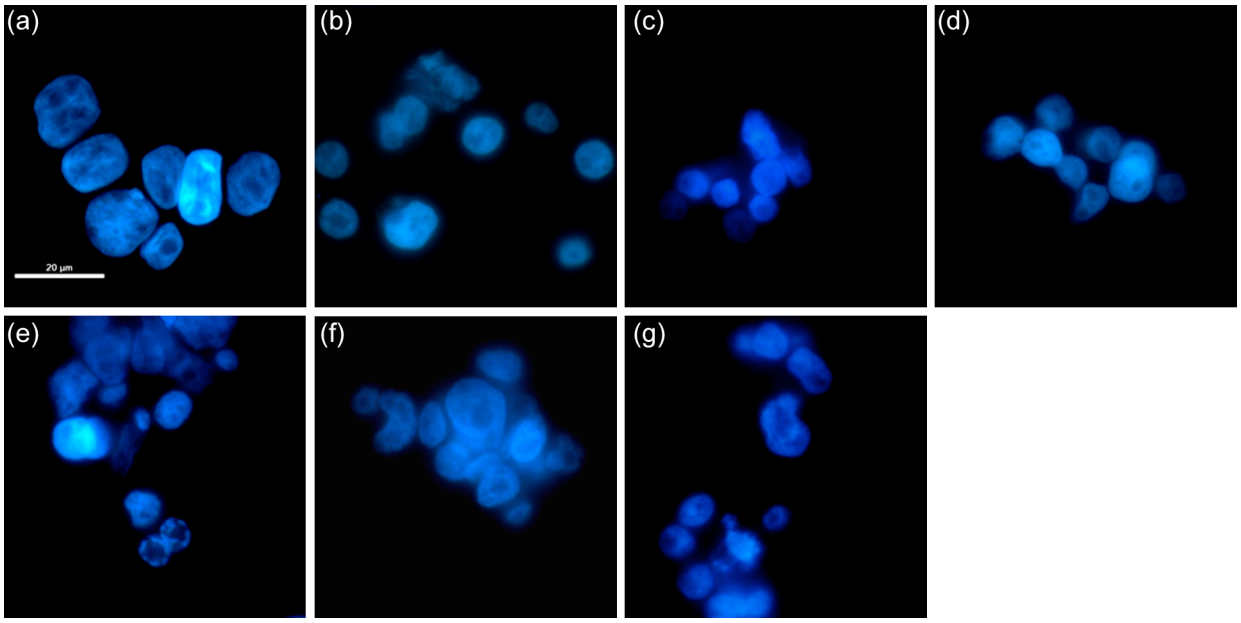

Figure S128. Hoechst 33342 staining of GLC4 cell line after 24 h exposure at different receptors (a) Untreated cells (control). (b) Cells treated with receptor **6**. (c) Cells treated with receptor **4**. (d) Cells treated with receptor **7**. (e) Cells treated with receptor **8**. (f) Cells treated with receptor **9**. (g) Cells treated with receptor **2**. In the case of (a), (b) and (g), cells show normal nuclear morphology, while in the case of (c), (d), (e) and (f) cells show condensation of the nuclei, apoptotic bodies (d) and nucleus with "bean shape"(e).

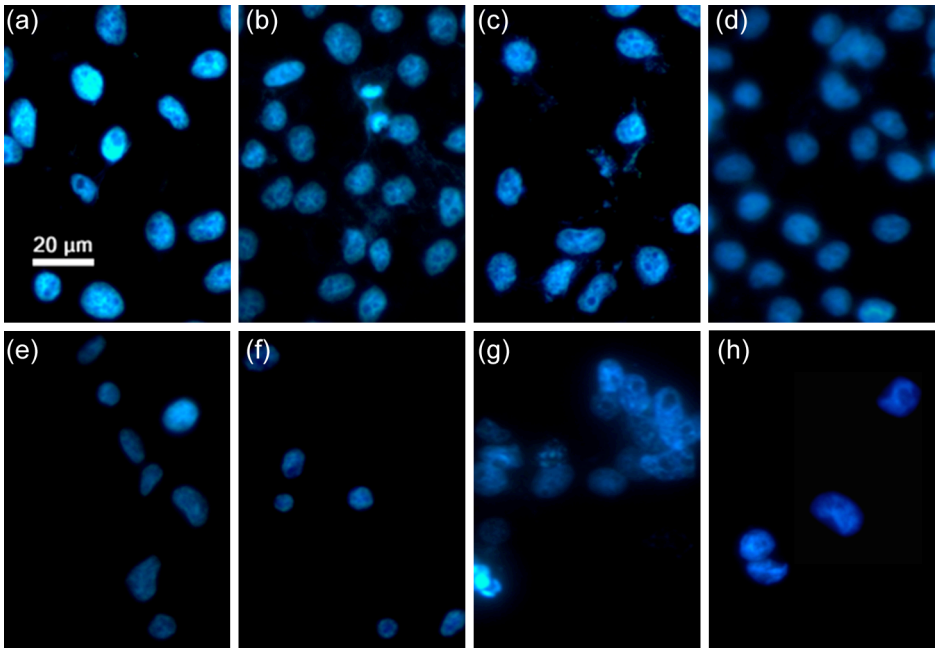

Figure S129. Hoechst 33342 staining of Cal27 cell line after 24 h exposure at different receptors (a) Untreated cells (control). (b) Cells treated with receptor **1**. (c) Cells treated with receptor **4**. (d) Cells treated with receptor **6**. (e) Cells treated with receptor **5**. (f) Cells treated with receptor **8**. (g) Cells treated with receptor **9**. (h) Cells treated with receptor **10**. In the case of (a), (b), (c) and (d) cells show normal nuclear morphology, while for (e), (f), (g) and (h) cells show condensation of the nuclei and nucleus with hole, apoptotic bodies (g) and "bean shape" (h).

S8. REFERENCES AND NOTES

1 Busschaert, N.; Gale, P. A.; Haynes, C. J. E.; Light, M. E.; Moore, S. J., Tong, C. C., Davis, J. T.; Harrell, W. A. Jr. *Chem. Commun.* **2010**, *46*, 6252.

2 Lakshminarayanan, P. S.; Ravikumar, I.; Suresh, E.; Ghosh, P. *Chem. Commun.* **2007**, *48*, 5214.

3 Hynes, M. J. *J. Chem. Soc., Dalton Trans.* **1993**, 311-312

4 Ravikumar, I.; Lakshminarayanan, P. S.; Arunachalam, M.; Suresh, E.; Ghosh, P. *Dalton Trans.* **2009**, 4160-4168.

5 Ravikumar, I. and Ghosh, P. *Chem. Commun.* **2010**, *46*, 1082-1084.

6 Duisenberg, A. J. M. *J. Appl. Cryst.* **1992**, *25*, 92-96.

7 Data collection software, R. Hooft, Nonius B.V., **1998**

8 Otwinowski, Z. and Minor, W. *Methods in Enzymology* **1997,** Vol. 276: *Macromolecular Crystallography*, part A, pp. 307−326; C. W. Carter, Jr. & R. M. Sweet, Eds., Academic Press

9 Sheldrick, G. M. SADABS - Bruker Nonius area detector scaling and absorption correction - V2.10

10 Sheldrick, G. M. *Acta Cryst.* **1990**, *A46***,** 467−473

11 Sheldrick, G. M. University of Göttingen, Germany, **1997**

12 v.d. Sluis, P. and Spek, A. L. *Acta Crystallogr., Sect A* **1990**, *46*, 194-201.

13 (a) Boon, J. M.; Smith, B. D. *J. Am. Chem. Soc.* **1999**, *121*, 11924-11925. (b) Sasaki, Y.; Shukla, R.; Smith, B. D. *Org. Biomol. Chem.* **2004**, *2*, 214-219.

From the main paper the full version of reference 38(b): Bok, D.; Galbraith, G.; Lopez, I.; Woodruff, M.; Nusinowitz, S.; BeltrandelRio, H.; Huang, W.; Zhao, S.; Geske, R.; Montgomery, C.; Van Sligtenhorst, I.; Friddle, C.; Platt, K.; Sparks, M. J.; Pushkin, A.; Abuladze, N.; Ishiyama, A.; Dukkipati, R.; Liu, W.; Kurtz, I. *Nat. Genet.* **2003**, *34*, 313-319;